SMALL GASES AND HYDROCARBON ADSORPTION AND SEPARATION IN MICROPOROUS METAL ORGANIC FRAMEWORKS (MMOFS)

by

HAOHAN WU

A dissertation submitted to the

Graduate School-New Brunswick

Rutgers, The State University of New Jersey

In partial fulfillment of the requirements

For the degree of

Doctor of Philosophy

Graduate Program in Chemistry and Chemical Biology

Written under the direction of

Professor Jing Li

And approved by

_____

_____

_____

_____

New Brunswick, New Jersey
MAY, 2013

ABSTRACT OF THE DISSERTATION

SMALL GASES AND HYDROCARBON ADSORPTION AND SEPARATION IN MICROPOROUS METAL ORGANIC FRAMEWORKS (MMOFS)

By HAOHAN WU

Dissertation Director:

Professor Jing Li

Microporous Metal Organic Frameworks (MMOFs) materials are very effective and efficient adsorbents for gas adsorption and separation due to their high surface area, large pore volume and relative low heat capacity. In this work, we focus on small gases and hydrocarbon adsorption and separation properties in MMOFs which typically have pore size smaller than 20Å. Nitrogen and argon adsorption isotherms were collected at 77K and 87K respectively for porosity characterization, e. g. surface area, pore volume and pore size distribution. Single component isotherms of small gases of CO_2, N_2, O_2, H_2, O_2, Alkanes (C_nH_{2n+2}) and Alkenes (C_nH_{2n}) were collected at ambient condition to preliminarily evaluate gas adsorption and separation properties. After screening, mixed gas adsorption and breakthrough experiment were performed using promising MMOFs candidates in order to mimic the real world situation. Besides experiment, molecular

simulation was studied in aid of learning adsorption behavior and separation mechanism in depth. An interesting phenomenon, so called "commensurate adsorption", was recognized and summarized in this thesis.

Acknowledgements

This dissertation was conducted in the department of Chemistry and Chemical Biology of Rutgers, the State University of New Jersey in Piscataway NJ. At this moment, I would like to thank many people who support, inspire and encourage me to be a disciplined researcher, an innovative student and a responsible man.

Thanks to Dr. Jing Li who leads me to chemistry program and offers me research opportunity in the field of MMOFs. She is not only a great advisor to my study, but a role model in my life teaching me to be a warm and responsible man. She is the ever closest person as a mother figure in U.S.

Thanks to Dr. David H. Olson who introduces zeolite and hydrocarbon adsorption and separation science which becomes a core business in my later PhD career. We have been interacting closely and sharing invaluable experience both in work and personal life for years.

Thanks to Dr. Matthias Thommes who is a great mentor in adsorption theory. His book in title of "Characterization of Porous Solids and Powders: Surface Area, Pore Size and Density" is the first ever book I read through twice from beginning to the very end though I still have to review some of contents once a while.

Thanks to all my past and present group members: Jeongyong Lee, Ke Wu, Min Wu, Sanhita Pramanik, Mojgan Roushan, Kunhao Li, Yonggang Zhao, Debasis Banerjee, Sujing Wang, Zhijuan Zhang, Zhichao Zhao, Jingming Zhang, Xiao Zhang, Yin Wang, Voshadhi Amarasinghe, Qihan Gong, Hao Wang et. al. Without their help, I can't go any further on my research career.

Last not the least, thanks to my family who always support my interest. Especially, I have to thank my Mom, Wenjun Wu again. It is hard to be a single Mom in China. I hope I made her be proud of me.

Contents

List of Tables

List of Figures

Chapter 1: Introduction

In the past decade, Metal Organic Frameworks (MOFs) has become one of hottest research fields across all disciplines due to its fancy structure and tunable porosity. [1-4] Generally, MOFs are fine crystalline solids with multi-dimensional structures. They are comprised by single or dual metal cations or metal clusters (secondary building unit or SBU) and organic ligands with multiple binding sites linked via coordinative bonds. According to the IUPAC definition, the pore size below 2nm is classified as micropore.[5] As such, Microporous Metal Organic Frameworks (MMOFs) are a subset of the general family of MOFs which embrace small porosity below 2nm. Being a new type of adsorbent materials, MMOFs possess numerous interesting and appealing features, including but not limited to, large internal surface area and pore volume,[6-27] high gas adsorption enthalpies, often significantly higher than those found in other adsorbates, characteristic of physisorption,[28-30] great structural flexibility,[31-36] remarkable adsorption selectivity,[37-40] interesting sorption kinetics,[41-45] catalytic functionality,[46-49] non-linear optical property,[50-52] and drug delivery in medical use.[53-55]

Although we explored MMOFs with wide collaboration in different disciplines,[52,56-65] we concentrated on gas adsorption and separation in this work as my major project.[58,66-77] One of big challenge is flue gas separation in which CO_2 and N_2 are two major components. There are thousands of tons of CO_2 was produced everyday as fossil fuels were consuming for energy generation. This rapid accumulation of carbon dioxide, a greenhouse gas, is becoming a major environmental issue worldwide.[78] Sea level rise, average temperature and ocean acidity increase, abnormal climate change and

other unpredictable natural occurrences are all signs of global warming as a indirect and direct consequence of such accumulation. We strived to develop a series of MMOFs to effectively and efficiently separate CO_2 from flue gas, such as $Zn_2(bpdc)_2(bpee)\cdot 2DMF$[76] (denoted as RPM3=Rutgers Recyclable Porous Materials), $Zn_2(bpdc)_2(bpe)\cdot 2DMF$[75] (denoted as RPM4), $[Cu_3(TDPAT)(H_2O)_3]\cdot 10H_2O\cdot 5DMA$ (TDPAT= 2,4,6-tris(3,5-dicarboxylphenylamino)-1,3,5-triazine).[69] Likewise, we also try to employ those promising materials for nature gas separation in which CH_4 and CO_2 are two major components and syngas separation in which CO and CO_2 are two major components.[66,69,72,74-76]

Besides research on small gases adsorption and separation work, hydrocarbon adsorption and separation became a big emphasis in my later PhD research. With the aid of simulation package by Materials studio, we are able to predict adsorption uptake of hydrocarbon as well as its orientation in MMOFs materials, which helps us to understand adsorption behavior and separation mechanism so as to design and modify desired MMOFs materials for specific separation process. Inspired from former hydrocarbon study in Zeolite, we conclude new concept of "commensurate adsorption" in MMOFs materials after closely examining many MMOFs adsorption cases.[67]

Chapter 2: Small gas adsorption and separation on MMOFs

2.1 Flue gas separation (CO_2 vs N_2)

Effective and efficient CO_2 capture from flue gases has become one of the most emerging issues concerning environmental conservation and protection as CO_2 is the most predominant greenhouse gas causing global warming.[78] Conventional technologies to remove carbon dioxide from the flue gases includes chemical absorption, but the solvents used, such as aqueous alkanolamines, usually requires high energy to regenerate (30% energy penalty) and often leads to environmental issues due to solvent loss and degradation. Adsorption-based separation methods have the advantages of easy control and low energy demand. However, a proper absorbent with low cost, high selectivity and adsorption capacity of CO_2, especially at relatively low pressure (e.g. 0.15 atm, the partial pressure of CO_2 in flue gases) and humid condition, is essential for making the process practical. Table 1 is a typical example of flue gas composition though it may be different case by case. MMOFs materials have become good candidates to selectively capture of CO_2 at given condition (0.15atm, 45°C). However, the stability of MMOFs is still a question mark. The CO_2 separation performance is abruptly degraded upon moisture existence since H_2O molecule is more competitively adsorbed than CO_2 onto active metal open site or "hot spots" on MMOFs surface. In order to employ MMOFs to the use of CO2 capture, pre-treatment of removal of Moisture is required.

Table 1 Typical Post-combustion Flue Gas Composition for a Coal-Fired Power Plant.[79] Reproduced with permission from ref 79. Copyright 2012 The American Chemical Society.

molecule	concentration (by volume)
N_2	73–77%
CO_2	15–16%
H_2O	5–7%
O_2	3–4%
SO_2	800 ppm
SO_3	10 ppm
NO_x	500 ppm
HCl	100 ppm
CO	20 ppm
hydrocarbons	10 ppm
Hg	1 ppb

2.1.1 $Zn_2(bpdc)_2(bpee)\cdot 2DMF$ (RPM3-Zn)

The structure of $Zn_2(bpdc)_2(bpee)\cdot 2DMF$ (**1**) (bpdc = 4,4′- biphenyl dicarboxylate, bpee = 1,2-bis(4-pyridyl)ethylene) is a three-dimensional (3D) network composed of one-dimensional (1D) open channels running along the crystallographic b-axis (see Fig. 1).[31,80]

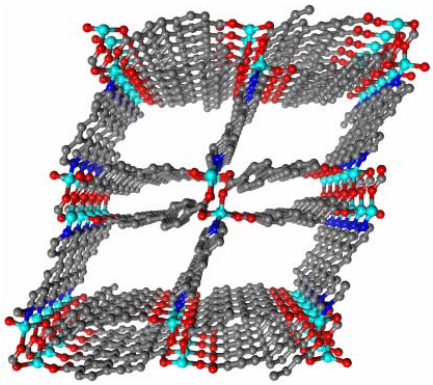

Figure 1: The structure of **1** showing 1D open channels. Color scheme: Zn: cyan, N: blue, O: red and C: grey. H atoms and DMF are omitted for clarify. Reproduced with permission from ref 31. Copyright © 2010 WILEY-VCH Verlag GmbH & Co. KGaA, Weinheim.

The size of the parallelogram shaped pore window is ~5×7 Å (excluding van der Waals radius of carbon, 1.7 Å). The solvent accessible volume was calculated to be 1171.9 $Å^3$ (27.6 % of the unit cell volume). The thermogravimetric (TG) profile of **1** was shown a weight loss of 15.43 wt% was observed experimentally in the temperature range of 80-140°C, in excellent agreement with the calculated percentage weight of gust DMF molecules, 15.6%.

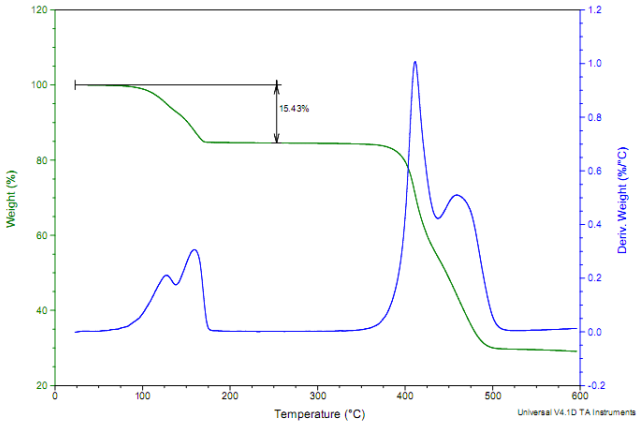

Figure 2. The thermogravimetric (TG) profile of **1.** Reproduced with permission from ref 31. Copyright © 2010 WILEY-VCH Verlag GmbH & Co. KGaA, Weinheim.

The structure is highly flexible and undergoes a fully reversible change after removal and refill of DMF guest molecules (See Fig. 3). The pore size of the outgassed structure (1′) is significantly reduced, as estimated from the PXRD data. The micropore volume of 1′ was calculated to be 0.171 cc/g based on the 87K Ar adsorption isotherm data (See Fig. 4).

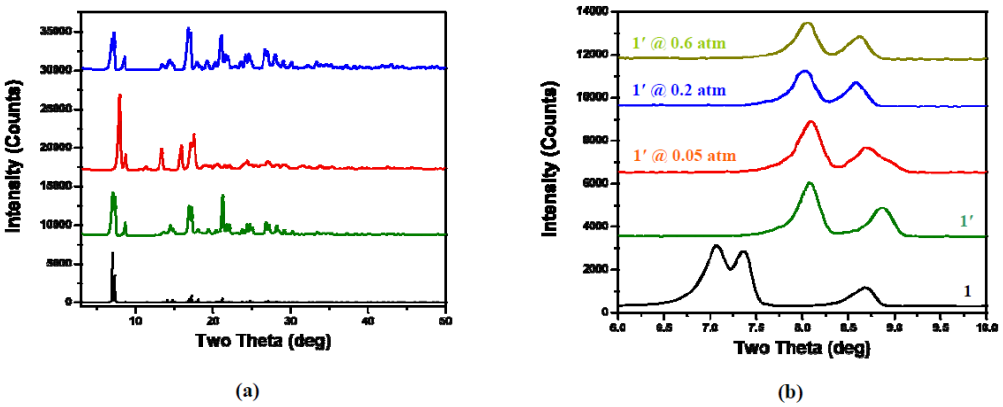

Figure 3. (a) PXRD patterns of the as-made (**1**, green, bottom), outgassed (**1**′, red, middle), and DMF regenerated (blue, top) samples along with the simulated one (black). Structure change is evident from the distinct difference in the peak positions of **1** and **1**′. It is also clear **1** is fully restored after **1**′ is refilled with DMF. (b) PXRD patterns taken in-situ on **1**′ (outgassed sample) as a function of CO_2 pressure (0.05, 0.2 and 0.6 atm, respectively). The PXRD of **1** (as-made sample) is included as reference (black, bottom). Reproduced with permission from ref 31. Copyright © 2010 WILEY-VCH Verlag GmbH & Co. KGaA, Weinheim.

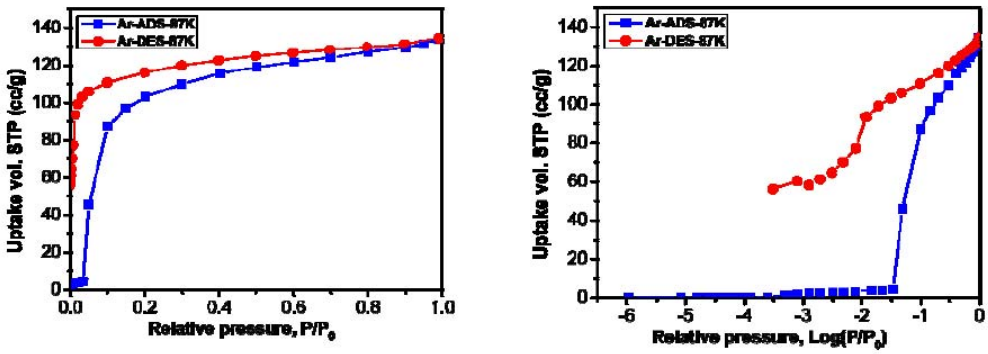

Figure 4. Ar adsorption-desorption isotherms at 87K, respectively, plotted as relative pressure P/P°(left) and log(P/P°) (right). Reproduced with permission from ref 31. Copyright © 2010 WILEY-VCH Verlag GmbH & Co. KGaA, Weinheim.

To examine the separation capability of this flexible MMOFs, single component gas sorption experiments were carried out on CO_2 and N_2 near room temperature and up to 1 atm. At 25 °C, the CO_2 shows very little adsorption at low pressure. An abrupt increase is observed as the pressure reaches ~0.1 atm, which is followed by a quick

increase to a maximum uptake of 25 cc/g (5 wt%) at 1 atm (Fig. 5). At 15, 5°C and 1 atm, the material takes up 5.4, 5.9 wt% of CO_2, respectively (Fig. 6) Unlike previously reported flexible structures,[81] the desorption curve of CO_2@1′ nearly retraces the adsorption one, showing practically no hysteresis. Repeated experiments confirmed this observation (Fig. 7). The shape of the isotherms is quite unusual but is similar to those of IRMOF-1 recently reported by Snurr and co-workers[82] at lower temperatures (e.g. 195 and 218 K), where the simulation assumed a rigid structure model.

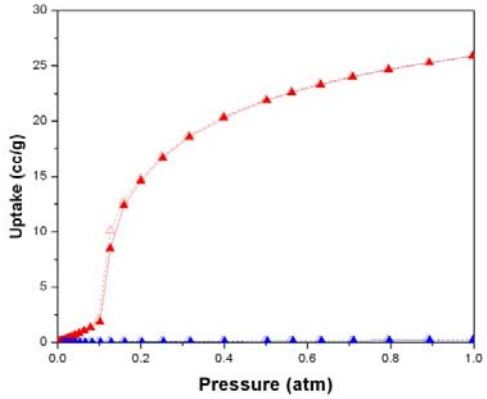

Figure 5. CO_2 (red) and N_2 (blue) adsorption-desorption isotherms at 25 °C and up to 1 atm. Filled symbols are adsorption data points and open dots, desorption data points. Reproduced with permission from ref 31. Copyright © 2010 WILEY-VCH Verlag GmbH & Co. KGaA, Weinheim.

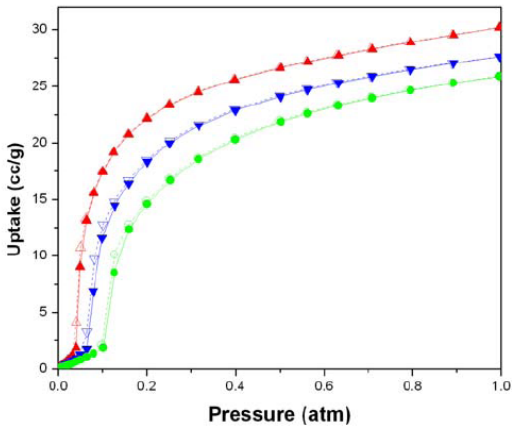

Figure 6. CO_2 adsorption-desorption isotherms at 5°C (red), 15°C (blue) and 25°C (green). Adsorption and desorption data are represented by filled and open symbols, respectively. Reproduced with permission from ref 31. Copyright © 2010 WILEY-VCH Verlag GmbH & Co. KGaA, Weinheim.

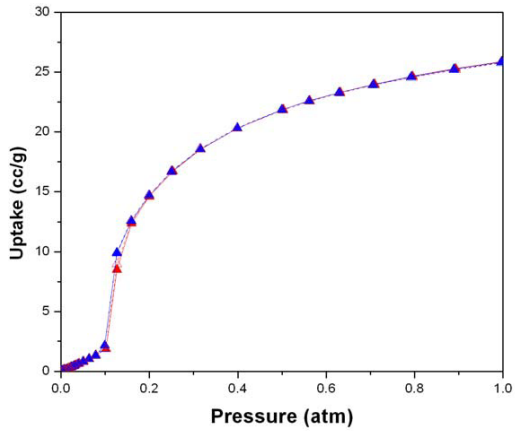

Figure 7. Repetitive runs of CO2 adsorption-desorption isotherms at 25°C up to 1 atm (Blue: first run, Red: second run). Reproduced with permission from ref 31. Copyright © 2010 WILEY-VCH Verlag GmbH & Co. KGaA, Weinheim.

Adsorption isotherms of N2 were measured under the same conditions and the results indicate very little uptake over the entire pressure range (See Fig. 2). The selectivity of CO2:N2 at 25 °C is calculated to be 294:1 at 0.16 atm and 116:1 at 1 atm, respectively. These numbers are significantly higher than the best values reported so far,

for example, 6:1 and 49:1 for SNU-M10[83] and MOF74-Mg,[84] respectively, at 25°C and 0.16 atm (See summary in table 2).

Table 2. Single-component separation ratios of CO2/N2 at 25 °C. Reproduced with permission from ref 31. Copyright © 2010 WILEY-VCH Verlag GmbH & Co. KGaA, Weinheim.

Pressure, atm	Separation Ratio (v/v)		
	1′	MOF74-Mg	SNU-M10[1]
0.16	294	49	6[2]
0.60	166	16	24[3]
1.00	116	12	98

In addition, H2, CO, O2 and CH4 adsorption-desorption isotherms were measured under identical experimental conditions (25 °C and up to 1 atm). All show very similar behavior to that of N2 (See Fig. 8). The selectivity ratios of CO2 over H2, CH4, and CO are 190, 257 and 440, respectively, at 0.16 atm and 25 °C, and 768 over O2 (0.2 atm, 25°C) (See summary in table 3).

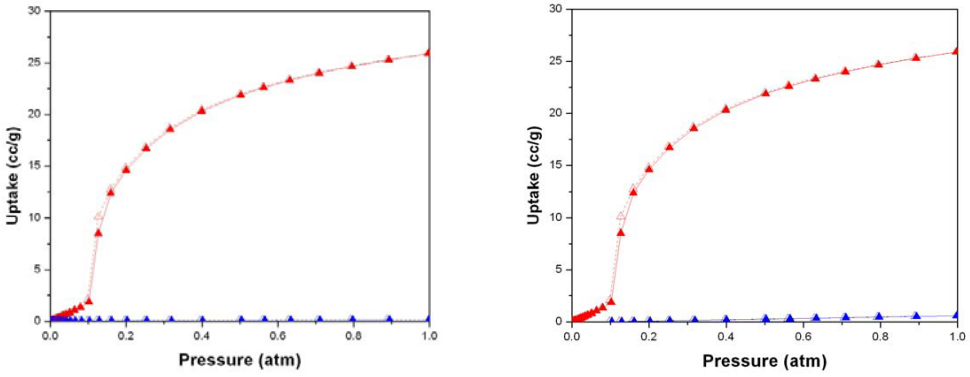

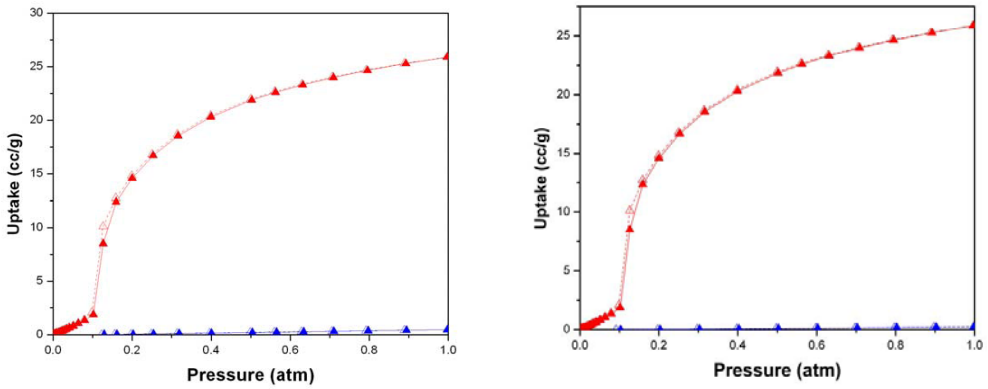

Figure 8. Comparison of CO_2 in red and H2 (top left), CH4 (top right), CO (bottom left) and O_2 (Bottom right) in blue adsorption-desorption isotherms at 25 °C up to 1 atm (Adsorption Branch: filled symbols, Desorption Branch: open symbols). Reproduced with permission from ref 31. Copyright © 2010 WILEY-VCH Verlag GmbH & Co. KGaA, Weinheim.

Table 3. Single-component gas uptake in 1′ and separation ratios of CO2/Gas at 25 °C. Reproduced with permission from ref 31. Copyright © 2010 WILEY-VCH Verlag GmbH & Co. KGaA, Weinheim.

Pressure (atm)	Gas	Gas Uptake (STP, cc/g)	Wt %	CO_2/Gas Ratio (v/v)
0.16	CO_2	12.36	2.43	
	N_2	0.042	0.0052	294
	H_2	0.065	0.00058	190
	CH_4	0.048	0.0035	257
	CO	0.028	0.0035	441
	O_2	0.019 [1]	0.0027 [1]	768
1.00	CO_2	25.89	5.09	
	N_2	0.22	0.028	116
	H_2	0.14	0.0012	185
	CH_4	0.58	0.041	45
	CO	0.46	0.057	56
	O_2	0.23	0.033	113

[1] at O_2 pressure of 0.2 atm.

The extent of adsorbent-adsorbate interactions was estimated by the heats of CO2 adsorption calculated based on the sorption isotherms obtained at 5, 15 and 25 °C. As shown in Fig. 9, the values are 28.5-28.9 and 32.5-33.5 kJ/mol, respectively, before and after the onset pressure of pore filling. These values compare very well with those having flexible structures and comparable pore size, including MIL-53(Cr) (32 kJ/mol) and MIL-53(Al) (35 kJ/mol), at similar temperatures.[85]

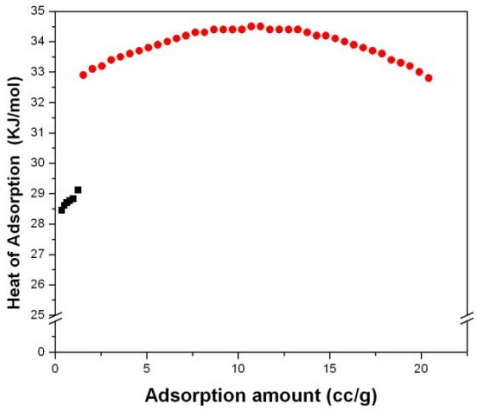

Figure 9. Heats of CO2 adsorption as a function of uptake. The values before pore opening are shown in black, and those after pore opening are in red. Reproduced with permission from ref 31. Copyright © 2010 WILEY-VCH Verlag GmbH & Co. KGaA, Weinheim.

Compound **1** was tested in a more real-world process with a gas mixture mimicking the industrial flue gas composition (See Fig. 10 and Fig. 11 for experimental setup and details).

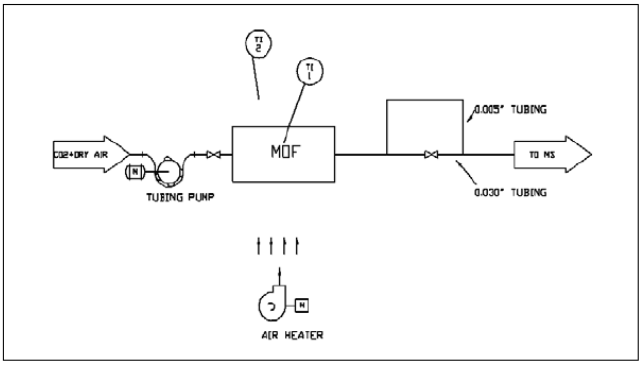

Figure 10. Equipment flow diagram for the mixed gas adsorption-desorption experiments. [86] Reproduced with permission from ref 31. Copyright © 2010 WILEY-VCH Verlag GmbH & Co. KGaA, Weinheim.

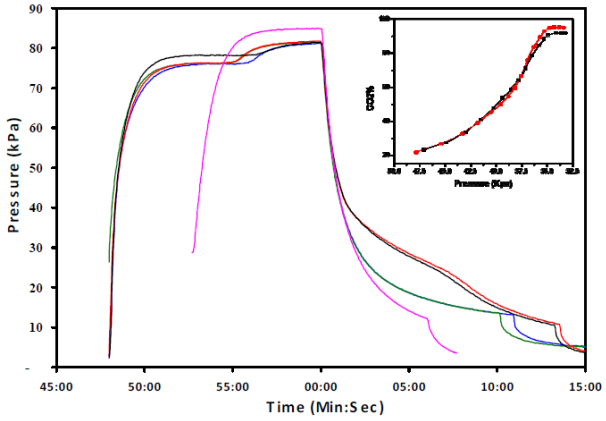

Figure 11. Changes in the system pressure in the chamber when gas was filled and emptied. Initial load was 20% of CO2 in air and initial load rate was 5.7scc/min with 0.5g of the sample in a tube of 127μm in diameter. Multiple runs indicate the consistency of performance. Pressure curves of two repetitive runs at 25°C (blue and green) and 50°C (red and black) are shown for 1′ (activated sample). Data for 1 (as-made sample) at 25°C are also included as reference (pink). Inset: CO2 concentration in the exhaust gas as a function of system pressure. CO2 reaches a max concentration of 93%±2% when system pressure drops to 34kPa in 2.2 mins. Reproduced with permission from ref 31.

Illustrated in Fig. 12 are the exhaust gas composition during the desorption phase of the experiment. At a feed concentration of 20% carbon dioxide (with 80% of dry air), the activated 1′ is able to recover 47% and 95% of CO2 at 25 and 50 °C, respectively, within 2.2 minutes. The recyclability of the samples was further examined by repeating the gas mixture adsorption experiment under identical conditions after the initial run. The results for both 25 and 50 ºC runs are plotted in Fig. 12. Data clearly suggest that the process is highly reproducible. A maximum separation ratio of CO2/N2 from this mixture gas was calculated to be 84 at 50 °C.

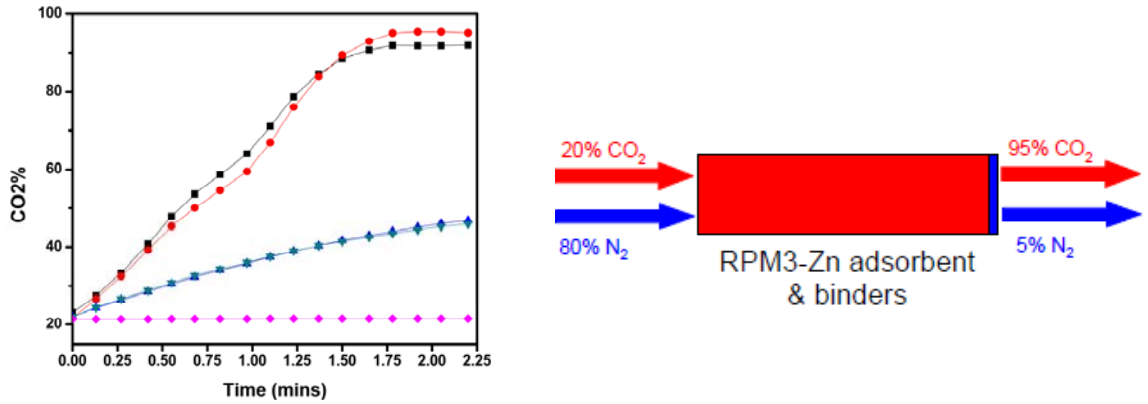

Figure 12. (left) The CO2 composition (vol %) of the exhaust from an activated MMOF (1′) at 25 °C (blue and cyan, two separate runs) and 50 °C (black and red), in comparison with the values from an as-made sample at 25 °C (1, pink). The initial feed concentration of CO2 is ~20%. (right) A brief scheme showing the pressure swing adsorption process: the N2 (80%, v/v) rich mixed gas was flow through RPM3-Zn adsorbent bed at high pressure. Concentrated 95% (v/v) of CO2 was recovered at low desorption pressure. Reproduced with permission from ref 31. Copyright © 2010 WILEY-VCH Verlag GmbH & Co. KGaA, Weinheim.

2.1.2 $Zn_2(bpdc)_2(bpe)\cdot 2DMF$ (RPM4-Zn)

Compound $Zn_2(bpdc)_2(bpe)\cdot 2DMF$ (**2**) (bpdc = biphenyldicarboxylate bpe = 1,2-bis(4-pyridyl)-ethane, DMF = N,N-dimethylformamide) crystallizes in monoclinic crystal system, space group C2/c.[32] All Zn atoms in **2** are tetrahedrally coordinated to three O from three bpdc and one N from a bpe ligand with approximately tetrahedral geometry. The second building unit (SBU) is an eight-member ring, $Zn_2(COO)_2$2+ that is formed by inversion symmetry related pairs of Zn(II) atoms and bidentate carboxylate group from bpdc ligands (Figure 13a). A monodentate carboxylate group from another bpdc ligand completes the SBU coordination. Each SBU is further connected to four neighboring SBU to form a 44 brick-like net (Figure 13b). Two such identical nets interpenetrate to generate a 2D layer.

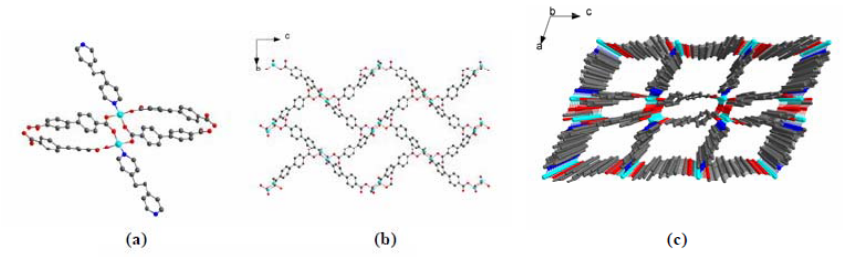

Figure 13. Views of the crystal structure of **2**. (a) the SBU and the coordination around the Zn(II)2 pair; (b) the single 44 brick-like net; (c) perspective view of 1 showing the 1D channels along the b-axis (DMF molecules and H atoms are removed for clarity). Zinc cyan, Carbon gray, Oxygen red, Nitrogen blue. Reproduced with permission from ref 32. Copy right 2010 Royal Society of Chemistry.

Adjacent 2D layers are connected by the bpe ligands via Zn-N bonds to complete the tetrahedral coordination of Zn(II) metal centers and to give rise to an overall 3D structure with 1D open channels extending along the crystallographic b-axis. These channels have a parallelogram-shaped cross section (5×7 Å, excluding Van der Waals radius of the carbon atom, 1.7 Å) and the DMF guest molecules reside in the channel (Figure 1c). The DMF molecules can be removed by heating **2** under vacuum at 160 °C for 12 hours. The TG analysis of **2** gave a weight loss of 15.13 wt% that maches very well with the calculated value (15.5 wt%) based on the crystal data (Fig. 14). Unpon removal of guest DMF, the guest-free compound (**2′**) underwent a minor structure change but remained highly crystalline, as confirmed by PXRD analysis (Fig. 15). The original structure was fully restored by heating **2′** in DMF at 80 °C for 6 hours. The solvent accessible volume of **2′** was calculated to be 1041.8Å^3 (25.1% of the unit cell volume) using program PLATON/SQUEEZE.

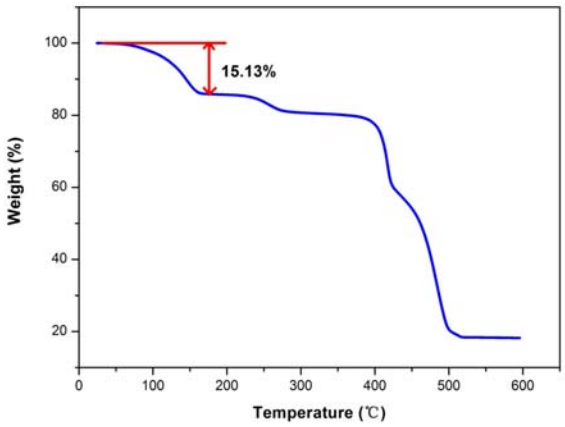

Figure 14. Thermogravimetric analysis of a freshly prepared sample of **2**, showing a good agreement between the observed weight loss of DMF (15.13 wt%) and the calculated value (15.5 wt%). Reproduced with permission from ref 32. Copy right 2010 Royal Society of Chemistry.

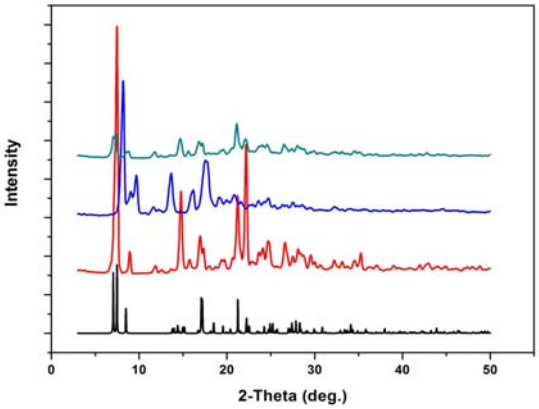

Figure 15. PXRD patterns of as-synthesized sample of **2** (red), guest-free **2′** (blue), and **2′** after being heated in DMF at 80 °C for 6 hours (dark-green). The pattern in black (bottom) is calculated from the single crystal structure of **2**. Reproduced with permission from ref 32. Copy right 2010 Royal Society of Chemistry.

The porosity and gas adsorption properties of **2′** were evaluated by the adsorption-desorption isotherm experiments employing volumetric methods at various temperatures. The activated samples (**2′**) were prepared by heating **2** under vacuum at 160 °C overnight. The pore volume and surface area were obtained from the CO_2 isotherm at 273K. The surface area was estimated to be 88.4 m^2/g (BET) and 137.8 m^2/g

(Langmuir) in the pressure range P/P_0 = 0.05-0.25. The total pore volume was estimated to be 0.08 cc/g, substaintially smaller than the value calculated based on the crystal structure of **2** (0.2 cc/g). This is consistent with the observation of structure change/distortion upon guest removal (Fig. 15), and confirms that the pores in **2'** are significantly shrunk with respect to the original structure of **2**. These data show that **2'** is a porous framework with relatively small surface area and pore size.

The adsorption isotherms for CO2 at 273, 288 and 298K are ploted in Fig. 16. The isotherms show a three-step adsorption profile. At 298K, about 0.55 wt% of CO_2 (2.8 cc/g at STP) is adsorbed in the first step (up to 0.08 atm). In the second step, 1' takes up ~3.5 wt% CO_2 (18.0 cc/g) in the pressure range of 0.08-0.6 atm. In the final step, the CO_2 uploading reaches 5.4 wt% (27.76 cc/g) at 1 atm. The isotherms at 273 and 288 K show a similar trend. Such observations are well documented for a number of previously reported flexible MMOFs where pressure-dependent structure changes occur during adsorption-desorption processes.[31,87-88] The structure change as a function of CO2 pressure in each of the three steps was monitored and confirmed by an in-situ powder X-ray diffraction experiment, (Fig. 17). As shown in Figure 16, the inflection becomes more pronounced as temperature decreases, and the on-set pressure of each inflection point also decreases as temperature is lowered, which is similar to several other cases and modeled by grand canonical Monte Carlo (GCMC) simulations.[82,87]

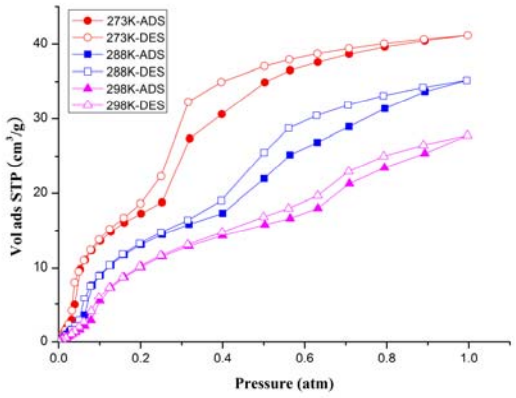

Figure 16. The CO_2 adsorption-desorption isotherms measured at 273, 288 and 298K. Reproduced with permission from ref 32. Copy right 2010 Royal Society of Chemistry.

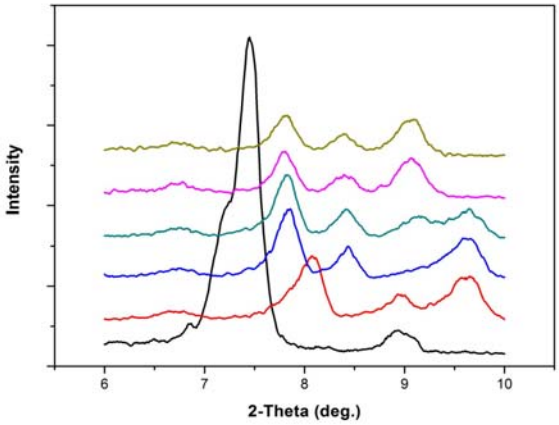

Figure 17. Room temperature PXRD patterns at low angles (2θ = 6-10°) for as-synthesized sample **2** (black), guest-free sample **2′** (red), **2′** after refilling CO_2 at 0.05 atm (blue, first step), **2′** after refilling CO_2 at 0.2 atm (green, second step), **2′** after refilling CO_2 at 0.6 atm (pink) and **2′** after refilling CO_2 at 1 atm (yellow, third step). Reproduced with permission from ref 32. Copy right 2010 Royal Society of Chemistry.

The heats of CO2 adsorption were calculated based on the adsorption isotherms obtained at 273, 288 and 298K using the virial coefficient (VC) method[89] (see detailed Programming for Origin software in appendix A) and are plotted in Figure 18. The highest value is obtained for the first step, namely ~37.6 kJ/mol at a very low loading of 0.064 cc/g. For the second and third steps, the values are 29.2-32.9 and 28.5-29.2 kJ/mol,

for a loading range of 2.93-17.86 and 18.11-28.06 cc/g, respectively. These values are comparable with other reported flexible structures having similar porosity, for example, MIL-53(Cr) (32 kJ/mol) and MIL-53(Al) (35 kJ/mol) and RPM3-Zn (33-35 kJ/mol)[31,85] at similar CO2 uptake and temperatures.

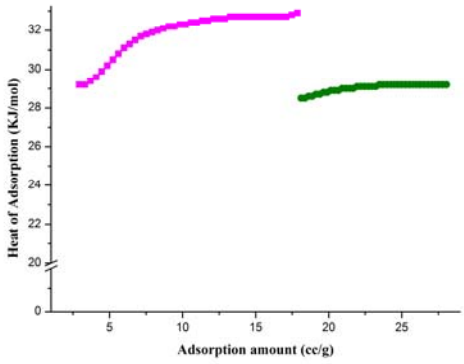

Figure 18. Heats of CO2 adsorption as a function of uptake. Heat of adsorption for the first step was shown in pink. To be contrast, the heat of adsorption for the second and third steps was shown in green. Reproduced with permission from ref 32. Copy right 2010 Royal Society of Chemistry.

To evaluate the adsorption selectivity and capacity of **2'**, the adsorption-desorption isotherms of other small gases such as CH4, N2, O2 and CO were also measured at room temperature. Figure 19 shows the N2 and CH4 isotherms compared with that of CO2. Clearly **2'** adsorbed essentially N2 and very little CH4 in the pressure range given. The single-component CO2/N2 separation ratios of **2'** at 0.09, 0.5 and 1 atm are 98:1 (v/v), 169:1 (v/v) and 360:1 (v/v), respectively, and for CO2/CH4 they are 74:1 (v/v), 25:1 (v/v) and 24:1 (v/v) at 0.09, 0.5 and 1 atm, respectively. These values are 99:1 (v/v) and 53:1 (v/v), respectively, at ~0.16 atm (a pressure that is well within a typical CO2 partial pressure range in flue gases). A more detailed comparison was presented in table 4.

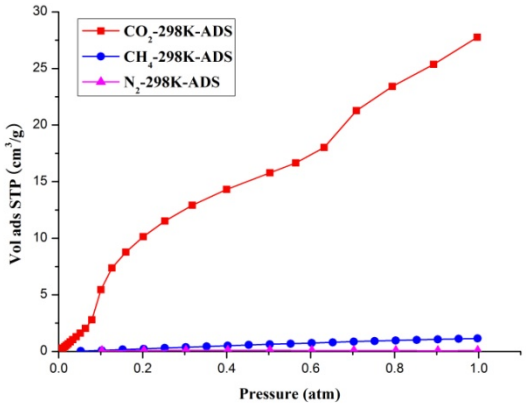

Figure 19. Room temperature adsorption isotherms of CO2, N2 and CH4 on **2'**. Reproduced with permission from ref 32. Copy right 2010 Royal Society of Chemistry.

Table 4. Single-component gas uptake in **2**' and separation ratios at 25 °C**.** Reproduced with permission from ref 32. Copy right 2010 Royal Society of Chemistry.

Pressure (atm)	Gas	Gas Uptake (STP, cc/g)	wt%	CO_2/Gas Ratio (v/v)
0.16	CO_2	8.77	1.72	
	N_2	0.088	0.011	99
	CH_4	0.160	0.012	53
	CO	0.041	0.005	213
	O_2	0.071	0.010	124
1	CO_2	27.76	5.46	
	N_2	0.077	0.0096	360
	CH_4	1.15	0.082	24
	CO	0.079	0.0098	351
	O_2	0.085	0.012	327

2.1.2 $Zn_2(bdc\text{-}R)_2(ted)\cdot 2DMF\cdot 0.2H_2O$ series (R=H, OH or NH_2)

In order to better understand how selected functional groups may affect the adsorption properties of a given structure type, we have targeted on three microporous MOFs, $Zn(BDC)(TED)_{0.5}$ (**3**), $Zn(BDC\text{-}OH)(TED)_{0.5}$ (**4**), and $Zn(BDC\text{-}NH_2)(TED)_{0.5}$ (**5**) in this study.[90-91] The three structures are closely related in such a way that (a) they are isostructural and (b) they differ only in the functional group (-R) of the terephthalate,

BDC-R. The mother structure of $Zn_2(bdc\text{-}H)_2(ted)$ and correlation among three compounds were shown in Fig. 20 and Fig. 21, respectively.

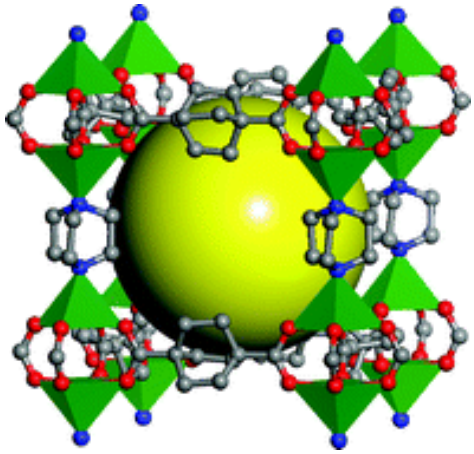

Figure 20. 3D structure of **3** with one cage shown in ball-and-stick model. The space inside one cage is highlighted by the yellow sphere. Color schemes: Zn, green square pyramids; C, gray; N, blue; O, red. Hydrogen and solvent molecules were omitted for clarity)[92] Reproduced with permission from ref 92. Copy right 2008 Royal Society of Chemistry.

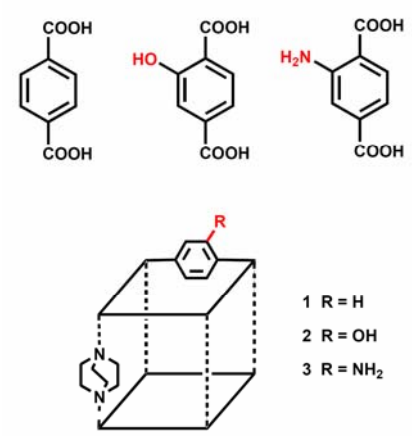

Figure 21. Brief scheme of correlation among three $Zn_2(bdc\text{-}R)_2(ted)$ derivatives. Reproduced with permission from ref 91. Copyright © 2010 WILEY-VCH Verlag GmbH & Co. KGaA, Weinheim.

All three structures contain paddle-wheel dinuclear Zn clusters $Zn_2(COO)_4$ (or secondary building unit, SBU) which are bridged by BDC–R ligands (R = –H, –OH, and –NH for **3**, **4** and **5**, respectively), to form a two-dimensional (2D) 4^4 grid. The BDC-R

ligands in the 2D nets bend significantly, making the grid highly non-symmetric. The neighboring 2D grids are pillared by TED molecules and extended to a three-dimensional (3D) framework. Upon the removal of solvent molecules, the BDC–R ligand in all three guest-free frameworks **3′**, **4′** and **5′** becomes linear and the 4^4 grid becomes symmetric. Inter-crossing channels of two different sizes are found in compound **3**the cross section of 7.5Å×7.5Å (measured between the C-C atoms in the two lateral BDC ligands excluding van der Waals radius of carbon) along the c axis; and of 4.8Å×3.2Å along a- and b- axes (measured between C-C and H-H atoms, excluding van der Waals radius of carbon or hydrogen atoms). In such an inter-connected porous structure, very large void (61.3%) is accessible for solvent and guest molecules. Differing from **3**, the two small windows along the a- and b- axes in compound **4** (4.8Å×2.6Å measured from the single crystal structure) become inaccessible for most of small gas molecules due to the grafting of –OH group on the benzene ring. Hydroxy groups were found almost parallel to the benzene ring without protruding into the channel along c-axis, thus compound 2 features a one-dimensional (1D) channel structure along the c-axis. As calculated by PLATON, 53.6% of the unit cell becomes accessible to guest molecules upon the removal of the solvent. Despite the unsuccessful attempt to produce qualified single crystal for structure analysis, the phase and purity of compound **5** were identified by the powder X-ray diffraction analysis. Both compounds **4** and **5** have very similar PXRD patterns as that of compound **3** (Fig. 22), confirming that the pillared 3D structure is retained upon ligand functionalization. Considering the size of amino group in **5**, a similar 1D channel structure to compound **4** is expected for **5**.

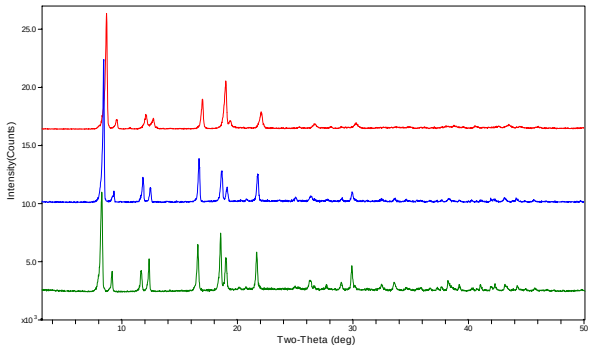

Figure 22. Powder X-ray diffraction (PXRD) patterns of compound **3** (bottom), **4** (middle) and **5** (top). Reproduced with permission from ref 91. Copyright © 2010 WILEY-VCH Verlag GmbH & Co. KGaA, Weinheim.

The thermal stability measurements by thermogravimetric analysis (TGA) indicate that all solvent molecules trapped in compound **3** (32.2%) can be removed at ca. 150 °C. The resulting framework was stable to 260 °C, followed by a decomposition at ca. 300 °C. For compound **4**, 29.5% of weight loss was observed upon heating to 180 °C, which corresponds well to the amount of solvent molecules. The guest-free structure was stable till 250 °C. TGA data show all guest molecules of compound **5** (30.3%) can be removed at ca. 200 °C, and the decomposition of the guest-free framework occurred at ca. 230 °C. The experimental mass losses are in good agreement with the solvent weight calculated from single crystal data: 34.4 % for **3** and 27.6 % for **4**. The PXRD analysis indicates that upon removal of solvent molecules, all three compounds (**3**′, **4**′, and **5**′) remain highly crystalline. A typical TGA (Fig. 23) and PXRD (Fig. 24) of **4** are as following.

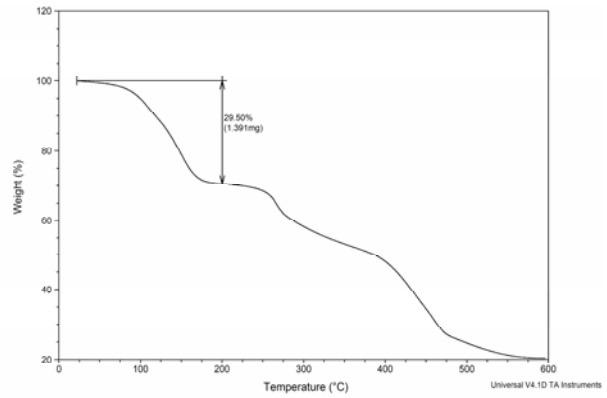

Figure 23. TGA plots of compound **4.** Reproduced with permission from ref 91. Copyright © 2010 WILEY-VCH Verlag GmbH & Co. KGaA, Weinheim.

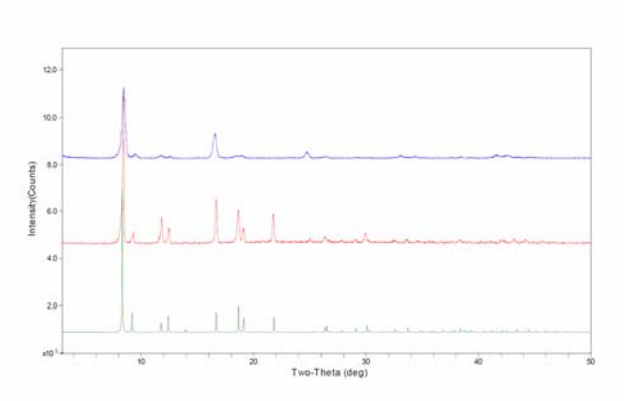

Figure 24. Powder X-ray diffraction (PXRD) patterns of compound 4. Top: evacuated sample 4′; middle: as-synthesized sample; bottom: simulated sample from single crystal data. Reproduced with permission from ref 91. Copyright © 2010 WILEY-VCH Verlag GmbH & Co. KGaA, Weinheim.

To determine the surface areas and porosity of the three compounds, argon and nitrogen adsorption-desorption experiments were carried out. The evacuated compound **3′** shows much higher N2 adsorption capacity than **4′** and **5′**. The Brunauer-Emett-Teller (BET) and Langmuir surface areas are summarized in Table 5. Apparently, the significantly lower surface areas and the pore volumes found in the functionalized compounds **4′** and **5′** are a direct result of occupation by the functional groups (–OH and –NH2) in the voids.

Table 5. Summary of porosity characterization, H_2 and CO_2 adsorption data for 3′, 4′ and 5′. Reproduced with permission from ref 91. Copyright © 2010 WILEY-VCH Verlag GmbH & Co. KGaA, Weinheim.

	Surface Area[m^2/g] Langmuir (BET)	Pore Volume [cm^3/g]	H_2 (77K and 1atm)		CO_2 (298K and 1atm)	
			Uptake (wt%)	Q_{st} (KJ/mol)	Uptake (wt%)	Q_{st} (KJ/mol)
3′	2057 (1937)	0.75	2.1	~5.0	7.4	19.8~20.3
4′	1111 (1023)	0.56	1.8	5.5~4.9	13.1	24.2~26.9
5′	1183 (1081)	0.46	1.5	4.4~3.9	9.5	22.8~22.9

The CO_2 adsorption isotherms for evacuated compounds **3′**, **4′** and **5′** were collected at 278, 288 and 298 K, and the results are plotted in Figure 25. In contrast to the adsorbed amount of H_2 (see table 5), an opposite trend is obtained for the CO_2 uptake in **3′** and **4′**, which is clearly not coincident with the order of surface area and pore size. As seen from the isotherm data, compound **4′** has a maximum CO_2 uptake of 23.7 and 13.0 wt% at 278 and 298 K (1 atm), respectively, corresponding to ~16 and ~10 CO_2 molecules per unit cell. For **3′**, the CO_2 uptake decreased to 18.4 and 7.4 wt% at 278 and 298 K (1 atm), respectively. Note the adsorbed amount of CO_2 is nearly doubled in **2′** with respect to that by its parent structure **3′** at room temperature.

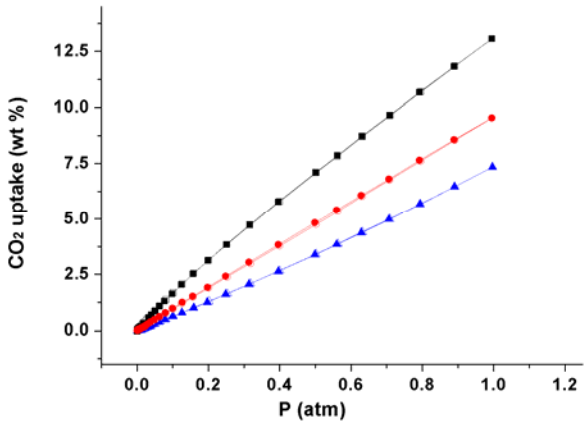

Figure 25. CO2 adsorption-desorption isotherms at 298 K for **3′** (blue), **4′** (black) and **5′** (red). (Adsorption Branch: open symbols, Desorption Branch: filled symbols). Reproduced with permission from ref 91. Copyright © 2010 WILEY-VCH Verlag GmbH & Co. KGaA, Weinheim.

The isosteric heats of CO_2 adsorption were calculated based on the adsorption raw data collected at 278, 288 and 298 K without fitting (Figure 26). The highest Q_{st} values for compound **4′** are 24.2-26.9 kJ mol^{-1} at the low loading (1-6 wt%), in comparison with those of **3′** (19.8-20.3 kJ mol^{-1}) and **3′** (22.8-22.9 kJ mol^{-1}), respectively. The trend in the Q_{st} values is clearly in accordance with the uptake amount. Both follow the order: **4′** > **5′** > **2′** and override the trend in surface area values (**3′** >> **5′** ≈ '**4′**). The higher adsorption enthalpies of CO_2 in **4′** and **5′** having functionalized BDC ligands compared to those of **3′** 'suggest stronger interactions between the functionalized frameworks and CO_2. For compound **4′**, the primary interaction between CO_2 and framework is considered as the electron donor-accepter reaction, in which the oxygen atom of hydroxyl group serve as electron-donor center while the C atom of CO_2 as electron-accepter center. In addition, the dipolar or quadrupolar interactions between the hydroxyl group and CO_2 molecule also contribute to the observed trend.

Accordingly, similar but weaker electron donor-accepter interaction may be expected in the CO_2 adsorption by amino group functionalized compound **5′**, due to the less electron donating ability of $–NH_2$ compared to the –OH group. Consequently, the enhanced CO_2 adsorption can be achieved by functionalizing MOF structures to increase gas-framework interactions.

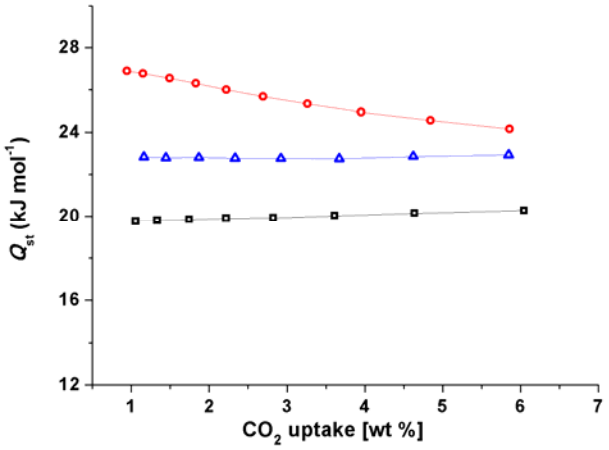

Figure 26. Isosteric heats of CO_2 adsorption (Q_{st}) values for **3′** (black), **4′** (red) and **5′** (blue). Reproduced with permission from ref 91. Copyright © 2010 WILEY-VCH Verlag GmbH & Co. KGaA, Weinheim.

The enhancement of CO_2 uptake found in functionalized MOF structures prompted us to further investigate their CO_2 selectivity over other important gases, including CH_4, CO, N_2 and O_2. The adsorption isotherms of CO_2, CH_4, CO, N_2 and O_2 on compound **3′** and **4′** were performed under the same conditions (298K, up to 1 atm), and are shown in Figure 27. Experimental data reveals that both compounds possess significantly higher affinity to CO_2 than CH_4, CO, N_2 and O_2. Compared to compound **3′**, slight decreases in the uptake capacity for other small gases, including CH_4, CO, N_2 and O_2, are found in compound **4′.** These changes coincide with the reduction of void size and surface area due to the space occupation by functional groups. Moreover, in virtue

of the significant enhancement of CO_2 uptake in compound **4'**, its selectivity of CO_2 to CH_4, CO, N_2 and O_2 will therefore be further improved. The single-component separation ratios of CO_2/CH_4, CO_2/CO, CO_2/N_2 and CO_2/O_2 at 298K and 1 atm are calculated to be 4:1(v/v), 10:1(v/v), 15:1(v/v) and 14:1(v/v) for compound **3'**, 7:1(v/v), 16:1(v/v), 23:1(v/v) and 15:1(v/v) for compound **4'**, respectively. And the selectivity will be further increased at higher pressure. In addition to the stronger electron donor-accepter interactions between the CO_2 molecule and hydroxyl group, other two factors should also be taken into account for the high CO_2 selectivity in **4'**. First, since the higher molecular polarity can lead to stronger interactions and faster sorption rates, it is expected that the introduction of polar –OH group will be in favor of the attraction of CO_2, which has the largest quadrupole moment (13.4 $C \cdot m^2$) and polarizability (2.93$C^2 \cdot M^2/J$) among all small gases investigated (the quadrupole moments of CO, N_2 and O_2 are 8.3, 4.7 and 1.3 $C \cdot m^2$ respectively, and CH_4 is nonpolar).[93] Second, the confinement by the pore and channel may also help the enhancement of selectivity.[94] The selectivity found in compound **4'** are comparable with those reported for zeolite and carbon adsorbents (e.g. zeolite 13X: CO_2/CH_4, 2-24; CO_2/N_2, 18), as well as some other MOFs (e.g. Cu-BTC: CO_2/CH_4, 6; CO_2/N_2, 20) at the similar conditions.[95-97] The relatively high CO_2 uptake capacity and selectivity of **4'** place it in the category of qualified candidates for further development of CO_2 capture and sequestration.

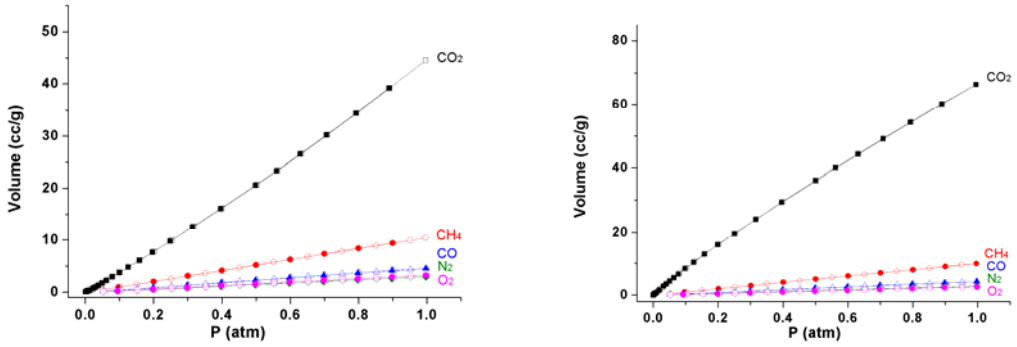

Figure 27. Comparison of CO_2 (black) and selected gases (CH_4, red; CO, blue; N_2, green; O_2, pink) adsorption-desorption isotherms of compound **3′** (top) and **4′** (bottom) at 298 K. (Adsorption branch: filled symbols, desorption branch: open symbols). Reproduced with permission from ref 91. Copyright © 2010 WILEY-VCH Verlag GmbH & Co. KGaA, Weinheim.

2.1.3 $[Cu_3(TDPAT)(H_2O)_3]\cdot 10H_2O\cdot 5DMA$

Compound $[Cu_3(TDPAT)(H_2O)_3]\cdot 10H_2O\cdot 5DMA$ (**6**) (TDPAT=2,4,6-tris(3,5-dicarboxylphenylamino)-1,3,5-triazine, DMA=Dimethylacetamide is highly porous MMOFs.[98] (see detailed structure description in ref 98) The total accessible volume after removal ofthe guest and coordinated solvent molecules is 70.2% using the Platon software, and the calculated density of the desolvated framework is 0.782 g/cm^3. Thermogravimetric (TG) and powder X-ray diffraction (PXRD) analysis at various temperatures show that the framework is stable up to 285°C (Fig. 28 and 29). The water/moisture stability was tested in boiling water (1 day) and in air (30 days). The framework remained intact as clearly indicated by the PXRD patterns of the samples taken after these tests (Figure 30).

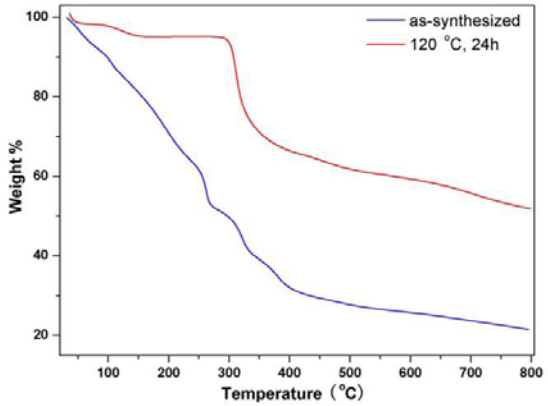

Figure 28. The TG profile of guest-free sample (**6′**, red) and as-synthesized sample (**6**, blue). **6′** was prepared by heating the activated sample for 24 h under dynamic high vacuum. The **6′** is prone to adsorb moisture, which could change its color quickly from deep purple to blue upon exposure to air. The minor weight loss of **6′** before 150 °C in the TG profile may be attributed to the re-adsorbed water molecules during sample weighting. Reproduced with permission from ref 98. Copyright © 2012 WILEY-VCH Verlag GmbH & Co. KGaA, Weinheim.

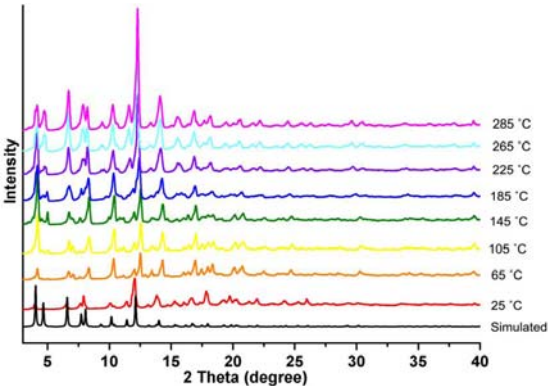

Figure 29. PXRD patterns of **6** taken at various temperatures under N_2. Reproduced with permission from ref 98. Copyright © 2012 WILEY-VCH Verlag GmbH & Co. KGaA, Weinheim.

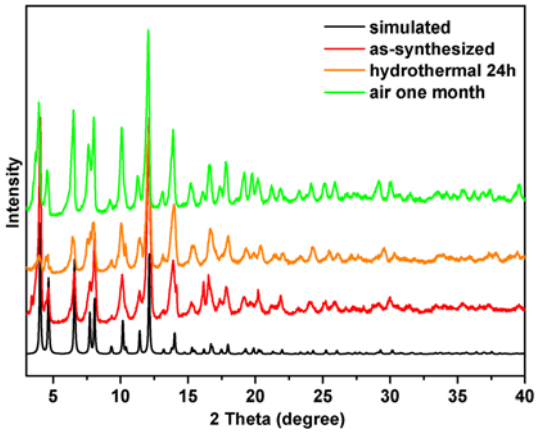

Figure 30. The XRD patterns of **6** under hydrothermal conditions for 24 h (orange) and in air for one month (green). Reproduced with permission from ref 98. Copyright © 2012 WILEY-VCH Verlag GmbH & Co. KGaA, Weinheim.

Permanent porosity of activated Cu-TDPAT was confirmed by N2 adsorption–desorption isotherms at 77 K which show a reversible type-I isotherm (Fig. 31). The Langmuir and BET surface area calculated based on data at the low-pressure region (P/Po=0.05–0.2) are 2608 and 1938 m^2/g, respectively. The total pore volume calculated from the N_2 isotherms is 0.93 cm_3/g, in good agreement with the value obtained from single-crystal data.

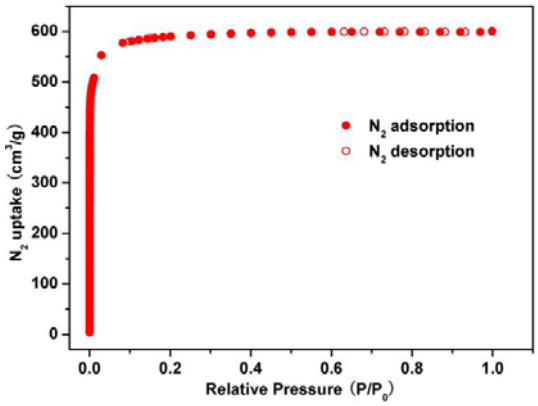

Figure 31. The N_2 sorption isotherm of **6′** at 77 K. Reproduced with permission from ref 98. Copyright © 2012 WILEY-VCH Verlag GmbH & Co. KGaA, Weinheim.

The CO2 low-pressure adsorption–desorption isotherms were measured at 273, 288, and 298 K (0–1 atm) (Fig. 32). Compound 1 has a very high CO2 adsorption capacity. At 298 K, the uptake amount is 132 cm^3/g (STP=standard temperature and pressure; 25.8 wt%, 103 v/v) and 31.3 cm^3/g (STP; 6.2 wt%, 24.5 v/v) at 1.0 and 0.1 atm, respectively. At 273 K, they are 227 cm^3/g (STP; 44.5 wt%, 177 v/v) and 52.8 cm^3/g (STP; 10.4 wt%, 41.3 v/v) at 1.0 and 0.1 atm, respectively. These values are substantially higher than all previously reported rht-type structures (See comparison in Fig. 33), and significantly larger than that of the best performing zeolitic imidazolate frameworks (ZIFs), namely ZIF-78 (60.2 v/v, at 298 K and 1 atm),[99] and that of zeolite 13X (20.7 wt%, at 298 K and 1 atm),[100] one of the best sorbents for CO2 separation.

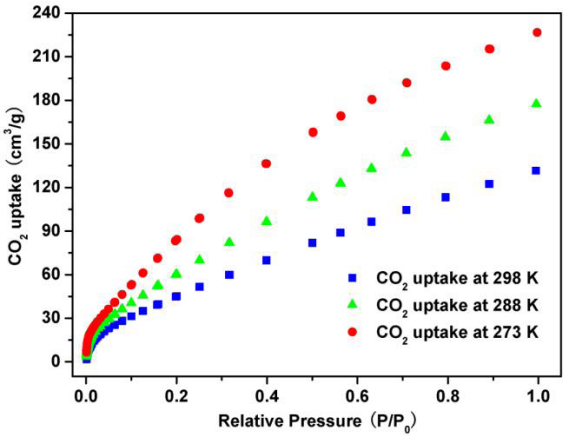

Figure 32. CO2 adsorption isotherms of **6′** at 273, 288, and 298 K. Reproduced with permission from ref 98. Copyright © 2012 WILEY-VCH Verlag GmbH & Co. KGaA, Weinheim.

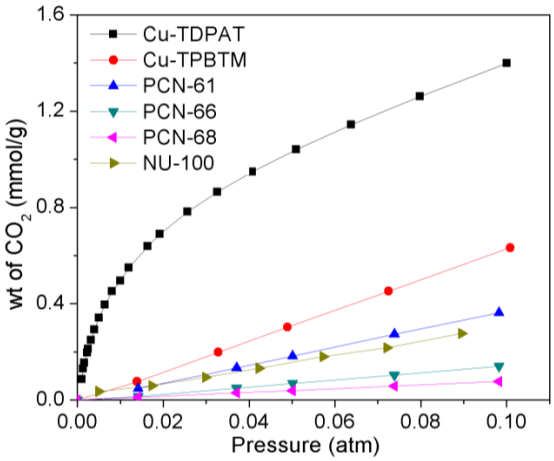

Figure 33. CO2 adsorption isotherms of rht-type structures at 298K. Reproduced with permission from ref 98. Copyright © 2012 WILEY-VCH Verlag GmbH & Co. KGaA, Weinheim.

To evaluate the extent of CO2–MOF interactions, isosteric heats (Qst) of CO2 adsorption were calculated by the virial method using experimental isotherm data at three temperatures. The Qst values (based on the Clausius–Clapeyron equation) were also obtained directly from experimental data at low loadings by interpolation (AS1Win 2.01). No fitting was involved in the latter case. The data plotted in Fig. 34 in the shows excellent agreement by the two methods. Compound **6′** shows a very high adsorption enthalpy (42.2 kJ/mol at zero loading), indicative of strong adsorbate–adsorbent interactions. The Qst values over the entire CO2 loading range are appreciably higher compared with all other rht-type structures reported thus far, following the same trend as the uptake amounts at low pressure. As all rht-type MOFs contain a high density of OMSs, this unusually high CO2 binding affinity can be attributed to the fact that **6** is the only member that also carries a high density of LBSs and that has the smallest cages.

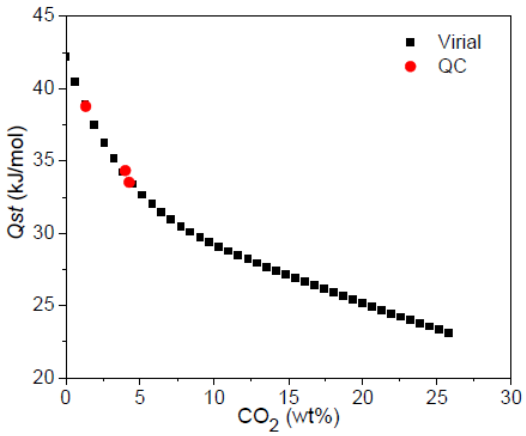

Figure 34. CO2 adsorption enthalpies (Qst) of **6′** based on the experimental isotherm data at 273, 288, and 298 K. Comparisons are made between the two methods. Reproduced with permission from ref 98. Copyright © 2012 WILEY-VCH Verlag GmbH & Co. KGaA, Weinheim.

In addition to its high uptake capacity and strong adsorption enthalpy for CO_2, 6′ also shows high adsorption selectivity of CO_2 over N_2 at 298 K. At 1 atm, the separation ratio for CO_2/N_2 calculated based on single-component gas adsorption isotherms is 16 (v/v), higher than those of MOF-74-Mg (12, v/v)[84] and ZIF-78 (about 13, v/v)[99] under the same conditions. At 0.16 atm (a pressure close to the CO_2 concentration in a power plant flue gas stream), the value is 34 (v/v) for 6′, second to the highest value reported for MOF-74-Mg (49, v/v). To imitate the separation behavior of 6′ under a more realworld setting, the CO_2/N_2 selectivity in a binary mixture was calculated employing the ideal adsorbed solution theory (IAST) method[101] with the experimental single-component isotherms fitted by the dual-site Langmuir (DSL) model.[102] At a total pressure of 1 atm and CO_2 concentration of 10% (partial pressure of 0.1 atm), a remarkable selectivity of about 79 is predicted by IAST (see Figure S9 in the Supporting Information).

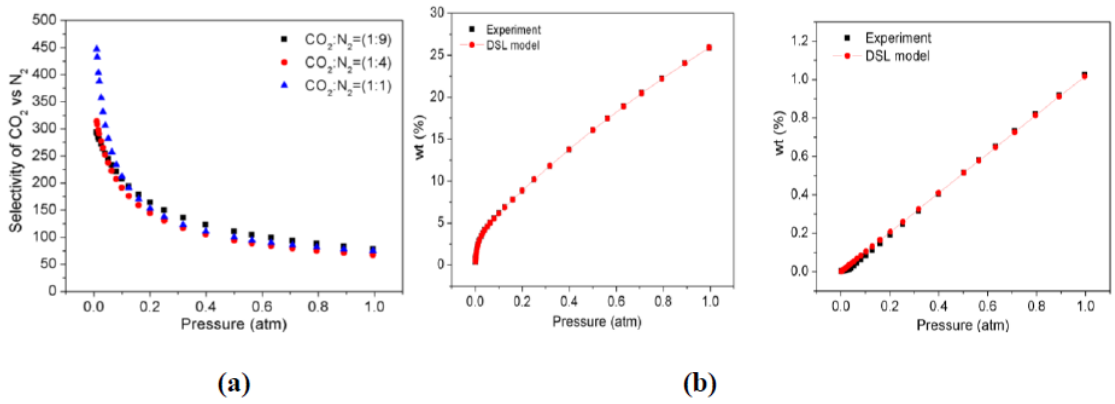

Figure 35. (a) The room temperature (298K) selectivity of CO2/N2 calculated by IAST method for three CO2 concentrations (CO2/N2: 1:9 (10%), 1:4 (20%), and 1:1 (50%). (b) Experimental single-component isotherms of CO2 (left) and N2 (right) and corresponding fitted isotherms by DSL model. Reproduced with permission from ref 98. Copyright © 2012 WILEY-VCH Verlag GmbH & Co. KGaA, Weinheim.

To evaluate the performance of compound 6′ in a real gas mixture, we carried out a series of breakthrough experiments to determine its CO_2 separation capacity from a CO_2/N_2 mixture under kinetic flow conditions (see Fig. 36 and 37). The results show that 6′ can effectively capture CO_2 from the mixed gas with an uptake of 6.7 wt% before breakthrough, comparable to that of MOF-74-Mg in a similar CO_2/CH_4 breakthrough experiment.[103] Moreover, compound 6′ saturated with CO_2 can be fully regenerated under relatively mild conditions. Successive breakthrough experiments revealed that 6′ retains a constant capacity of 5.7 wt% upon repeated regenerations at 80°C. These values reflect the kinetic aspect of separation, suggesting that 6′ is a promising candidate for CO_2 capture and separation from gas mixtures.

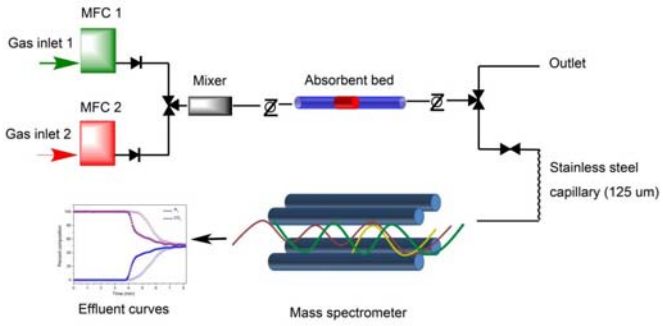

Figure 36. Schematic illustration of the apparatus used for the breakthrough experiments. In a typical experiment, 130 mg of **6** crystals were thoroughly ground and packed into a stainless column (1.6 mm I.D. × 50 mm) with silica wool filling the void space. The sample was in-situ activated under vacuum (6.5×10^{-4} Pa) at 120 °C for 10 hours to remove the solvent molecules and make the active sites accessible. The sample was then purged with N2 flow (2.0 ml/min) for 1 hour while the temperature of the column was decreased to 25 °C. CO2 flow was then introduced at 2.0 ml/min without changing the N2 flow, resulting in a 50:50 CO2/N2 mixture by volume. Effluent from the column was monitored using a mass spectrometer (MS). Breakthrough is defined to be the time point when CO2 starts to be detectable by MS. The dead time was determined using an empty column with exactly the same dimensions. Breakthrough times were calculated by subtracting the dead time from the observed breakthrough time. Reproduced with permission from ref 98. Copyright © 2012 WILEY-VCH Verlag GmbH & Co. KGaA, Weinheim.

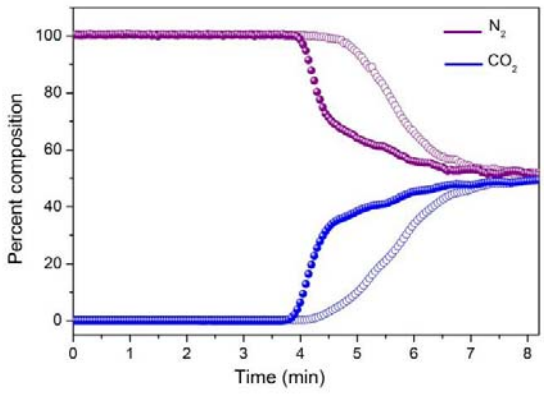

Figure 37. Breakthrough curves of **6′** for a CO2/N2 gas mixture (feed concentration: 50:50 by volume). The curves with open and solid symbols represent the data of fully activated and regenerated samples, respectively. Reproduced with permission from ref 98. Copyright © 2012 WILEY-VCH Verlag GmbH & Co. KGaA, Weinheim.

2.2 Nature gas storage and separation (CH_4 vs N_2)

Hydrogen used to be a hot field for next generation of clean energy.[104] However, hydrogen has a very low boiling point which needs high energy to be liquefied in order to ease storage and transportation. Physisorption of hydrogen in porous MOFs provides an intriguing approach to hydrogen storage. Since the initial study of hydrogen storage with MOF-5,[14] significant progress has been made in this area, with a great number of MOFs examined for their hydrogen uptake capacities.[28,105-106] No MOF has yet met the DOE targets of reaching 0.055 kg/kg for system gravimetric capacity and 0.040 kg/L for system volumetric capacity by 2015. Most of the MOFs synthesized to date function best only at low temperatures due to their weak interactions (dominated by van der Waals forces) with H_2. More efforts are needed to increase MOF hydrogen uptake capacities and to enhance MOF hydrogen interactions before they can be considered for practical hydrogen storage applications.

As an alternative, methane has huge amount preserved in underground mineral world wide.[107] It has been used as an alternative to gasoline for large-scale transportation applications. A typical nature gas composition is listed in table 6.[108] As we see, there is significant amount of CO_2 existed, which has to be removed before refinery work. Besides, nature gas was exploited at high pressure (up to 35-45 bar), which requires separation at high pressure. So, many MOFs have recently shown great potential for methane storage at desired condition.[30,43,109-112]

Table 6. A typical composition of nature gas.

Methane	CH_4	70-90%
Ethane	C_2H_6	0-20%
Propane	C_3H_8	
Butane	C_4H_{10}	
Carbon Dioxide	CO_2	0-8%
Oxygen	O_2	0-0.2%
Nitrogen	N_2	0-5%
Hydrogen sulphide	H_2S	0-5%
Rare gases	A, He, Ne, Xe	trace

2.2.1 $[Cu_3(TDPAT)(H_2O)_3]\cdot 10H_2O\cdot 5DMA$

As previously discribed in 2.1.3, **6** is a highly porous MMOFs. In additional to flue gas separation study, we evaluated its application to nature gas separation. The high pressure single component adsorption was collected up to 80 bar at ambient temperature as shown in Fig. 38 and 39. **6** shows extremely high gas uptake capacity [CO2 (excess): 310 v/v, 298 K, 48 bar; CH4 (total): 181 v/v, 298 K, 35 bar].

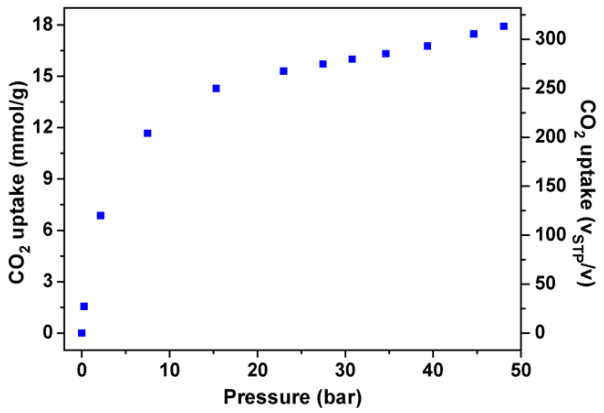

Figure 38. The high-pressure CO2 excess uptake of **6** at 298 K. Reproduced with permission from ref 98. Copyright © 2012 WILEY-VCH Verlag GmbH & Co. KGaA, Weinheim.

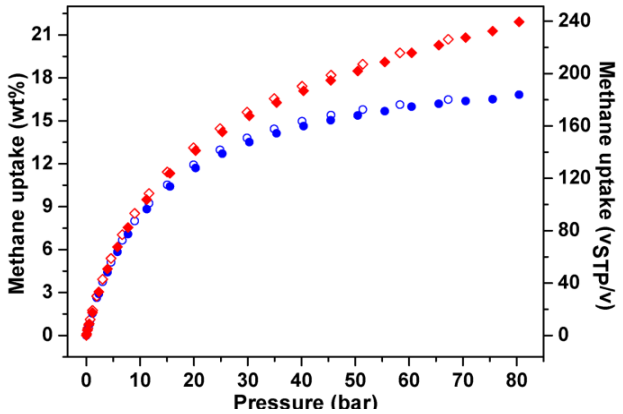

Figure 39. The high-pressure CH4 isotherms of Cu-TDPAT at 298 K (adsorption: filled; desorption: open), excess uptake (blue circles) and total uptake (red squares). Reproduced with permission from ref 98. Copyright © 2012 WILEY-VCH Verlag GmbH & Co. KGaA, Weinheim.

2.2.2 $\{[Zn_3(\mu_3\text{-}OH)(H_2O)]_4(L)(L\text{-}H_2)_2\}\cdot 45DMF\cdot 44H_2O$

$[\{[Zn_3(\mu_3\text{-}OH)(H_2O)]_4(L)(L\text{-}H_2)_2\}\cdot 45DMF\cdot 44H_2O$ (L=TBCPPM, tetrakis{3,5-bis[(4-carboxyl)phenyl]phenyl}methane) is a highly porous MMOFs with surface area of 3120m^2/g.[113] (detailed structufe description and synthesis can be found in ref 113) To evaluate the gas uptake capacity of **7**, high-pressure volumetric (excess) methane adsorption experiments were carried out on the freeze-dried sample of **7** under a pressure of up to 80 bar. As shown in Fig. 40, impressively, **7** adsorbs up to 276 mg/g of CH4 at room temperature and 80 bar without showing any saturation. With the data for the pore volume and the density of methane, the total gravimetric uptake was calculated to be 344 mg/g, corresponding to a volumetric (v/v) uptake of 329 v(STP)/v. **7** has an excess CH4 uptake of 175 mg/g (167 v(STP)/v) at room temperature and 35 bar. Both high pressure hydrogen and methane adsorption isotherms are reproducible on the same sample, indicating the stability of **7** under high pressures. The pore size of **7** (around 6 Å) is ideal for methane uptake, which is consistent with a previous

computational study that indicated an ideal pore size of 4~8 Å for methane storage.[30] These values placed 2 among the leading MOF materials for fuel gas storage applications (Table 7). **7** has the highest gravimetric and volumetric methane uptakes at 298 K and 80 bar among all the MOFs.[30,43,109,114]

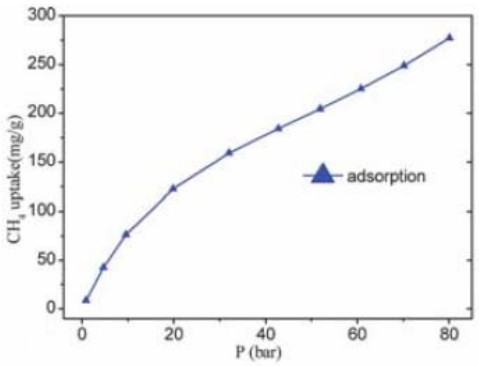

Figure 40. Excess high pressure methane sorption isotherms of **7** at 298 K. Reproduced with permission from ref 113. Copyright © 2012 Royal Society of Chemistry

Table 7. Comparison of **7** with selected MOFs with the highest gas uptake capacities

				Excess CH_4 uptake
MOF	BET surface area ($m^2 g^{-1}$)	Pore volume ($cm^3 g^{-1}$)	Pressure (bar)	@ 298 K (wt %)/ volumetric ($g L^{-1}$)
7	2718	1.46	80	27.6/189
MOF-200	4530	3.59	80	23.4/114
MOF-205	4460	2.16	80	25.8/167
MOF-210	6240	3.6	80	26.4/135
MOF-177	4526	1.59	70	N/A
NOTT-112	3800	1.62	35	N/A
NOTT-140	2620	1.07	20	15.3/105
UTSA-20	1156	0.63	15	14/123
PCN-14	1753	0.87	45	18/149
PCNP-66	4000	1.63	45	17.5/78
PCN-68	5109	2.13	50	18.6/71
NU-100	6143	2.82	70	N/A
Cu-TDPAT	1938	0.93	52	16.8/131
Mn-BTT	2100	0.795	90	N/A
SNU-77 H	3670	1.52	90	17.7/104
FJI-1	4043	1.21	62	24.5/99

Chapter 3: Commensurate adsorption of alcohol and hydrocarbons in MMOFs

3.1 Introduction

3.1.1 Background and History

Commensurate adsorption is an interesting and important phenomenon occurring during adsorption processes, where adsorbed amount and orientation of an adsorbate molecule (at equilibrium) correlate to the symmetry of the crystal and pore structure of the adsorbent.[67] Some early examples referred to adsorption of noble gas and small molecules on two-dimensional (2D) surfaces of organic substrates, such as CH_4[115-116], Kr[117-118], N_2[119], benzene[120], and Xe[121] on graphite at low temperatures. Later studies included both organic and inorganic surfaces, for example, CH_4[122] Kr[123], Xe[124], H_2[125-127], D_2[126-128], HD[126-127], CF_3Cl[129], ^4He[130-131], CO[132-133] and N_2[134-135] on graphite substrate, Xe[136-138], Kr[139], Ar[140] on Pt(111), Xe on Cu(110)[141-142], H_2 on Fe(211)[143], H_2 on Rh(311)[144], Ar on Ag(111)[145], CO on Pd(100)[146] and Ar on several surfaces of ZnO.[147] The surface structures were characterized and confirmed both experimentally and theoretically, for example by neutron diffraction, high resolution X-ray scattering, density functional theory (DFT) and molecular simulations. In the late 1980's, the concept was introduced to porous materials of three-dimensional (3D) network structures such as zeolites[148-180], where more complex interactions exist between adsorbate molecules and adsorbent systems. Commensurate adsorption (in some cases referred as freezing/locking) of hydrocarbons (e.g. *p*-xylene, *n*-hexane, *n*-heptane, benzene, etc.) was found in several

different types of zeolites, for instance, MFI, ITW, ERI, CHA, LTA, and silicalites (Table 9).[151,153,156-157,161,163-167,173-178] The observed adsorption of an integral number of adsorbate molecules that correlates with adsorbent structure was attributed to the close match of the size and/or shape of the hydrocarbon molecules to the zeolite pore features such as channel/cage size, shape, and segment length, crystal symmetry and multiplicity of special and general crystallographic positions, which determine the location and orientation of the adsorbate molecules, their packing order and level of adsorption. Accordingly, when the geometry of an adsorbate is commensurate with the pore structure or topology of a zeolite/silica adsorbent, highly ordered packing of the adsorbed molecules will result.

Table 8. Summary of commensurate adsorption of hydrocarbons in selected zeolites. Reproduced with permission from ref 67. Copyright © 2012 American Chemical Society.

Zeolite	**Crystal & Pore Features**	**Adsorbate**	**Adsorbed Amount (mo/UC, mo/cage) @ T, P***		**Note**	**Ref.**
			Experimental	**Theoretical#**		
ZSM5/ Silicalite -1, MFI type zeolite	3D framework with 2 intersecting 1D channels (window sizes: 5.4×5.6 Å (straight) and 5.1×5.5 Å (sinusoidal)). There are 4 of each intersections, straight channel segments and sinusoidal channel segments per unit cell.	*p*-Xylene	~4 mo/UC @ 343K, P/Po=0.03	8 mo/UC @ 180K	Adsorption hierarchy: intersections > sinusoidal	48-153,156-158,160-172,176,179
			7.63 mo/UC @ 313.2K, P/Po=0.048,			
		n-Hexane	7.1 mo/UC @ 363K	8 mo/UC @ 180K	Adsorption hierarchy: sinusoidal > straight	
			7.85 mo/UC @ 308.1K, P/Po=0.138,			
			~8 mo/UC @ 298K			
		n-Heptane	7.3 mo/UC @ 298K	8mo/UC @ 180K	Adsorption hierarchy: straight > sinusoidal	

		Benzene	~8 mo/UC @ 273K, 10 torr or 303K, 80 torr	8 mo/UC @ 303K	Adsorption hierarchy: intersections > sinusoidal	
		Propane	11.7 mo/UC @ 303K, 4atm	12 mo/UC @ 303K	Adsorption hierarchy: sinusoidal > straight > intersections	
		2,2-Dimethyl-butane	~4 mo/UC @ 298K	4 mo/UC @ 362K, 1atm	Only adsorbed in intersection	
ITQ-12, ITW type zeolite	3D frameworks with 2 of 1D channels (narrow window along (100), 2.4 ×5.3 Å, and wide window along (001), 3.8 × 4.1 Å).	Propene	~2 mo/UC @ 303K, 640 torr	2 mo/UC @ 303K, 640 torr	Only wide window channels are accessible to propene	54-155,159
ERI type zeolite	3D frameworks with elongated cylindrical cages of 13Å in length and 6.3 Å in diameter connected by 3.6 × 5.1 Å windows.	*n*-C7,*n*-C8, *n*-C9		1mo/cage @ 300K		173-177
CHA type zeolite	3D frameworks with ellipsoidal cage of about 10 × 6.7 Å across connected by 3.8 × 3.8 Å windows	*n*-C6-, *n*-C7, *n*-C8	<1 mo/cage	1mo/cage @ 300K		73-178,180

* mo/UC = Number of molecules per unit cell, mo/cage = Number of molecules per cage, T = Temperature, P = pressure. # Theoretical adsorbed amount was determined either from simulation or structure refinement.

3.1.2 Examples of Commensurate Adsorption of Hydrocarbons

A well-known case is the adsorption of *p*-xylene in ZSM-5 (a zeolite material crystallized in orthorhombic system with cell parameters a = 20.07, b = 19.92, c = 13.42 Å, and Si/Al = 86). The framework has a 2D pore structure containing two intersecting 1D channels (Fig. 41). The straight channels running parallel to [010] and zig-zag (sinusoidal) channels running parallel to [100] have a window size of ~5.4×5.6 Å and 5.1×5.5 Å, respectively (both defined by 10-rings).[148] Three distinct adsorption sites

(straight and zig-zag channels, and their intersections) were identified. Every unit cell contains 4 of each straight, zig-zag channel, and channel intersection sites. The adsorption isotherms showed two distinct steps at loadings of 4 and 8 *p*-xylene molecules.[148] The first four *p*-xylene molecules are located in the channel intersection sites with their methyl groups along the straight channels and the next four *p*-xylene molecules occupy the four zig-zag channel positions (giving a total number of 8 *p*-xylene molecules per unit cell). Both the crystal structure determination and simulation studies showed such arrangement is energetically most favorable.[149,169]

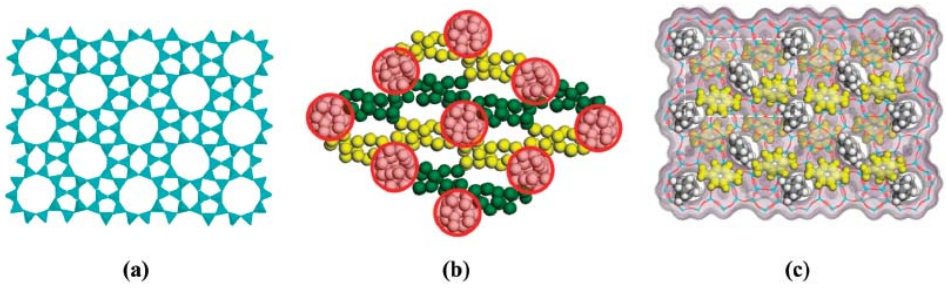

Figure 41. (left) The framework of ZSM-5 projected along the [010] direction. (middle) Simulated helium adsorption in ZSM-5 at 70 °C, viewed along the [010] direction. Helium atoms are modeled as spheres and give an outline of the channel and cross-section shapes. The red circles outline the cross section of straight channels. The two sets of the zig-zag channels running along the [100] direction are outlined by He atoms in green and yellow at different height. (right) Simulated *p*-xylene adsorption viewed along the [010] direction. Within a unit cell, the first four molecules loaded occupy the intersection sites of the straight and zig-zag channels (grey), and the second four molecules take the positions within the zig-zag channels (yellow). Color scheme: Si and Al (blue), O (red), *p*-xylene (grey and yellow) and the Connolly surface[181] (purple). The unit cell is outlined by white dotted line. Reproduced with permission from ref 67. Copyright © 2012 American Chemical Society.

A second example concerns adsorption of benzene molecules in silicalite, an aluminum-free form of ZSM-5.[153,182-183] The sorption kinetics study suggested that the initial stage of benzene adsorption took place preferentially at the channel intersections

until a critical concentration of four molecules per unit cell was reached. This absorbed amount corresponds to one molecule occupying each available channel intersection site (4 per unit cell).

Propene adsorption in ITQ-12 represents another typical example of commensurate adsorption in zeolites.[154-155] ITQ-12 is a 3D framework having 2D pore structure (Fig. 42a). The channel running along the [100] has a narrow window made of 8-member ring with a size ~2.4×5.3 Å. The channel along [001] has a more circular window aperture, ~3.8×4.1 Å. The cage between the windows has a flat shape and size that gives a good match with the molecular geometry of propene, allowing it to diffuse in and be adsorbed much more rapidly than propane. At both 30 and 80 °C, the adsorbed amount of propene corresponds to 1 molecule per cage. Illustrated in Fig. 42b is a simulated structure showing adsorbed propene molecules.

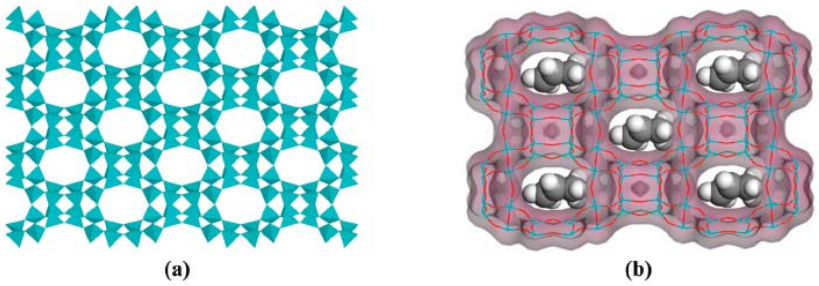

Figure 42. (left) The framework of ITQ-12 projected along the [001] direction. (right) Simulated structure showing adsorbed propene molecules in the cages with a window size of ~3.8×4.1 Å. Color scheme: Si and Al (blue), O (red), C (gray sphere), H (white sphere) and the Connolly surface[181] (purple). Reproduced with permission from ref 67. Copyright © 2012 American Chemical Society.

3.2. Hydrocarbon adsorption in MMOFs

3.2.1. Gas Adsorption and Adsorptive Separation

The past three decades have witnessed an exponential growth in research and development of crystalline microporous materials. The discovery of a new family of such materials, microporous metal organic frameworks (MMOFs), has offered emerging opportunities for revolutionizing industrial applications, in particular, separation and purification of hydrocarbons.[2-4,6-9,37,40]

MMOFs are crystalline solids with extended network structures. They are comprised of single metal cations (primary building unit or PBU) or metal clusters (secondary building unit or SBU) and organic ligands with multiple binding sites linked via coordinative bonds. As a subset of the general family of metal organic framework (MOFs, also known as coordination polymers or CPs), they possess perfectly ordered and well-defined pore structures and their pore dimensions are in the range of micropore (less than 2 nm) according to the IUPAC definition. Being a new type of adsorbent materials, MMOFs possess numerous interesting and appealing features, including but not limited to, large internal surface area and pore volume;[6-27] high gas adsorption enthalpies, often significantly higher than those found in other adsorbates characteristic of physisorption;[28,184-187] great structural flexibility;[74,99,103-105] remarkable adsorption selectivity;[37-40] and interesting sorption kinetics.[39,188] Their crystal structures (e.g. framework dimensionality, connectivity, and topology), chemical composition (e.g. the type and form of metals and ligands) and pore characteristics (e.g., pore size and shape, pore volume and the chemical functionality of

the pore walls) can be systematically and deliberately tuned to enhance targeted properties and to achieve improved performance.

The initial interests in gas adsorption on MMOF materials were largely driven by the search for appropriate structures to store small gas molecules (i.e., hydrogen, methane and carbon dioxide).[14-17,22-23,28,34,43,84-85,96,101,109-110,114,185,187,189-197] More recent efforts are geared towards selective adsorption and adsorptive separation of small gases (e.g. N_2, O_2, CH_4, H_2, CO, CO_2, NO_x, NCCl, NH_3, SO_2, and H_2S) [13,34,85,89-90,101,103,193,198-238] and various hydrocarbons.[33,38-39,45,80,154-155,186,200,216,232,239-261] Selected examples of hydrocarbon adsorption in MMOFs are given in Table 9. Adsorption based separation is one of the most important separation technologies utilized in petroleum refining industries and has been extensively developed for zeolites and related materials since the 1960s.[262-266] Adsorptive separation of a hydrocarbon mixture may be achieved via equilibrium, steric or kinetic mechanism, or combinations of these in more complex systems.[263,267] In an equilibrium process, separation is based on differences in the relative amounts of various hydrocarbon species adsorbed in the adsorbent once equilibrium is established. The process is dictated by the difference in the binding energies (i.e. isosteric heat of adsorption, Q_{st}). Separation based on steric mechanism is a consequence of shape/size exclusion or molecular sieving effect, when some adsorbate species cannot get through the pore openings while others can. The kinetic mechanism is based on the differences of the rates of adsorption and transport for different adsorbates. Hydrocarbons with substantially faster

adsorption kinetics will adsorb on an adsorbent well before those with slower kinetics.

Table 9. Summary of experimental hydrocarbon and alcohol adsorption in selected MMOFs. [33,80,88,90,240,242,244-246,248-249,251,268-269] Reproduced with permission from ref 67. Copyright © 2012 American Chemical Society.

MMOF[&]	Crystal & Pore Structure	Adsorbate	T(K)	Phase[#]	P or R.C.[%]	Experimental Adsorbed Amount	Note	Refs.
[V^{IV}O(bdc)] (MIL-47)	3D framework with 1D	*p*-Xylene (*p*X)	298	L	0.8 M	37 wt%,		[33,240, 244,246]
			343	V	0.04 bar	40 wt%,		
		o-Xylene	298	L	0.8 M	35 wt%		

	diamond shaped channels along *a* axis (window size ~7.0×5.7 Å)	(oX)	343	V	0.04 bar	37 wt%		
		m-Xylene (*m*X)	298	L	0.8 M	30 wt%	NRS^	
			343	V	0.04 bar	37 wt%		
		Ethyl-benzene (EB)	298	L	0.8 M	17 wt%	NRS	
			343	V	0.04 bar	33 wt%		
		Styrene	298	L	0.45 M	21 wt%		
		Ethane	303	V	25 bar	6.0 mo/UC		
		Propane	303	V	10 bar	4.5 mo/UC		
		Butane	303	V	10 bar	4.2 mo/UC		
		n-Octane	343	V	0.05 bar	23 wt%		
[Al^{III}(OH)(bdc)] (MIL-53-Al)	3D framework with 1D diamond shaped channels along the *a* axes (window size ~7.2×5.3 Å)	*p*-Xylene	298	L	0.55 M	43 wt%		240,242,245,251
			343	V	0.035 bar	36 wt%		
		o-Xylene	298	L	0.55 M	46 wt%		
			343	V	0.035 bar	42 wt%		
		m-Xylene	298	L	0.55 M	25 wt%	NRS	
			343	V	0.035 bar	37 wt%		
		Ethyl-benzene	298	L	0.55 M	16 wt%	NRS	
			343	V	0.035 bar	28 wt%		
		Styrene	298	L	0.45 M	24 wt%		
		Ethyl-toluene isotherms	298	L	0.55 M	Competitive adsorption	Ortho- is preferable	
		Cymene isotherms	298	L	0.55M	Competitive adsorption		
		Hexane	313	V	0.95 P/Po	2.4 molec/UC	Inflection at different pressure and different uptake	
		Heptane	313	V	0.95 P/Po	2.2 molec/UC		
		Octane	313	V	0.95 P/Po	1.5 molec/UC		
		Nonane	313	V	0.95 P/Po	1.3 molec/UC		

[Cr^{III}(OH)(bdc)] (MIL-53-Cr)	Same as MIL-53-Al	Ethane	303	V	30 bar	~0.33 cc(liquid)/g		33,88,248,251
		Propane	303	V	10 bar	~0.35 cc(liquid)/g		
		Butane	303	V	1.8 bar	~0.39 cc(liquid)/g		
		Hexane	313	V	0.95 P/Po	3.0 molec/UC		
		Heptane	313	V	0.95 P/Po	2.5 molec/UC		
		Octane	313	V	0.95 P/Po	1.8 molec/UC		
		Nonane	313	V	0.95 P/Po	1.4 molec/UC		
[Fe^{III}(OH)(bdc)] (MIL-53-Fe)	Same as MIL-53-Al	Ethane	303	V	30 bar	6.6 mmol/g	Inflection at 1.2 mmol/g	270
		Propane	303	V	10 bar	4.0 mmol/g	Inflection at 2.8 mmol/g	
		Butane	303	V	1.8 bar	3.9 mmol/g	Inflection at 2.8 mmol/g	
[Cu_2(pzdc)$_2$(dpyg)]	3D framework with 1D channel along the *a* axis (window size ~4×6 Å)	Methanol	298	V	1.0 P/Po	6.2 mmol/g	hysteresis	271
[Cu_2(pzdc)(b	3D	Methanol	298	V	1.0 P/Po	35 cc(STP)/g	hysteresis	256

pee)]	framework with 1D channel along the *c* axis (window size ~3.5×4.5 Å)	Ethanol	298	V	1.0 P/Po	Negligible		
[Cd(4-btapa)$_2$(NO$_3$)$_2$]	Two-fold Interpenetrating 3D framework with 3D zig-zag channels (window size 4.7×7.3 Å)	Methanol	298	V	0.9 P/Po	130 cc(STP)/g	hysteresis	[272]
[Ni(bpe)$_2$(N(CN)$_2$)](N(CN)$_2$)	Two-fold Interpenetrating 3D framework with 1D hexagonal channel along the *c* axis (window size 6.5×4.7	Methanol	298	V	0.9 P/Po	85 cc(STP)/g	hysteresis	[232]
		Ethanol	298	V	0.9 P/Po	32 cc(STP)/g		

	Å							
[Cu(etz)]	3D framework containing large cages (d = 9 Å) connected by small flexible hydrophobic apertures (window size, d = 1.5 Å)	Methanol	298	V	1.0 P/Po	175 mg/g		[255]
		Ethanol	298	V	1.0 P/Po	245 mg/g		
		Benzene	298	V	1.0 P/Po	200 mg/g		
		cyclo-Hexane	298	V	1.0 P/Po	negligible		
[Ce(tci)(H_2O)]	3D framework with 1D channel along a axis (window size 2.8×2.7 Å)	Methanol	298	V	0.9 P/Po	2 molec/UC		[254]
		Ethanol	298	V	0.9 P/Po	negligible		
$Ag_2[Cr_3O(OOCC_2H_5)_6(H_2O)_3]_2[\alpha$-$SiW_{12}O_{40}]$	Nonporous flexible ionic 2D layers of polyoxometalates ($[\alpha$-$SiW_{12}O_{40}]^{4-}$) and	Ethane	298	V	0.7 P/Po	~0.2 mol/mol		[253]
		Propane	298	V	0.7 P/Po	~0.2 mol/mol		
		n-Butane	298	V	0.7 P/Po	~0.2 mol/mol		
		Ethylene	298	V	0.3 P/Po	~2.0 mol/mol		
		Propylene	298	V	0.4 P/Po	~2.0 mol/mol		
		n-Butene	298	V	0.6 P/Po	~1.0 mol/mol		
		n-	298	V	0.8 P/Po	~0.2 mol/mol		

	macrocations ([$Cr_3O(OOCC_2H_5)_6(H_2O)_3$]$^+$) stacking along the *b* axis	Penetene						
		Isobutene	298	V	0.8 P/Po	~0.4 mol/mol		
		Acetylene	298	V	~0.03 P/Po	~1.2 mol/mol		
		Methyl Acetylene	298	V	0.18 P/Po	~1.7 mol/mol		
$[Zn_2(bpdc)_2(bpee)]$ ·2DMF (RPM3-Zn)	3D Framework with 1D channels along the *b*-axis (window size: ~5.1×8.8 Å)	Methanol	303	V	85 torr	126 mg/g		80,249, 268
		Ethanol	303	V	41 torr	115 mg/g		
		n-Propanol	303	V	12 torr	143 mg/g		
		n-Butanol	303	V	3.5 torr	152 mg/g		
		n-Pentanol	303	V	1.2 torr	155 mg/g		
		Benzene	303	V	74 torr	192 mg/g		
		p-Xylene	303	V	6.0 torr	124 mg/g		
		o-Xylene	303	V	3.9 torr	130 mg/g		
$[Zn_2(bpdc)_2(bpe)]$ ·2DMF (RPM4-Zn)	3D frameworks with 1D channel along the *b*-axis (window size: ~4.5×8.0 Å)	Ethanol	303	V	41 torr	82 mg/g		31,273
		n-Propanol	303	V	12 torr	126 mg/g		
		n-Butanol	303	V	3.5 torr	128 mg/g		
		n-pentanol	303	V	1.2 torr	106 mg/g		
		Benzene	303	V	74 torr	139 mg/g		
		p-Xylene	303	V	6.0 torr	125 mg/g		
		o-Xylene	303	V	3.9 torr	80 mg/g		

$Cu_4O(OH)_2(Me_2trzpba)_4$	3D framework with 3D channel system (window size: 4.5×5.5 Å along the *a*- and *b*-axes, 3.5×8.5 Å along the *c*-axis)	Methanol	298	V	0.9 P/Po	14 mmol/g		[259]
$[Cu(dhbc)_2(4,4'\text{-bpy})]\cdot H_2O$	2D framework with 1D channels along the *a*-axis (pore size: 2.9×4.8 Å and 4.7×2.5 Å)	Benzene	313	V	61 torr	202 mg/g		[67]
		Toluene	313	V	17.6 torr	153 mg/g		
		p-Xylene	313	V	5.1 torr	55 mg/g		
		Propane	303	V	664 torr	39 mg/g		
		n-butane	303	V	640 torr	43 mg/g		
		n-Pentane	303	V	352 torr	49 mg/g		
		n-Hexane	303	V	100 torr	54 mg/g		
$[Mn_3(fa)_6]$	3D framework with 1D zig-zag channels	Acetylene	196	V	1 bar	68.2 cc(STP)/g		[274]
			275	V	1 bar	57.7 cc(STP)/g		
			298	V	1 bar	51.2		

						cc(STP)/g		
$[Mg_3(fa)_6]$	3D framework with 1D zig-zag channels	Acetylene	196	V	1 bar	72.5 cc(STP)/g		274
			275	V	1 bar	69.4 cc(STP)/g		
			298	V	1 bar	65.7 cc(STP)/g		
$[Zn_2(bptc)]$	Two types of interconnecting pores with openings of 3.9 × 5.1 Å and 3.9 × 5.2 Å	Ether	298	V	1 P/Po	13 wt%		257
		Methanol	298	V	1 P/Po	10 wt%		
		Benzene	298	V	1 P/Po	9 wt%		
		Toluene	298	V	1 P/Po	13 wt%		
		n-Pentane	298	V	1 P/Po	7 wt%		
		n-Hexane	298	V	1 P/Po	8.5 wt%		
$[Cu(gla)(4,4'\text{-bipy})_{0.5}]$	1D hydrophobic elliptical channels of window size 3.3×5.1 A	Methanol	298	V	0.96 P/Po	2.1 mmol/g		209
$[Al_{12}O(OH)_{18}(H_2O)_3(Al_2(OH)_4)(btc)_6]\cdot 24H_2O$ (MIL-96)	Three types of cages, of which two are accessible with small window opening of ~5 Å after	*trans*-Piperylene	298	L	0.65 M	12 wt%		205,241
		trans-1,3-Hexadiene	298	L		<1 wt%	Length exclusion	
		cis-Piperylene	298	L	0.35 M	0.6 molec/Cage (A/B)	Steric constraint	
		Isoprene	298	L	0.35 M	0.5	Steric constraint	

	removal of water molecules					molec/Cage (A/B)		
$[Cu_2(pzdc)_2(pyz)]\cdot 2H_2O$	3D framework consisting of 1D channels with window size of 4×6Å	Acetylene	270 300 310	V	1 bar	42 cc(STP)/g		[191]
$[Zn_2(bdc)_2(dabco)]\cdot 4DMF\cdot 0.5H_2O$	Tetragonal 3D framework having two 1D interconnected channels (pore apertures ~7.5×7.5 Å and 3.2×4.8 Å)	Methanol	298	V	0.42 P/Po	5.02 mg/g		[90,269]
		Ethanol	298	V	0.42 P/Po	418 mg/g		
		Isopropanol	308	V	0.9 P/Po	160 cc(STP)/g	Inflection at 3mo/UC	
$[Zn(bim)_2]$ (ZIF-7)	Sodalite topology with a window opening of ~3 Å	Propane, propene, ethane, ethene	298	V	1 bar	4 mo/cage	Quick loading of 3mo/UC	[275]
[Zn(tbip)]	3D frameworks with 1D	Methanol	298	V	90 torr	110 mg/g		[38]
		Dimethyl-	303	V	650 torr	30 mg/g		

	channel along the *c*-axis (window size: 4.5 Å)	ether (DME)						
[Cu(hfipbb)(H_2hfipbb)$_{0.5}$]	3D frameworks with 1D straight channel along the *b*-axis (window size: 3.2Å)	Methane	298	V	760 torr	0.39 wt%		39,249
		Ethane	298	V	760 torr	1.2 wt%		
		Propane	298	V	0.063 P/Po	2.6 wt%		
		Propene	298	V	0.019 P/Po	2.0 Wt%		
		n-Butane	298	V	0.33 P/Po	4.0 wt%		
		Methanol	298	V	0.6 P/Po	2.0 wt%		
[Co_3(fa)$_6$]	1D zig-zag channel along the *b*-axis (window size: 4.5Å)	Methane	303	V	684 torr	14 mg/g		200,27 4,276-278
		Ethane	303	V	684 torr	64 mg/g		
		Propane	303	V	684 torr	91 mg/g		
		Propene	303	V	684 torr	87 mg/g		
		n-Butane	303	V	684 torr	124 mg/g		
		n-Pentane	303	V	353 torr	94 mg/g		
		n-Hexane	303	V	100 torr	102 mg/g		
		n-Heptane	303	V	28 torr	110 mg/g		
		Methanol	303	V	85 torr	99 mg/g		
		Ethanol	303	V	41 torr	106 mg/g		
		n-Propanol	303	V	12 torr	143 mg/g		
		n-Butanol	303	V	3.5 torr	168 mg/g		
		n-Pentanol	303	V	1.2 torr	108 mg/g		
		Benzene	303	V	74 torr	174 mg/g		
		Toluene	303	V	18 torr	148 mg/g		

		p-Xylene	303	V	6.0 torr	48 mg/g		
		Ethylbenzene	303	V	5.8 torr	130 mg/g		

[&] bdc = 1,4-benzenedicarboxylate, pzdc = pyrazine-2,3-dicarboxylate, dpyg = 1,2-di(4-pyridyl)glycol, 4-btapa = 1,3,5-benzene tricarboxylic acid tris[N-(4-pyridyl)amide], bpee = 1,2-bis(4-pyridyl)ethane, bpe = 1,2-bis(4-pyridyl)ethane, dhbc=2,5-dihydroxybenzoic acid, Me_2trzpba=4-(3,5-dimenthyl-4H-1,2,4-triazol-4-yl)benzoate, etz = 3,5-diethyl-1,2,4-triazolate, tci = 3,3′,3″-(2,4,6-trioxo-1,3,5-triazinane-1,3,5-triyl)tripropionate, fa = formate, bptc = 4,4′-bipyridine-2,6,2′,6′-tetracarboxylate, gla = glutarate, 4,4′-bipy = 4,4′-bipyridine, btc = 1,3,5-benzenetricarboxylate, pyz = pyrazine, dabco = 1,4-diazabicyclo[2.2.2]-octane, bim = benzimidazole , H_2hfipbb = 4,4′-(hexafluoroisopropylidene)bis(benzoic acid), tbip = 5-*tert*-butylisophthalicate, bpdc = 4,4′-biphenyldicarboxylate. [#] L = Liquid phase adsorption, V = Vapor phase adsorption. [%] For vapor phase adsorption, the pressure (P) is used. For liquid phase adsorption, R. C. = relative concentration of adsorbate in a non-interacting solvent, in unit of mol/L (M). ^ NRS = Not Reaching Saturation.

3.2.2. Selective Adsorption of Hydrocarbons in MMOFs

Recent reports focusing on the adsorption behavior of hydrocarbons in MMOF structures have provided numerous examples where selective adsorption and sorptive separation may be achieved via one or combination of the aforementioned mechanisms.

Among possible olefin/paraffin separation via equilibrium-based adsorption processes,[240-241,243,262,279-280] preferential adsorption of styrene (also known as vinyl benzene, VB) over ethylbenzene (EB) in MIL-53-Al serves a good example.[240] The crystal structure of MIL-53-Al[281] is very similar to that of MIL-47.[282] Both are built on octahedral metal vertices of V^{IV} (MIL-47) and Al^{III} (MIL-53-Al) interconnected by bdc linkers. Both contain 1D channels of diamond-shaped cross-section, but they are more rigid in MIL-47 than in MIL-53-Al.[251] Liquid-phase competitive adsorption experiments using heptane as non-interacting solvent were carried out at room temperature (298 K).[240] Both compounds displayed preferred adsorption of VB over EB. A comparison of apparent adsorption enthalpies of the two showed that they are comparable in MIL-47, but significantly different in MIL-53-Al. The values are -9.0 kJ/mol (VB) and -10.1 kJ/mol (EB) for MIL-47,

and -24.2 kJ/mol (VB) and -13.1 kJ/mol (EB) for MIL-53-Al, respectively. The enthalpy loss of EB in MIL-53-Al was attributed to the structure distortion induced by EB which took place only in the more flexible framework of MIL-53-Al. The same trend was found from vapor-phase adsorption experiments where adsorption enthalpies obtained at low-loading were consistent with the liquid-phase data (-59.1 and -48.9 kJ/mol for VB and EB, respectively). The selective adsorption of dimethylether (DME) over methanol in Zn(tbip) represents another interesting example of sorptive separation based on equilibrium mechanism. [Zn(tbip)] is a guest-free MMOF featuring 1D microchannels[38]. Tetrahedral zinc metal centers (as PBU) are linked by tbip ligands to yield a 3D framework containing hexagonal close-packed 1D open channels of a small window diameter (~4.5 Å, excluding the van der Waals radius of hydrogen). The phenyl rings of the tbip ligands that form the channel walls are oriented in such a way that all tert-butyl groups protrude into the channels, making the material highly hydrophobic and essentially absorbs no water (< ~1 mg/g at room temperature and $P/P^o = 0.65$). The DME adsorption shows a typical Type-I profile while no MeOH adsorption occurs until a pressure threshold is reached, at which point, capillary condensation takes place. The pressure threshold increases as a function of temperature. Thus, Zn(tbip) exhibits potential for the separation of DME from MeOH. For example, facile separation of DME can be performed by selective adsorption at a given T and P that is below the MeOH capillary condensation point. Clearly, such a process is based on the difference in the adsorbate-adsorbent interactions. The isosteric heats of DME adsorption computed from

adsorption isotherms at Q = 10 mg/g loading is 51 kJ/mol, is much higher than that of MeOH when adsorbate-adsorbate contribution is excluded.

Industrial separation of C2-C4 olefins from paraffins is one of the most energy- and cost-intensive distillation-based technologies.[283-284] Our recent studies reveal that kinetic separation of propane ($C_3°$) and propene ($C_3^=$) by metal-imidazolate zeolitic framework (ZIF) materials is highly feasible as a result of the remarkable differences in their diffusion rates through the pores.[45] Under equilibrium conditions, [Zn(2-mim)$_2$] (ZIF-8, 2-mim = methylimidazole)[285-286] adsorbs essentially the same amount of $C_3°$ and $C_3^=$, 155 and 160 mg/g at 30 °C and 600 torr, respectively. Additionally, their isosteric heats at low loading are 34 and 30 kJ/mol, respectively, indicative of similar adsorbate-adsorbent interactions for the two systems. While thermodynamic separation is impractical for this particular case, striking difference in the adsorption rates was noticed. At 30 °C, the ratio of their diffusion rate coefficients, $D(C_3°)/D(C_3^=)$, is 125, suggesting a high possibility in kinetic separation of these two very similar molecules. Of course, for a more rigorous treatment of diffusion control in a separation process the measurement of counter-diffusivities is required.[90,287] It should be mentioned that in this case, although the size difference is minimal (0.2-0.3 Å) for the two molecules,[288] the energy barriers can be very different. The activation energies of propene and propane to pass through the pore openings are calculated to be 9.7 and 74.1 kJ/mol, respectively, for [Zn(2-cim)$_2$] (2-cim = 2-chloroimidazole). The very large variation in their activation energies for diffusion is clearly the main reason for the remarkable difference in their diffusion rates. The effective size of the pore opening is believed to be the dominating

factor for the separation capability in a number of previously reported systems, including several crystallographic 8-membered ring (8MR) zeolites, where separation was controlled critically by the window size of the cages,[154-155,289-294] although the window flexibility effects observed in zeolites may sometimes be quite different from those found in MMOFs.[287,295] In addition, $[Cu_3(btc)_2]$[296] and MIL-100 (Fe)[297] also show capability for separation of propane and propene via preferential adsorption of propene. Separation of ethane and ethene may be achieved using ZIF-8 membrane.[298]

A case where dual-effects on the sorptive separation of three hexane isomers, *n*-hexane (nHEX), 3-methylpentane (3MP) and 2,2-dimethylbutane (22DMB), in $Zn(bdc)(ted)_{0.5}$ have been discussed in several recent experimental and simulation studies[239,278,299]. $Zn(bdc)(ted)_{0.5}$ is a 3D framework structure composed of three intersecting channels.[12,90] Two types of intersecting 1D channels exist in this tetragonal crystal system. The large channel runs along the *a*-axis with a cross section of ~ 7.5 × 7.5 Å. The two smaller and identical channels are parallel to the *b*- and *c*-axis (cross section: ~ 3.8 × 4.7 Å). While all three hexane isomers can be adsorbed in the larger channel, the smaller channels can only take up linear nHEX (having smaller kinetic diameter) and exclude branched 3MP and 22DMB, due to size exclusion (steric effect). The nHEX also interact more strongly with the framework than the other two isomers (equilibrium effect). As a result, $Zn(bdc)(ted)_{0.5}$ adsorbs a significantly larger amount of nHEX than those of 3MP and 22DMB. Separation of nHEX from 3MP and 22DMB could be achieved by fixed-bed adsorption as indicated in binary breakthrough curves.[239]

Numerous MMOFs are found to be capable for separating hydrocarbons based on steric effect. MIL-96, with a formula of $Al_{12}O(OH)_{18}(H_2O)_3(Al_2(OH)_4)[btc]_6 \cdot 24H_2O$ (btc = 1,3,5-benzenetricarboxylate), was first reported in 2006.[205] It has three types of cages, among which only two (A- and B-type) are accessible after removal of water molecules by thermal activation. Both have small window size of ~5 Å. The compound adsorbs a large amount of *trans*-piperylene (or *trans*-1,3-pentadiene, ~12 wt%), but significantly less of both *cis*- piperylene and isoprene (3-4 wt%).[241] While all three hydrocarbons are C5 diolefins with similar zero-coverage adsorption enthalpies (-52.1, -53.0 and -54.6 kJ/mol for isoprene, *cis*- and *trans*-piperylene, respectively), the geometry of *trans*-piperylene allows a much better fit of this C5 isomer to the shape and size of the pores, resulting in packing of multiple molecules within a single cage. This is not possible for the other two C5 species. Similarly, C6 diolefins such as *trans*-1,3-hexadiene is only one $-CH_3$ longer than *trans*-piperylene, but its uptake is negligibly small (< 1 wt%), as a result of length exclusion. The separation between the C5 isomers (e.g. trans- and cis-piperylene) or between C5 and C6 diolefins (e.g. *trans*-1,3-pentene and *trans*-1,3-hexadiene) can thus be regarded as a steric-based mechanism. [Cu(hfipbb)(H_2hfipbb)$_{0.5}$], a 3D structure containing segmented channels of small pore diameter, has demonstrated strong capability of separating short-chain normal hydrocarbons (C4 or less) from all branched and all long-chain normal hydrocarbons (> C4) via a size exclusion effect.[39] This unusual behavior is due to the shape of the MOF pore structure: the straight 1D channel is composed of a periodic array of cages (~ 5.1 × 5.1 Å) with small neck (~ 3.2 × 3.2 Å) at a length of ~ 7.3 Å. This length is just greater than that of *n*-C4 (~ 6.4 Å) and just

smaller than that of *n*-C_5 (~ 7.7 Å). Thus, normal paraffins and olefins of C4 and shorter chains can fit in the cage while those of normal C5 or longer chains cannot. Although the neck is large enough to allow passage of the latter group, it is too small for this region to be an equilibrium position for them. On the other hand, all branched paraffins and olefins are excluded from entering the channels. To the best of our knowledge, all zeolites that adsorb *n*-C4 also take up normal hydrocarbons of longer chains, and do not show such adsorption selectivity with a cut-off in carbon numbers.

3.2.3. Adsorption: Methods and Characterization

3.2.3.1. Experimental Methods

One of the most important and commonly adopted experimental methods for characterization of an adsorption process is the measurement of gas adsorption isotherms at a fixed temperature.[300-304] Gas adsorption isotherms, namely the adsorbed amount as a function of pressure can be obtained by volumetric or gravimetric method, carrier gas and calorimetric techniques, nuclear resonance as well as by a combination of calorimetric and impedance spectroscopic measurements.[300-303] Among these, the most frequently used are the volumetric (manometric) and gravimetric methods. The gravimetric method is based on a sensitive microbalance and a pressure gauge. The adsorbed amount can be measured directly, but a pressure dependent buoyancy correction is necessary. The gravimetric method is very accurate and convenient to use for the adsorption measurements not too far from room temperature. The adsorbent is not in direct contact with the thermostat and it is thus more difficult to control and

measure the exact temperature of the adsorbent at both high and cryogenic temperatures. Therefore, the volumetric method is recommended to measure the adsorption of nitrogen, argon and krypton at the temperatures of liquid nitrogen (77.35 K) and argon (87.27 K)[304]. The volumetric method is based on calibrated volumes and pressure measurements by applying the general gas equation. The adsorbed amount is calculated by determining the difference of the total amount of gas admitted to the sample cell with the adsorbent and the amount of gas in the free space. Hence, the void volume needs to be known very accurately. One way to determine this is to introduce a non-adsorbing gas such as helium prior to (or after) every analysis in order to measure the void (free space) volumes at room temperature and at the temperature at which the adsorption experiment is performed. The helium void volume measurement procedure is based on various assumptions: (i) Helium is not adsorbed on the adsorbent; (ii) Helium does not penetrate into regions which are inaccessible for the adsorptive (e.g., nitrogen). However, these pre-requisites are not always fulfilled – in particular in the cases of microporous adsorbents. The use of helium can be avoided if the measurement of the void volume can be separated from the adsorption measurement by applying the so-called NOVA (NO Void Analysis) concept (see ref. 292, chapter 14). Further, the determination of the void volume can be completely avoided by using difference measurements, that is, an apparatus consisting of identical reference and sample cells, and the pressure difference being monitored by a differential pressure transducer. Correction for non-ideality of the adsorptive in the cold zone also needs to be applied. Another complication is that for gas pressures below ca. 80-100 millitorr (i.e., $P/Po < 10^{-4}$

for nitrogen and argon adsorption at 77 K and 87 K, respectively) pressure differences along the capillary of the sample bulb on account of the Knudsen effect need to be taken into account (i.e., thermal transpiration correction).

Many hydrocarbons are in liquid phase at room temperature and ambient pressure. For adsorption isotherm measurements of these molecules under ambient conditions, a special design of vapor bubbler can be used to generate vapor of hydrocarbons from its liquid phase. In such cases, the temperature at which vapor is being generated is controlled to be below the room temperature in order to avoid condensation in the pipe line during transportation of hydrocarbon vapors. The vapor pressure is controlled by a mass flow controller, ranging from 0~0.9 P/Po with the aid of nitrogen gas.[38-39,45,80,90,150,155,200,249,268,305]

Alternatively, adsorption of hydrocarbons in liquid phase can be measured using gas chromatography (GC).[240-241,243-246,306-307] A solvent that is incapable of being adsorbed and has no competitive effect with the adsorbate is selected as a carrier. The desired adsorbate concentration can be achieved by mixing appropriate amount of the solvent and adsorbate, in the same manner as the pressure control in the vapor phase adsorption. It is interesting to compare isotherms obtained by vapor- and liquid-phase adsorption.[242,244-246] Comparable level of adsorption can be achieved in both cases for a given range of temperature, pressure or relative concentration (R.C.), whereas the adsorption strength may vary. For example, the adsorption strength of C8 aromatics on MIL-47 is in the descending order of *p*-xylene, *o*-xylene, *m*-xylene and ethylbenzene based on liquid-phase adsorption data at 298 K,[246] which is consistent with those of

vapor-phase adsorption at 343 K.[244] However, such order changes at higher temperature. The adsorption strength of *p*-xylene in vapor phase decreases much faster than other isomers and becomes weaker than *o*-xylene and even *m*-xylene as temperature rises. As thermal energy increases along with increasing temperature, *p*-xylene as the longest isomer will have the most difficult time to achieve a dense and efficient packing at low pressure regime. Effectively packing and an ordered state may be reached only when pressure is sufficiently high.

Another method, gas adsorption microcalorimetry, has recently been developed and reported for several zeolite and related microporous materials.[308] This technique can provide information on the surface state of an adsorbate, adsorption enthalpy, phase transition during an adsorption process, and adsorption mechanisms. Specifically, isotherms and adsorption enthalpy of various adsorbates can be obtained simultaneously at low temperature (77 K) and room temperature using a volumetric apparatus coupled with a Tian-Calvet type microcalorimeter. This method is currently being successfully applied to a number of MOF materials.[33,88,309-310] For example, hydrogen and alkane adsorption behavior in MIL-47(V) and MIL-53(Cr) as well as their interaction energies have been fully characterized.[33,88,309]

Diffusion studies of hydrocarbons in microporous MOF materials represent another new topic in adsorption related research. Transport properties of guest molecules are investigated by measuring their transport diffusivity and surface permeability employing state-of-the-art and high temporal and spatial resolution IR micro-imaging and interference (IF) microscopy.[311] For example, the diffusion behaviors

of selected paraffins (e.g. ethane, propane, and n-butane) in Zn(tbip) have been analyzed in depth. Direct measurements of surface and transport resistances are made possible by these two techniques.[312-316]

3.2.3.2. Modeling and Simulations

Atomic and molecular level modeling and simulations provide essential tools to complement experimental methods to explain the adsorption associated phenomena, to help understand the principle of adsorption and to provide insight and guidelines for future experiments.[187,317-318] Grand canonical Monte Carlo (GCMC) simulation is the most extensively used method for calculation of equilibrium adsorption isotherms and isosteric heats of adsorption. The conventional Monte Carlo method works very well for noble gases and small molecules, but is insufficient for long chain hydrocarbons.[164,319-323] The configurational-bias Monte Carlo (CBMC) method has subsequently been developed to deal with long chain molecules.[324] The original CBMC technique was developed for lattice models[325-326] and later extended to continuous models.[327] The method has been successfully used in simulating long chain, branched and cyclic hydrocarbon adsorption in zeolites.[159,164,328-359]

The many unique and useful gas adsorption properties of microporous MOFs have prompted intense investigations not only by the experimentalists but also by theorists. Molecular simulation studies have been performed on a large number of systems with a variety of different structures. The computational studies are powerful and often complementary to the experiments.[187,190,195,278,299,360-365] Methane adsorption in IRMOF-1[190], one of most extensively investigated MOFs, illustrates a good example. The

simulated CH4 adsorption isotherm at 298 K and up to 40 atm matches almost perfectly with the experimental data over the entire pressure range, revealing that simulation can be a powerful tool to assess and predict the adsorption behavior and capacity of MMOFs, and to quantify adsorption energy and guest-host interactions. More recent simulation work on the adsorption of n-alkanes in Co3(fa)6 serves another excellent case.[278] Isotherms of C3 through C8 alkanes are simulated employing the CBMC method and molecular self-diffusivities are computed via molecular dynamics (MD) simulation. The simulation study not only confirms the experimentally observed commensurate-incommensurate adsorption phenomena but also offers helpful explanations and insight to such observations. The calculations show that for these alkane species, the chain length, which correlates with the commensurate-incommensurate behavior of the molecules, plays a key role in their non-monotonic behavior in Henry coefficients and self-diffusivities.

In this work, we have included numerous simulation results using Cerius2 Sorption software (Accelrys, Inc.). This program module employs GCMC method and Burchard Universal Force Field.[366] In a typical calculation, a box of 35~40 Å in each dimension is selected, which usually consists of multiple unit cell length along each crystallographic axis. Periodic boundary conditions are applied in all three dimensions. Usually $n\times10^7$ (n = 1-3) configurations are selected for a single simulation, depending on the energy convergence. Helium adsorption is simulated at a temperature of 1 K and pressure of 1 kPa. Simulations on hydrocarbon gas adsorbates are generally carried out under the same conditions used in experiments to mimic real-world conditions.

3.2.3.3. Physical Properties of Adsorbates

Physical properties of adsorbates are an important aspect regarding commensurate adsorption. The adsorption behavior and mechanism are largely affected by the type and degree of adsorbate-adsorbent interactions, for which the molecular composition, shape and size, polarity, polarizability, diffusivity and other properties of the adsorbate all play a dominant role.

The molecular models of selected hydrocarbons are built and their energies are optimized by Visualizer module (Matarial Studio 4.4, Accelrys Software Inc.). The optimized molecular structures are exported to Crystal Maker program (Version 6.1 for Mac OS, Crystal Maker Software Ltd.) from which physical dimensions of the molecules are determined. The size of each molecule is measured by its molecular length and the cross section, defined in Fig. 43. Covalent radii (from built-in database of Material Studio 4.4) of the outmost atoms are added to both the length and diameter values. The saturated vapor pressure of hydrocarbons is calculated from Antoine equation if the data are not directly available from the NIST chemistry web book on thermophysical properties of fluid systems:

$$\mathrm{Log}_{10}P = \mathrm{A}\text{-}\mathrm{B}/(\mathrm{C}+T)$$

Where P is the vapor pressure of a hydrocarbon at given temperature T, and A, B and C are component-specific constants.

Relevant physical properties of hydrocarbon adsorbates are tabulated in Table 10, including the physical dimensions (length and diameter), kinetic diameter, critical temperature and vapor pressure. The length of an adsorbate, L1, is defined to be the

longest dimension of the molecule and is the distance between the centers of the two outmost atoms projected onto the *z*-axis, taken as molecular axis. (Fig. 43a, c). The diameter of the molecule, D1, is taken to be the distance between the centers of the two outmost atoms projected onto the *xy* plane (Fig. 43b, d).

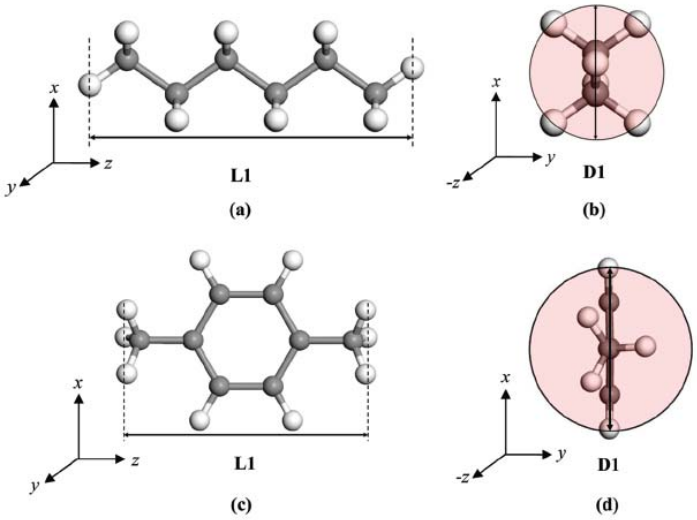

Figure 43. Illustration of molecular dimensions in the Cartesian coordinate system (*x*, *y*, *z*). L1 is along the *z*-axis and D1 is in the *xy* plane. (a)-(b) *n*-Haxane, and (c)-(d) *p*-xylene. Color scheme: C (grey), H (white). Reproduced with permission from ref 67. Copyright © 2012 American Chemical Society.

Table 10. Physical properties of hydrocarbon adsorbates.[367-377] Reproduced with permission from ref 67. Copyright © 2012 American Chemical Society.

		size (Å)[a]						vapor pressure (Torr)[b]		
		length		diameter						
	adsorbate	L1	L2	D1	D2	kinetic diameter (Å @298 K)	critical temp (K)	291 K[c]	298 K	303 K
paraffins and olefins	methane	1.9	2.6	2.1	2.8	3.8	190	N/A	N/A	N/A
	ethane	3.2	3.9	2.9	3.6	4.443	305	27049.0	31441.0	32369.9
	acetylene	3.5	4.2	0.0	0.7	3.3	308	31412.2	36864.2	41147.0
	propane	4.4	5.1	2.9	3.6	4.3−5.1	370	6115.4	7327.8	34904.0
	1-propene	4.2	4.9	3.3	4.0	4.7	365	7263.9	8687.0	9813.7
	n-butane	5.6	6.4	2.9	3.6	4.7	425	1459.5	1821.2	2119.8
	n-pentane	6.9	7.7	2.9	3.6	4.5	470	392.4	512.5	614.9
	n-hexane	8.2	8.9	2.9	3.6	4.3	508	110.7	151.3	187.1
	n-heptane	9.5	10.2	2.9	3.6	N/A	540	31.2	45.1	58.0
	n-octane	10.8	11.5	2.9	3.6	N/A	569	8.5	12.9	17.2
	n-nonane	12.1	12.8	2.9	3.6	N/A	594	2.3	3.4	4.6
	trans-butene	5.3	6.0	3.3	4.0	N/A	429	1401.5	1759.3	2054.8
	cis-butene	4.7	5.5	3.2	3.9	4.2	436	1271.0	1602.1	1876.2
	2-methylpropane	4.4	5.1	3.9	4.6	5.3	408	2133.3	2630.9	3035.8
	2-methylbutane	5.6	6.4	3.9	4.6	5	460	534.2	688.0	823.1
	3-methylpentane	6.9	7.7	3.9	4.6	5.5	504	140.6	189.8	232.9
	2,2′-dimethylpropane	4.4	5.1	5.2	5.9	6.2−6.6	434	1022.1	1285.8	1503.8
	trans-piperylene	7.1	7.9	3.3	4.0	N/A	∼484	182.4	200.9	215.1
	cis-piperylene	6.1	6.9	3.2	3.9	N/A	∼484	166.1	183.2	196.4
	isoprene	6.0	6.7	4.5	5.2	N/A	∼484	253.1	277.6	296.3
	trans-1,3-hexadiene hexadiene	8.4	9.1	3.3	4.0	N/A	527	N/A	N/A	N/A
	2,2′-dimethylbutane	5.6	6.4	5.2	5.9	6.2	489	241.9	319.1	385.4
aromatics	cyclohexane	5.1	5.8	4.4	5.1	6.0−6.2	554	70.5	97.6	121.7
	benzene	5.1	5.8	4.4	5.1	5.3−5.9	562	68.2	95.1	119.2
	toluene	5.8	6.6	4.4	5.1	5.3	592	19.6	28.5	36.7
	p-xylene	6.7	7.4	4.4	5.1	5.8	610	5.8	8.9	11.7
	o-xylene	5.8	6.6	5.5	6.3	6.8	630	4.3	6.6	8.8
	m-xylene	6.6	7.3	5.2	5.1	6.8	617	5.5	8.3	11.1
	styrene	7.6	8.4	4.4	5.1	N/A	646	37.7	51.6	64.0
	ethylbenzene	7.1	7.9	4.4	5.1	5.8	617	6.3	9.5	12.6
alcohols	methanol	3.3	4.1	2.1	2.8	3.6	513	87.4	127.1	164.0
	ethanol	4.3	5.1	2.9	3.6	4.5	514	38.9	59.0	78.5
	n-propanol	5.6	6.3	2.9	3.6	4.7	537	13.3	21.1	29.0
	n-butanol	6.8	7.6	2.9	3.6	5.0	553	3.9	6.7	9.6
	n-pentanol	8.1	8.8	2.9	3.6	6.7	582	1.3	2.3	3.5
	n-hexanol	9.3	10.1	2.9	3.6	6.2	610	0.5	0.8	1.2
others	dimethylether	4.3	5.1	2.2	2.9	4.3	467	3534.7	4349.0	5010.5

[a] L1 = longest dimension of the molecule and is the distance between the centers of the two outmost atoms projected onto the *z*-axis, taken as molecular axis (Figure 3a,c), L2 = L1 + covalent radii of the two outmost atoms. D1 = distance between the centers of the two outmost atoms projected onto the *xy* plane (Figure 3b, d), D2 = D1 + covalent radii of the two outmost atoms. [b] The saturated vapor pressure of hydrocarbons [calculated from Antoine equation as described above: $\log_{10}P = A - B/(C + T)$]. [c] 291 K is the temperature typically used to activate vapor from liquid hydrocarbons in our experiments.

3.3. Commensurate adsorption of hydrocarbon and alcohol in MMOFs

3.3.1. Crystal and Pore Structures

Commensurate adsorption of hydrocarbons has been reported only in a few zeolite structure types. Most adsorption occurs incommensurately, meaning adsorbate molecules are randomly distributed in the pores. This is most likely due to the following two reasons: (a) the dimensions of the cages or channels in zeolite frameworks are generally much larger than the adsorbate molecules, and (b) the topology and symmetry of the cavities/pores do not correlate well to the shape and geometry of the adsorbate molecules. Adsorption of benzene and toluene in zeolite-Y serves a good example to illustrate these points.[378-385] A random packing of 5 benzene molecules and 3 toluene molecules in a single supercage is shown in Fig. 44a and 44b, respectively.[378,385]

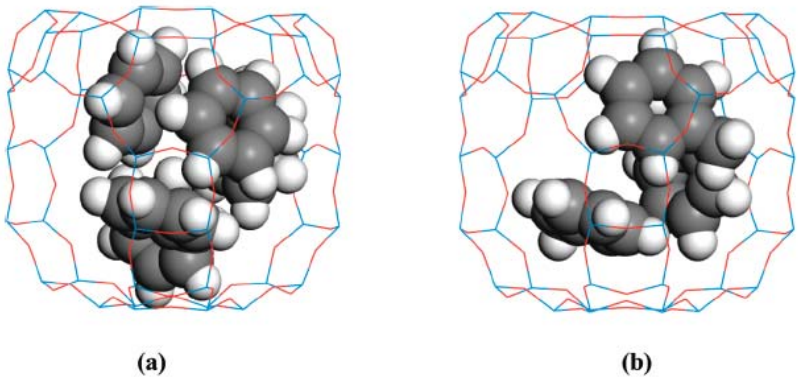

Figure 44. Random packing of (a) benzene and (b) toluene in a single supercage of zeolite-Y. Color scheme: Si (blue), O (red), C (gray sphere), H (white sphere). Reproduced with permission from ref 67. Copyright © 2012 American Chemical Society.

Unlike zeolites, commensurate adsorption is much more commonly occurred in metal organic frameworks in the vicinity of room temperature,[249,386] especially in ultramicroporous structures (a sub-family of MMOFs with pore diameters less than 7 Å)

or in supermicroporous structures (a sub-family of MMOFs having pore diameters between 7 and 20 Å) with small pore window size.[185,200] In addition to small pores or windows, their pore structures usually possess a rich hierarchy of complexity, as a result of a vast variety of framework types and broad range of surface functionalization. Among numerous MMOFs for which commensurate hydrocarbon adsorptions have been observed, a majority have 1D open channel structures built on cavities (segment) with distinct shapes. For example, $[M_3(fa)_6]\cdot DMF$ (M = Mn, Co, Ni) crystallize in a monoclinic crystal system in which the metal network has a diamondoid connectivity. The overall framework gives rise to a 1D zig-zag channel system proceeding along the *b* axis.[200] The diameters of the cage and window of the "zig" or "zag" segment are 5.5 and 4.5 Å, respectively with a repeating length of 7.1 Å. Both $[M_3(bpdc)_3(bpy)]\cdot 4DMF\cdot H_2O$ (M = Co, Zn)[185,305] and $[Cu(hfipbb)(H_2hfipbb)_{0.5}]$[39] are characterized as 1D pore systems having straight channels. In the former, these channels are composed of alternating large diameter cages (~ 10.6×10.6×5 Å, calculated based on van der Waals radius of carbon) and smaller windows (triangular in shape with an effective maximum dimension of ~ 8 Å), while in the latter, the 1D channels consist of oval-shaped cages (~ 5.1 Å in diameter) at ~ 7.3 Å interval connected by narrow windows of ~ 3.2 Å in diameter. A brief description of pore structures (e.g. type of channels and pores, shape and dimensions of channel/pore segments) for selected compounds are presented in Table 11.

Table 11. Summary of pore structures of selected MMOFs exhibiting commensurate hydrocarbon adsorption. Reproduced with permission from ref 67. Copyright © 2012 American Chemical Society.

MMOFs[&]	Pore structure	No. Segment/UC	Segment Dimension (Å)[@]	Refs.

$[M_3(fa)_6]$·sol (M = Mg, Mn, Co, Ni, sol = solvent)	1D zig-zag channel along the *b*-axis	4	Cage diameter: 5.5 Window size: 4.5 Length: 7.1*	200,274,276-277
[Cu(hfipbb)(H_2hfipbb)$_{0.5}$]	1D straight channel along the *b*-axis	2	Cage diameter: 5.1 Window size: 3.2 Length: 7.3	39
$[Cu_2(pzdc)_2(pyz)]$·2 H_2O	1D straight channel along the *a*-axis	2	Channel cross-section: 4.0×6.0 Length: ~4.7	387-388
$[Al_{12}O(OH)_{18}(H_2O)_3$ $(Al_2(OH)_4)(btc)_6]$·24 H_2O (MIL-96)	Two types of cages (Pore A and Pore B)	2 for A 2 for B	Pore A: Cage diameter: ~8.8 Window size: 4.5-5.5 Length: 8.9* Pore B: Cage diameter: ~8.8 Window size: 4.5-5.5 Length: 9.8*	205,241
$[Zn_2(bpdc)_2(bpee)]$· 2DMF (RPM3-Zn)	1D straight channel along the *b*-axis	4	Cage size: 5.3×9.8*,# Window size: ~5.1×8.8*,# Length: 6.75	80,268
$[Zn_2(bpdc)_2(bpe)]$·2 DMF (RPM4-Zn)	1D straight channel along the *b*-axis	4	Cage size: 5.6×10.1*# Window size: ~4.5×8.0*# Length: 6.6	273
$[V^{IV}O(bdc)]$ (MIL-47)	1D straight channel along the *a*-axis	2	Cage dimensions: ~9.7 × 8.2 Window size: ~7.0 × 5.7* Length: 6.8	282
$[M^{III}(OH)(bdc)]$ (M = Al, Cr, Fe and Ga) (MIL-53ht)	1D straight channel along the *a*-axis	2	Cr: Cage dimensions: 8.6×8.6,# Length: ~6.8 Al: Cage dimensions: 8.5×8.5# Window size: ~7.2 × 5.3*	245,281,389-390

			Length: ~6.6	

[@] Taken from reported crystal data or based on simulated results when data are not available.

* Distance between the centers of the two outmost He atoms calculated from the simulation data.

[#] The window and cage size after removal of guest is approximated from the reported as-made structure.

[&] fa = formate, H_2hfipbb = 4,4′-(hexafluoroisopropylidene)bis(benzoic acid), pzdc = pyrazine-2,3-dicarboxylate, pyz = pyrazine, btc = 1,3,5-benzenetricarboxylate, bpdc = 4,4′-biphenyldicarboxylate, bpee = 1,2-bis(4-pyridyl)ethene , bpe = 1,2-bis(4-pyridyl)ethane, bdc = 1,4-benzenedicarboxylate.

Hydrocarbon adsorptions that are commensurate with the MMOF structures have been found in both flexible and rigid frameworks. In this review, a rigid framework is referred to one that remains intact or is accompanied with only very minor changes in its crystal structure when guest or solvent molecules are removed. On the contrary, a flexible framework is associated with notable structure changes upon removal of guest/solvent molecules. In the following section, examples from both categories will be discussed and results from experimental adsorption measurements and simulation work will be analyzed and compared. The crystal structures of MMOFs selected from both groups are drawn in Fig. 45. When crystal structures of guest-free compounds are not available simulations are generally performed using the as-synthesized (guest-containing) structures. In such cases, the results may deviate significantly from the real situation and should always be verified by experimental data.

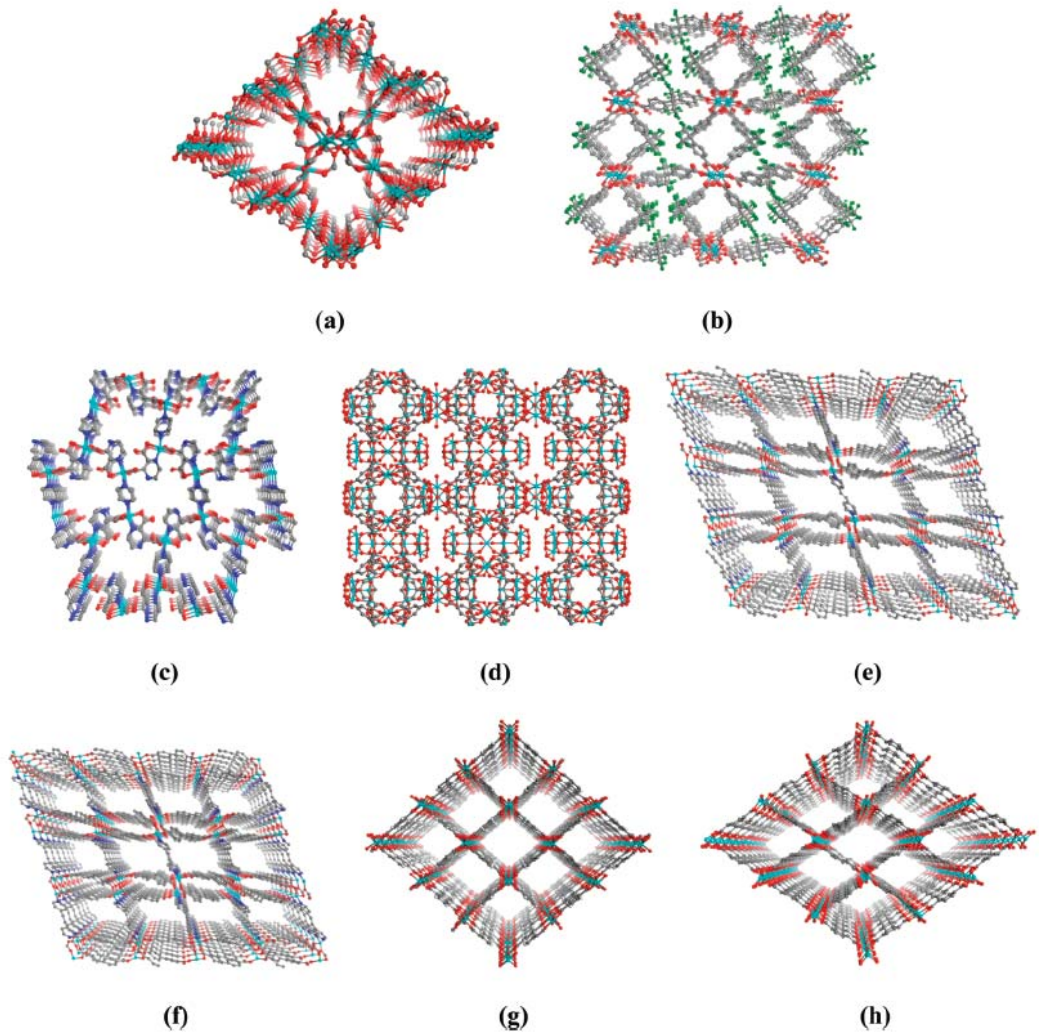

Figure 45. Crystal structures of guest-free MMOFs: (a) $[Co_3(fa)_6]$, (b) $[Cu(hfipbb)(H_2hfipbb)_{0.5}]$ (Cu(hfipbb)), (c) $[Cu_2(pzdc)_2(pyz)]$, (d) $[Al_{12}O(OH)_{18}(H_2O)_3(Al_2(OH)_4)(btc)_6]$, (MIL-96) (e) $[Zn_2(bpdc)_2(bpee)]$ (RPM3-Zn), (f) $[Zn_2(bpdc)_2(bpe)]$ (RPM4-Zn), (g) $[V^{IV}O(bdc)]$ (MIL-47), (h) $[Al^{III}(OH)(bdc)]$ (MIL-53ht). All structures are projected along channel direction except (e), which has two types of accessible cages. Color scheme: metal center (cyan), O (red), C (gray), N (blue), and hydrogen is omitted for clarify. Reproduced with permission from ref 67. Copyright © 2012 American Chemical Society.

3.3.2. Commensurate Adsorption in Selected MMOFs

3.3.2.1. $[M_3(fa)_6]$·sol (M = Mg, Mn, Co, Ni)

The $[M_3(fa)_6]$·sol (M = Mg, Mn, Co, Ni; fa = HCOO or formate, sol = solvent molecule) series of compounds have very similar crystal structures (Fig. 45a). Their frameworks are considered rigid since the crystal structures remain intact upon removal of the solvent molecules, evident from the powder X-ray diffraction (PXRD) patterns taken before and after guest removal. All $[M_3(fa)_6]$ frameworks embrace 1D zig-zag channels.[200,274,276-277] Simulated helium filling in the channels outlines such feature nicely, as shown in Fig. 46a. The repeating unit of the channel comprises of a "zig" and "zag" segment with the segment diameter of ~5.5 Å and window opening of ~4.5 Å. The length of a zig (or zag) segment is estimated to be ~7.1 Å (between the centers of the two outmost He atoms). Each unit cell (UC) contains two pairs of zig-zag units or 4 distinct segments. Data from experimental adsorption isotherms (Table 12) indicate light alcohols such as ethanol, propanol and butanol, and alkanes such as ethane, propane and *n*-butane, all achieve an adsorption level of ~4 molecules/UC (or 1 molecule per channel segment).[200] The simulations reveal that the packing of these molecules is commensurate with the zig-zag shaped pore structure of the channel, which also correlates very well with the shape outlined by He simulation (see Fig. 46b-c). On the other hand, the uptake of methanol is 5.5 molecules/UC and those of pentanol and *n*-hexane are 2.2 and 2.1 molecules/UC, one-half loading with respect to short-chain alcohols and alkanes. For methanol, the strong intermolecular interactions coped with the short length of the molecule (~ 4.1 Å) give rise to 3 molecules within a zig-zag unit. Pentanol and *n*-hexane, with a molecular length of 8.8 and 8.9 Å, respectively, are too long to fit in a single segment.

Table 12. Summary of commensurate-incommensurate adsorption in selected MMOFs. Reproduced with permission from ref 67. Copyright © 2012 American Chemical Society.

MMOFs[&]	Adsorbate	Temp. (K)	Pressure (Torr) or	Adsorbed amount (No. Molecule/UC)	Q*st* (Exptl)	Refs.

			R.C (M)[@]	Experiment[%]	Simulation/Structure Refinement	(kJ/mol)	
$[M_3(fa)_6]\cdot sol$ (M = Mg, Mn, Co, Ni, sol = solvent)[$]	Methane	303	684 torr	NRS*	4	29	200,274,276-278
	Ethane	303	684 torr	3.74	4	43	
	Propane	303	684 torr	3.82	4	43	
	Propene	303	684 torr	3.81	4	49	
	n-Butane	303	684 torr	3.75	4	61	
	n-Pentane	303	353 torr	2.23	2	-	
	n-Hexane	303	100 torr	2.1	2	54	
	n-Heptane	303	28 torr	1.95	2	-	
	n-Octane	303	-	-	2	-	
	Methanol	303	85 torr	5.47	6	58	
	Ethanol	303	41 torr	4.06	4	62	
	n-Propanol	303	12 torr	4.2	4	76	
	n-Butanol	303	3.5 torr	4.0	4	56	
	n-Pentanol	303	1.2 torr	2.2	2	60	
	Benzene	303	74 torr	3.94	4	54	
	Toluene	303	18 torr	2.84	-	64	
	p-Xylene	303	6.0 torr	0.71	-	62	
	Ethylbenzene	303	5.8 torr	2.16	-	56	
	Acetylene	196	760 torr	4.0	4	-	
$[Cu(hfipbb)(H_2hfipbb)_{0.5}]$	Methane	298	760 torr	0.64	-	-	39,249
	Ethane	298	760 torr	1.06	2	-	
	Propane	298	760 torr	1.53	2	47.8	
	Propene	298	760 torr	1.23	2	-	
	n-Butane	298	684 torr	1.79	2	52.3	
	Methanol	298	85 torr	1.62	2	81.1	
$[Cu_2(pzdc)_2(pyz)]\cdot 2H_2O$	Acetylene	270, 300, 310	760 torr	2.0	2	42.5	191,387-388,391
$[Al_{12}O(OH)_{18}(H_2O)_3(Al_2(OH)_4)$(bt	*trans*-Piperylene	298	0.65M	7.3 (L)	8	-	205,241
	cis-Piperylene	298	0.35M	2.4 (L)	-	-	

c)$_6$]·24H$_2$O (MIL-96)	Isoprene	298	0.35M	2.0 (L)	-	-	
[Zn$_2$(bpdc)$_2$(bpee)] ·2DMF (RPM3-Zn)	Methanol	303	85 torr	12.5	-	50.4	80,249,268
	Ethanol	303	35 torr	8.0	8[#]	45.5	
	n-Propanol	303	11.8 torr	8.0	8	57.3	
	n-Butanol	303	3.1 torr	7.8	8	65.6	
	n-Pentanol	303	1.2 torr	5.6	-	-	
	Benzene	303	61 torr	7.8	8	44.5	
	p-Xylene	303	5.1 torr	3.7	4	65.6	
	o-Xylene	303	3.8 torr	3.9	4	55.6	
[Zn$_2$(bpdc)$_2$(bpe)] ·2DMF (RPM4-Zn)	Methanol	303	85 torr	7.9	-	-	31,273
	Ethanol	303	41 torr	5.7	8[#]	-	
	n-Propanol	303	12 torr	6.0	8	-	
	n-Butanol	303	3.5 torr	5	4	-	
	n-pentanol	303	1.2 torr	3.5	4	-	
	Benzene	303	74 torr	4.8	4	-	
	p-Xylene	303	6.0 torr	3.4	4	-	
	o-Xylene	303	3.9 torr	2.2	4	-	
[V^{IV}O(bdc)] (MIL-47)	*p*-Xylene	298	0.8M	3.1 (L)	4	61.2	240,244,246
		343	30 torr	3.4			
	o-Xylene	298	0.8M	2.9 (L)	4	59.6	
		343	30 torr	3.1			
	m-Xylene	298	0.8M	NRS* (L)	4	59.7	
		343	30 torr	3.1			
	Ethylbenzene	298	0.8M	NRS (L)	4	59.7	
		343	30 torr	NRS			
	Styrene	298	0.45M	1.8 (L)	8/3[#]	57.0	
	n-Octane	343	38 torr	1.9	2	65.7	
[Al^{III}(OH)(bdc)] (MIL-53ht)	*p*-Xylene	298	0.55M	3.3 (L)	4	N/A	240,242,245
		343	27 torr	2.8			
	o-Xylene	298	0.55M	3.5 (L)	4	N/A	
		343	27 torr	3.3			
	m-Xylene	298	0.55M	NRS (L)	4	N/A	
		343	27 torr	2.9			

	Ethylbenzene	298	0.55M	NRS (L)	4	48.9	
		343	27 torr	NRS			
	Styrene	298	0.45M	1.9 (L)	8/3^	59.1	

@ R. C. = relative concentration of adsorbate in a non-interacting solvent, in unit of mol/L (M).
% Vapor adsorption experiments. Those marked by (L) refer to liquid-phase adsorption Experiments.
* NRS = Not reaching saturation.
$ All data are for $[Co_3(fa)_6]$ except those of acetylene where the measurements were on $[Mg_3(fa)_6]$ and $[Mn_3(fa)_6]$.
# Crystal structure without guest removal is used in the simulations.
^ 4 pairs of styrene per triple unit cell
& fa = formate, H_2hfipbb = 4,4′-(hexafluoroisopropylidene)bis(benzoic acid), tbip = 5-tert-butylisophthalicate, pzdc = pyrazine-2,3-dicarboxylate, pyz = pyrazine, btc = 1,3,5-benzenetricarboxylate, bpdc = 4,4'-biphenyldicarboxylic, bpee = 1,2-bis(4-pyridyl)ethane, , bpe = 1,2-bis(4-pyridyl)ethane, bdc= 1,4-benzenedicarboxylate.

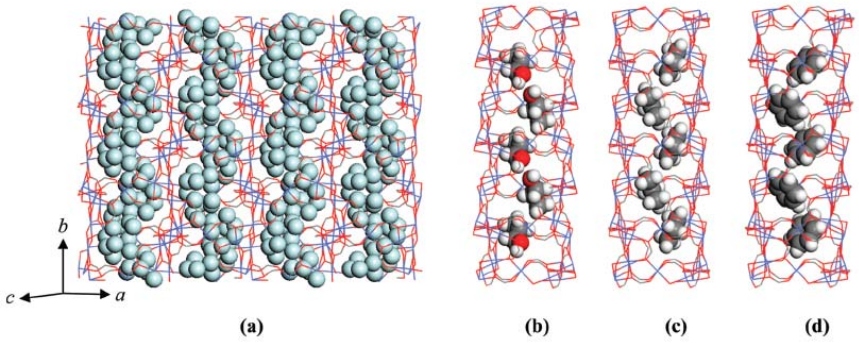

Figure 46. The simulated gas adsorption in the $[Co_3(fa)_6]$ structure. The 1D channels run along the crystallographic *b*-axis. (a) He at 1 K and 760 torr; (b) *n*-propanol at 303 K and 12 torr; (c) propane at 303 K and 684 torr; and (d) benzene at 303 K and 61.4 torr. Color scheme: Co (blue), O (red), C (gray), He (powder blue), H (white). Reproduced with permission from ref 67. Copyright © 2012 American Chemical Society.

The commensurate and incommensurate adsorption of linear alkanes (C1~C3 and *n*-C4~*n*-C7) in the $[Co_3(fa)_6]$ structure was also investigated by simulations employing CBMC method.[278] For C1~C3 that are shorter than the segment length, the adsorption level was found to be 4 molecules/UC, while for *n*-C5~*n*-C7 that are longer than the length of a single segment, the loading is one-half of the C1~C3 group, with one molecule bestriding the two adjacent channel segments. This corresponds to 2 molecules/UC. With its molecular length slightly longer than the channel segment, *n*-C4 tends to extend slightly into the adjacent segment at lower pressure. At higher pressure,

however, it adopts a more constrained conformation to fully fit within one segment. The simulation data are in excellent agreement with the experimental uptake values for C3 and *n*-C6, which yield 3.8 and 2.1 molecules per unit cell, respectively (Fig. 47, Table 12). The simulation results also show that adsorption strength is in the order of C3 > C2 > C1, C3 > *n*-C4 > *n*-C5 and *n*-C7 > *n*-C6 > *n*-C5. In the case of short alkanes C1~C3, the channel segment is sufficiently large to house one molecule per segment but C3 has a length that is more commensurate with the segment size, and therefore, interacts more effectively with the MMOF pore walls (higher adsorption strength). For longer alkane group *n*-C5~*n*-C7, the adsorption is incommensurate and each molecule occupies two adjacent segments (the zig-zag pair). The length of *n*-C7 has a better fit to the pore size and thus, a more effective interaction (higher adsorption strength) with the MMOF pore walls. A commensurate-incommensurate transition occurs at alkanes of intermediate length, *n*-C4 and *n*-C5.

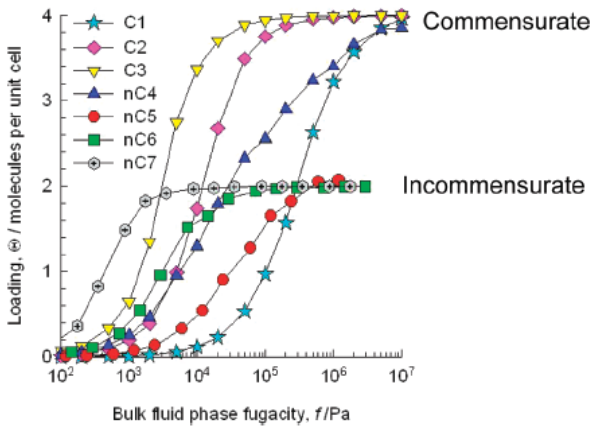

Figure 47. Adsorption isotherms of normal alkanes (C1~*n*-C7) in Co-FA at 300K simulated by the CBMC method. Similar effects for both alkanes and alcohols were observed in cage type zeolite structures.[177,392] Reproduced with permission from ref 67. Copyright © 2012 American Chemical Society.

It is interesting to note that methane behaves distinctly differently from methanol. While both molecules have a length that well fits within a channel segment, the shorter methane (2.6 Å) molecules show commensurate packing based on the simulation results, whereas the packing of longer methanol (4.1 Å) molecules is incommensurate and for each segment second molecule is adsorbed but straddles over to the adjacent segment. This is made possible because of strong intermolecular interactions among the CH_3OH molecules, as indicated by a very high isosteric heat (Q_{st} = 58 kJ/mol) which compensates the energy loss from straddling (~1.5 molecules/segment). Such hydrogen bonding interaction is absent in the case of CH_4 (Q_{st} = 29 kJ/mol) and thus, no driving force for the straddling of a 2nd molecule. The strong hydrogen bonding effect on adsorption of alcohols has also been found in several different zeolite structures.[393-395]

The adsorption of acetylene in the $[M_3(fa)_6]\cdot DMF$ (M = Mg, Mn) represents another case where the adsorbed molecules commensurate with the pore and crystal structure. With the aid of single-crystal X-ray diffraction technique, the structure of acetylene-adsorbed metal formate was determined at 90K.[274] The acetylene molecules occupy one of the two independent positions (A and B) in a zig (or zag) channel at an uptake of 4 molecules per unit cell. This result is fully consistent with the data obtained from sorption experiments.[274]

In addition to linear hydrocarbons and alcohols, aromatic molecules were examined for their adsorption behavior. Interestingly, benzene also shows a strong sign of commensurate adsorption confirmed by adsorption experiment (3.94 molecules/UC),

simulation and single crystal X-ray diffraction (Fig. 46d, Table 12).[200,396] Longer aromatic hydrocarbons, such as toluene, *p*-xylene, and ethylbenzene, are characterized by incommensurate adsorption because their sizes exceed the channel segment length. It is interesting to note that a significantly higher uptake amount of ethylbenzene (2.16 molecules/UC) than *p*-xylene (0.71 molecules/UC) is observed, regardless of the fact that the former is longer than the latter (7.9 and 7.4 Å, respectively).[200] This can be understood by examining the shapes and flexibility of the two molecules with respect to the zig-zag pore segment. In ethylbenzene, the ethyl group is flexible and can be relatively easily extended and fit into the adjacent segment, whereas *p*-xylene is too rigid to be bent over into the neighboring segment, resulting in a very low uptake (Table 12).

3.3.2.2. [Cu(hfipbb)(H$_2$hfipbb)$_{0.5}$]

Cu(hfipbb)(H$_2$hfipbb)$_{0.5}$ is a guest-free rigid 3D framework built on a common paddle-wheel SBU (Fig. 45b). Its pore structure features straight 1D channels composed of oval shaped cages (diameter ~5.1 Å) that are connected by small necks (diameter ~3.2 Å) at ~7.3 Å intervals.[305] This feature is clearly observable from the He simulation data depicted in Fig. 48a. The compound displays unique adsorption properties which have been analyzed by both experimental methods and theoretical modeling.[39,249] Generally, [Cu(hfipbb)(H$_2$hfipbb)$_{0.5}$] adsorbs quickly normal paraffins and olefins up to C4. Any normal paraffins and olefins longer than C4 and all branched hydrocarbons are excluded. Commensurate adsorption is observed for several gases, including propane and *n*-butane, where each cage takes one molecule (2 molecules/UC, see Table 12 and Fig. 48b). Pentane has a molecular length that exceeds the cage limit, forcing it to extend

into the adjacent cage through the small neck. Unlike [$Co_3(fa)_6$], where the window opening is 4.5 Å, the very narrow neck in [Cu(hfipbb)(H_2hfipbb)$_{0.5}$] will lead to a very short H···H intermolecular distance (~1.86 Å) within this region, making it impossible as an equilibrium position for pentane to straddle. Gas-sorption simulations indicate that the channels are sufficiently large to allow passage of normal alkanes (diameters ~3.6 Å) of C5 and higher members, but will exclude all branched alkanes which typically have diameters larger than those of normal alkanes.

The adsorption strength of alkanes follows the following order: propane > ethane > methane and propane > *n*-butane according to the Henry constants calculated from experimental isotherms at low loadings. Again this can be explained based on the commensurability of the adsorbates to the pore structure. Propane molecule has an optimal length and shape to best fit the cage cavity, showing highest Henry constant among all alkanes. Butane adopts a slightly twisted configuration, similar to that observed in [$Co_3(fa)_6$]. The experimentally adsorbed 1.8 butane molecules/UC at 298 K and 1 atm is in excellent agreement with the uptake value of 2 molecules/UC modeled by molecular simulation. [Cu(hfipbb)(H_2hfipbb)$_{0.5}$] is the first MMOF that shows capability of separating normal C4 from higher paraffins and olefins. Such behavior is unique with respect to zeolites, for which a cutoff carbon number for the adsorption of linear hydrocarbons has not been observed. Other MMOFs with small pore opening or narrow neck sections between larger cages also demonstrate alkane separation capabilities following a similar mechanism.[241,397] In addition to paraffins and olefins, adsorption experiments and simulation are performed on methanol. The results are consistent and

indicate that the adsorption of this molecule is also commensurate with the pore structure of [Cu(hfipbb)(H_2hfipbb)$_{0.5}$] (Fig. 48c).

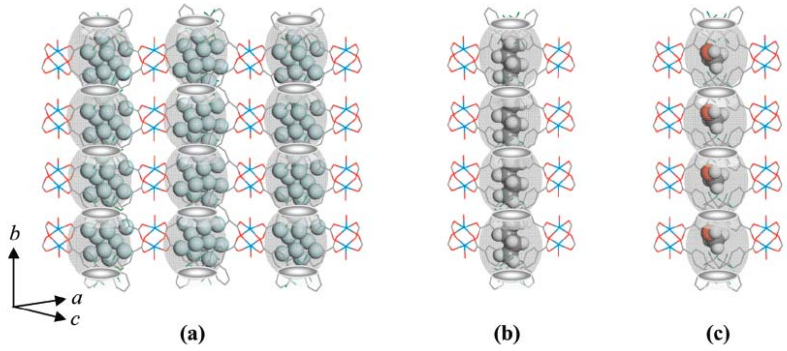

Figure 48. The simulated gas adsorption in the [Cu(hfipbb)(H_2hfipbb)$_{0.5}$] structure. The 1D channels run along the crystallographic *b*-axis. (a) He at 1 K and 760 torr; (b) *n*-butane at 303 K and 684 torr; (c) methanol at 303 K and 78.7 torr. Color scheme: Cu (light blue), O (red), C (gray), F (green), He (powder blue), H (white). Reproduced with permission from ref 67. Copyright © 2012 American Chemical Society.

3.3.2.3. [Cu_2(pzdc)$_2$(pyz)]·2H_2O

The framework of [Cu_2(pzdc)(pyz)]·2H_2O (pzdc = pyrazine-2,3-dicarboxylate, pyz = pyrazine, Fig. 45c) is considered "rigid" with the understanding that while there is a gas pressure associated structure change, such a change is considerably smaller in comparison with those classified as "flexible" structures. Its pore structure consists of 1D cylindrical channels with a cross-section of 4 × 6 Å.[387-388,398] The channels are straight and run along the crystallographic *a*-axis, as easily visualized from Fig. 49a. The adsorption isotherms of C_2H_2 measured at various temperatures (e.g. 270, 300, and 310 K) show that in all cases a maximum loading of 42 cm^3/g (STP) is reached at relatively low pressure (between 5 and 60 kPa depending on the temperature), corresponding to one molecule per pore segment and two molecules/UC.[191] The uptake of CO_2, which has a similar size as C_2H_2 (both having a kinetic diameter of 3.3 Å), is significantly less at such pressures.

The strong adsorption of acetylene was attributed to its high adsorption enthalpy as a result of strong hydrogen bonding between the uncoordinated oxygen atoms from the framework ligand and the hydrogen atoms in acetylene. The channel shape and relative positions of the O atoms, and the orientation and size of C_2H_2 allow the molecules to be packed in such a way to fit perfectly within the segments. (Fig. 49b). The periodic structure with adsorbed C_2H_2 at 10 kPa and 170 K was confirmed by the maximum entropy method (MEM) and Rietveld analysis using synchrotron X-ray powder diffraction method.[191,388,391] Fig. 50 shows that C_2H_2 molecules are located at the center of the pore segment and align along the *a*-axis with an inclination of 78.1°. The structure refinement shows that they are densely packed with an intermolecular distance of 4.7 Å, commensurate with the length of *a*-axis and in excellent agreement with the experimental adsorption results.

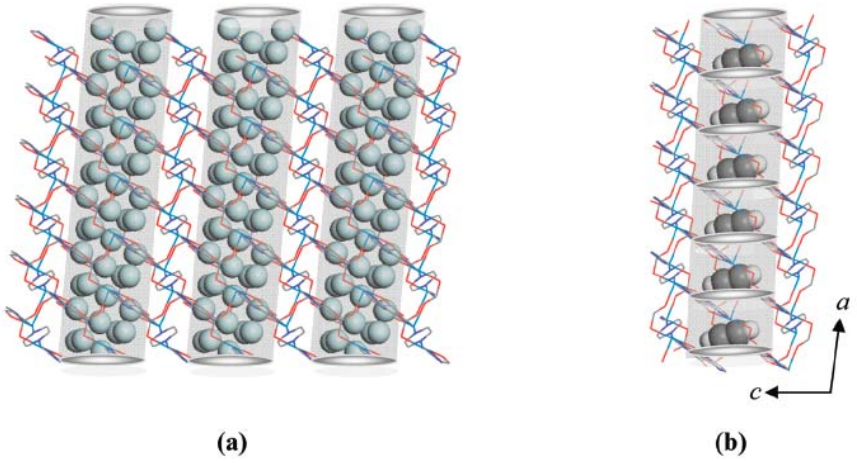

Figure 49. The simulated gas adsorption in the $[Cu_2(pzdc)_2(pyz)]$ structure. The 1D straight channels run along the crystallographic *a*-axis. (a) He at 1 K and 760 torr; (b) acetylene at 303 K and 684 torr. The channel is divided into "segments" to guide the eyes. Color scheme: Cu (light blue), O (red), C (gray), N (dark blue) He (powder blue) and H (white). Reproduced with permission from ref 67. Copyright © 2012 American Chemical Society.

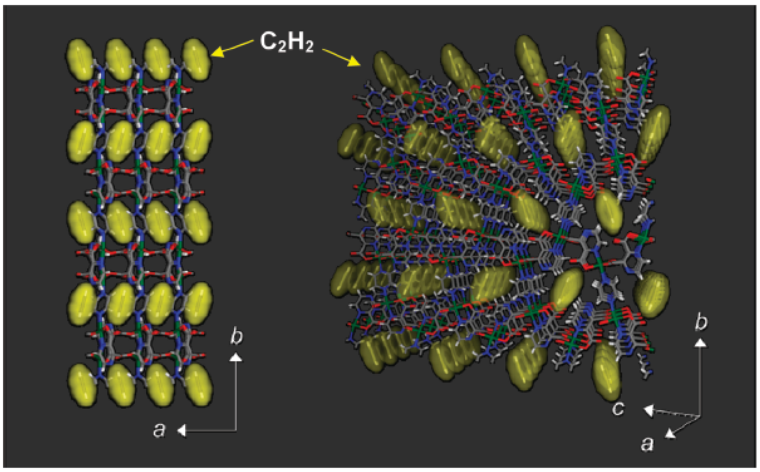

Figure 50. The C_2H_2 loaded $[Cu_2(pzdc)_2(pyz)]$ structure (170K) from MEM/Rietveld analysis. (a) View along the *c*-axis. (b) Perspective view along the *a*-axis. Color scheme: Cu (green), O (red), C (gray), N (blue) and H (white). Reproduced with permission from ref 67. Copyright © 2012 American Chemical Society.

3.3.2.4. $Al_{12}O(OH)_{18}(H_2O)_3(Al_2(OH)_4)[btc]_6 \cdot 24H_2O$ (MIL-96)

MIL-96 is a rigid 3D framework constructed from two inorganic structural motifs, a trimeric unit made of three corner sharing $AlO_5(H_2O)$ octahedra via a μ_3-O and a 2D net built on 1D interconnecting chains of corner-sharing octahedral $AlO_2(OH)_4$ and $AlO4_2(OH)_2$ (Fig. 45d).[205] The overall structure contains three types of cages, of which only two (A-type and B-type, two of each within a unit cell) are accessible to hydrocarbons. Both A-type and B-type cages have a very small window opening (between 2.5-3.5 Å) but large cage diameters (minimum ~8.8 Å). The pore volumes estimated from PLATON are ~420 and ~635 $Å^3$ for cages A and B, respectively. Upon removal of water molecules the window aperture is enlarged to ~4.5-5.5 Å,[205] The cross-sections of these cages estimated from our He simulations are 10.0×8.9 Å and 15.1×9.8 Å (center-to-center distances) for A and B, respectively. Their shape and size outlined by simulated He are shown in Fig. 51. Single-component and competitive liquid-phase

adsorption experiments on C5 hydrocarbons demonstrate high capability of MIL-96 for the separation of isoprene, *cis*- and *trans*-piperylene via selective adsorption.[241] The experimental single-component isotherms yielded a maximum uptake of 12 wt% for *trans*-piperylene (heptane as solvent, 298 K) which matches reasonably with the theoretical value of 13.2 wt% that corresponds to 2 molecules per cage or 8 molecules/UC. The uptakes of *cis*-piperylene and isoprene are considerably lower under the same experimental conditions, giving 0.6 and 0.5 molecules per cage, respectively. This difference was attributed to steric effect as the molecular geometry of *trans*-piperylene allows a much better fit to the pore shape and more than one molecule can be packed within a single cage. Our simulated gas-phase adsorption of *trans*-piperylene gives 8 molecules per unit cell which agrees with the liquid-phase experiments, although the number of molecules in cages A and B is found to be 1 and 3, respectively, rather than 2 and 2 as previously assumed.[241]

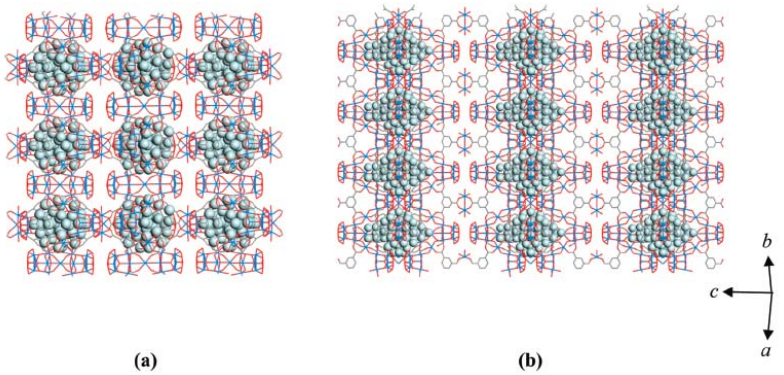

Figure 51. The simulated He adsorption in the MIL-96 structure at 1 K and 760 torr. The size and shape of the two types of accessible pores are outlined by He atoms: (a) Type-A, and (b) Type-B. Color scheme: Al (light blue), O (red), C (gray) and He (powder blue). Reproduced with permission from ref 67. Copyright © 2012 American Chemical Society.

3.3.3.5. $[Zn_2(bpdc)_2(bpee)]\cdot 2DMF$ (RPM3-Zn)

$[Zn_2(bpdc)_2(bpee)]\cdot 2DMF$ (or RPM3-Zn, RPM = Recyclable Porous Material) is a highly flexible 3D structure containing 1D straight channels running along the *b*-axis (Fig. 45e). The channel is made of repeating segment (length of 6.75 Å, coincident with the unit cell length of the *b*-axis) having parallelogram-shaped cross-section (cage and window sizes of ~5.3×9.8 Å and ~5.1×8.8 Å, respectively, estimated from the He simulated data using the as-synthesized $[Zn_2(bpdc)_2(bpee)]\cdot 2DMF$ structure (Fig. 52a and Table 11). Each unit cell contains 4 segments.[80,268] Gas adsorption experiments and simulations on selected hydrocarbons show that the uptake levels of benzene, *p*- and *o*-xylene are all indicative of adsorption commensurate with the pore and crystal structure.[80,249] For benzene, each segment takes up 2 molecules (or 8 molecules/UC) and the ring planes of the pair are not perfectly parallel but with an angle. The molecules pack in zig-zag fashion within the 1D channel[399] (Fig. 52b). *p*-Xylene (length of 7.4 Å), on the other hand, is significantly longer than benzene (5.8 Å) and thus, is limited to 1 molecule per segment (4 molecules/UC). Simulations show that it packs in either a "zig" or a "zag" orientation (Fig. 52c) within a single channel of ~40 Å, which is presumably affected by how the first molecule enters the channel. Once the first molecule is adsorbed, subsequent molecules in that channel will pack along the same orientation. Simulations also show that *p*-xylenes in adjacent channels appear to pack independently with respect to the neighboring channels. *o*-Xylene, a bulkier isomer with lower symmetry, also follows an ordered adsorption pattern at a uptake of 1 molecule per channel segment (4 molecules/UC). The orientations of these molecules are slightly different in the adjacent channels.

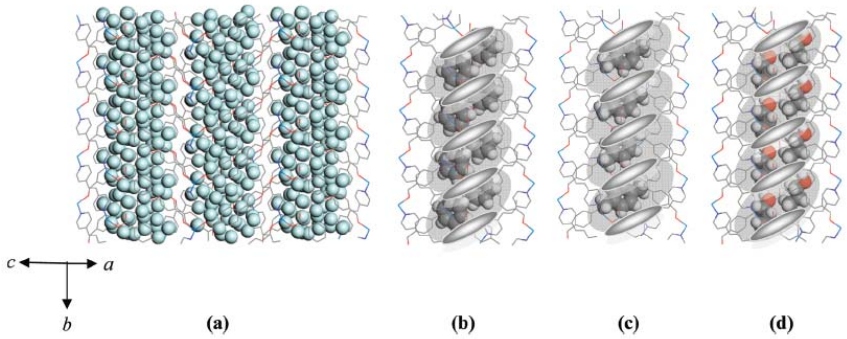

Figure 52. The simulated gas adsorption in the RPM3-Zn structure. The 1D channels run along the crystallographic *b*-axis. (a) He at 1 K and 760 torr; (b) Benzene at 303 K and 61.4 torr; (c) *p*-Xylene at 303 K and 5.2 torr; (d) *n*-Propanol at 303 K and 12.0 torr. Color scheme: Zn (light blue), O (red), C (gray), N (dark blue) He (powder blue) and H (white). Reproduced with permission from ref 67. Copyright © 2012 American Chemical Society.

The normal C2-C4 alcohols also exhibit commensurate adsorption in RPM3-Zn near room temperature. The adsorption isotherms of both propanol and butanol display some interesting features. At 25 and 30 °C, a plateau approaching 2 molecules per pore segment (8 molecules/UC) is clearly visible (see Fig. 53), which is also confirmed by simulation (Fig. 52d). Having a similar length as benzene (5.8 Å), propanol (6.3 Å) also adapts the same zig-zag packing configuration as benzene molecules within each channel. At higher temperatures (e.g. 50-75 °C), however, its adsorption isotherms show an inflection at a loading of ~2 molecules. Whether this behavior is due to a structure change will need to be verified by further study. For butanol, the 25 °C experimental adsorption isotherm is a classical type-I adsorption but at higher temperatures (30-40 °C), its isotherms resemble more of a type-II adsorption.[300] At and above 45 °C, the curves are essentially type-I with an adsorption limit of ~5.5 molecules/UC. Having a linear chain length of 7.6 Å, butanol seems too long to have the same adsorption

capacity as propanol (8 molecules/UC), as it is more comparable with *p*-xylene (7.4 Å) of similar length (4 molecules/UC). A possible explanation is that at lower temperature (e.g. 25 °C), the butanol molecule adopts a non-linear conformation, allowing it to pack 2 molecules per pore segment. This conformation becomes unstable at higher temperatures, therefore reducing the amount adsorbed.

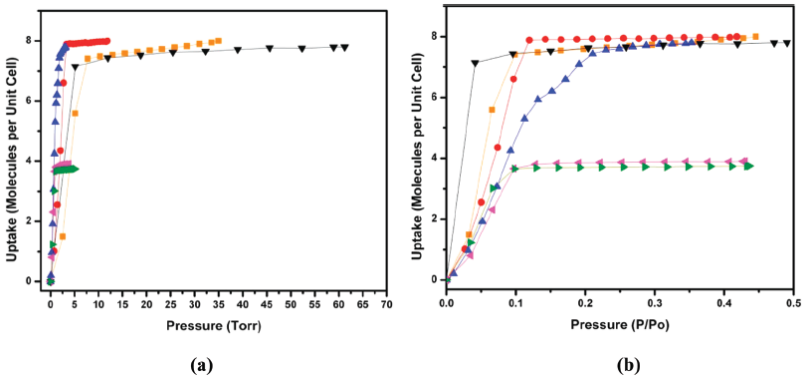

Figure 53. Adsorption isotherms of selected hydrocarbons and alcohols in RPM3-Zn at 30 °C plotted in (a) absolute pressure, and (b) relative pressure, P/Po. Color scheme: ethanol (orange), *n*-propanol (red), *n*-butanol (blue), benzene (black) *o*-xylene (pink) and *p*-xylene (green). Reproduced with permission from ref 67. Copyright © 2012 American Chemical Society.

3.3.3.6. [Zn$_2$(bpdc)$_2$(bpe)]·2DMF (RPM4-Zn)

[Zn$_2$(bpdc)$_2$(bpe)]·2DMF (RPM4-Zn, Fig. 45f) is isotypic to RPM3-Zn, with the pillar ligand bpee replaced by bpe,[273] and thus, has a very similar 1D channel structure as RPM3-Zn before removal of solvent (guest) molecules. The 1D open channels are made of identical segments (6.6 Å in length) with cage and window dimensions of 5.6×10.1 Å and 4.5×8.0 Å, respectively. Compared to RPM3-Zn, the carbon-carbon single bond between the two pyridine rings of the bpe ligand in RPM4-Zn leads to a higher degree of flexibility and further distortion of the pore structure upon evacuation of guest molecules. This is evident both from their PXRD patterns (before and after guest

removal) and from their room temperature CO_2 adsorption isotherms that exhibit a hysteresis-free three- and two-step sorption for RPM4-Zn and RPM3-Zn, respectively.[31,273]

RPM4-Zn takes up a significantly less amount of benzene and *o*-xylene compared to RPM3-Zn. This is due to the more severe distortion of its framework upon guest removal which leads to further reduction of its cage dimensions in the guest-free form. The benzene experimental adsorption isotherm at 30 °C only corresponds to a loading of ~1 molecule per channel segment, half of that of RPM3-Zn under the same conditions. For *o*-xylene, the uptake is reduced to ~0.5 molecule per channel segment, also about one-half of that for RPM3-Zn. In the case of *p*-xylene a loading of 0.84 molecules per channel segment is achieved, comparable to 0.93 molecules per channel segment for RPM3-Zn. Simulated adsorption of *p*-xylene gives a loading limit of 1 molecule per channel segment, consistent with the experimentally observed uptake. The different adsorption levels of benzene, *o*-xylene and *p*-xylene can be explained by molecular size. All three molecules lie approximately parallel to the longest side of the cage. As shown in Fig. 54, such orientation requires the molecular width to be comparable with the length of pore segment (or the length of *b* axis, 6.6 Å). The widths of benzene and *p*-xylene are both ~6.6 Å (hydrogen VDWs radius included), slightly tilting allows each to fit fully within a segment. However, the *o*-xylene is more bulky with a width of 7.7 Å, too long to fit completely within a single segment, thereby reduced the uptake level of about one-half of benzene and *p*-xylene (one molecule per two segments).

As in the cases of aromatic hydrocarbons, all alcohols tested also show significantly lower adsorption amount in RPM4-Zn. Methanol and *n*-pentanol have an adsorption level of 2 and 1 molecule per channel segment, respectively, indicating commensurate adsorption, while they are not commensurate in the case of the RPM3-Zn. On the other hand, ethanol, *n*-propanol and *n*-butanol no longer show commensurate adsorption, giving less than 2 molecules per channel segment. These observations are consistent with the relative pore size and pore volume in the two structures and suggest that the cut-off limit of molecule length for commensurate adsorption shifts to lower value in RPM4-Zn.

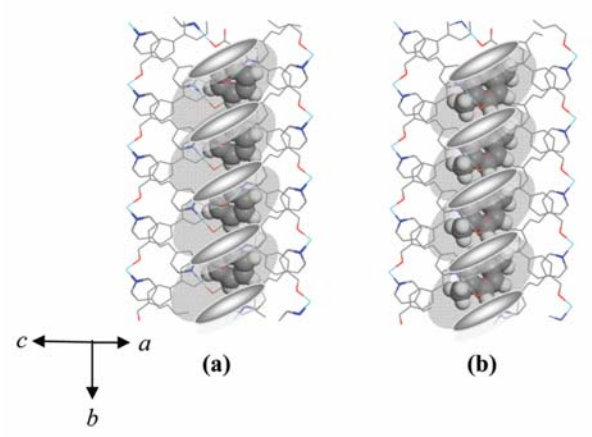

Figure 54. The simulated gas adsorption in the RPM4-Zn structure. The 1D channels run along the crystallographic *b*-axis. (a) Benzene at 303 K and 61.4 torr; (b) *p*-Xylene at 303 K and 5.2 torr. Color scheme: Zn (light blue), O (red), C (gray), N (dark blue) and H (white). Reproduced with permission from ref 67. Copyright © 2012 American Chemical Society.

3.3.3.7. [$V^{IV}O$(bdc)] (MIL-47)

[$V^{IV}O$(bdc)] (MIL-47) is the guest-free form of [$V^{III}OH$(bdc)]·0.75(H_2bdc) (MIL-47as). The crystal structure of MIL47as is made of 1D chains of corner-sharing VO_6 octahedra interconnected by 1,4-benzenedicarboxylate (bdc) to give a 3D network.[282] Upon

heating, the guest H_2bdc molecules filling the pores can be removed, and the μ_2-OH groups are converted to μ_2-O, resulting in a porous framework [V^{IV}O(bdc)] (Fig. 45g). MIL-47 embraces large-pore 1D straight channels parallel to the crystallographic *a*-axis with a diamond-shaped cross-section. These channels contain repetitive segments having cage and window sizes of 9.7 × 8.2 Å and 7.0 × 5.7 Å, respectively (2 segments/UC). The length of the channel segment is 6.82 Å, coinciding with the length of *a*-axis. These features are apparent from the simulated He pattern shown in Fig. 55. It should be pointed out that we have classified MIL-47 as a "flexible" structure based solely on the fact that its crystal structure is significantly different from that of MIL-47as, the as-synthesized parent structure before evacuation (to be consistent with our grouping for all other structures included in this review). The framework of MIL-47 itself is generally considered "rigid", as it does not undergo a substantial structure change upon adsorption and desorption of hydrocarbons (with a few exceptions).[33,240,246,400]

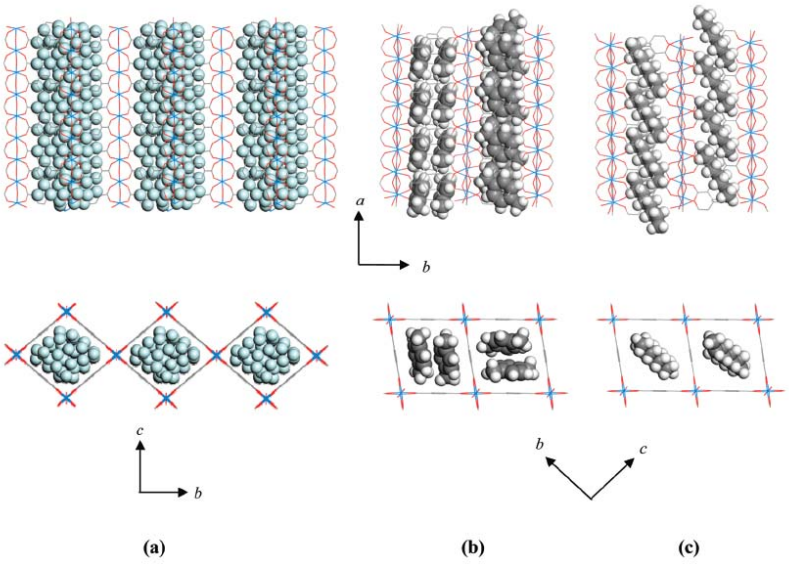

Figure 55. The simulated gas adsorption in the MIL-47 structure shown in two directions. (a) He at 1 K and 760 torr; (b) *p*-Xylene at 303 K and 11.7 torr; (c) *n*-Octane at 303 K and 17.2 torr. The 1D channels run along the crystallographic *a*-axis. Color scheme: V (light blue), O (red), C (gray), and He (powder blue) and H (white). Reproduced with permission from ref 67. Copyright © 2012 American Chemical Society.

A number of recent experimental and simulation studies have centered on its adsorption properties with regard to C8 hydrocarbons. Liquid-phase single-component and competitive adsorption experiments of C8 alkylaromatics on MIL-47 were performed in hexane solution at room temperature. *p*-Xylene and *o*-xylene show high uptakes and reach saturation at a loading of 37% and 35%, respectively, whereas a considerably lower adsorbed amount of *m*-xylene and ethylbenzene is noted[246]. Vapor-phase adsorption experiments carried out at various temperatures (e.g. 343, 383 and 423 K) yielded values that are consistent with liquid-phase experiments. At 343 K and up to 0.05 bar, the uptake amount approaches 4 molecules/UC for both *p*- and *o*-xylene and slightly lower for *m*-xylene and ethylbenzene[244]. The GCMC simulated adsorption isotherms at these temperatures show excellent agreement with the experimental results,

giving a saturated loading of 4 *p*- and *o*-xylene molecules per unit cell[400]. As all four isomers have similar adsorption enthalpies, the higher adsorption level of *p*-xylene and *o*-xylene is attributed to their more effective packing.[244,246,400]

The location and orientation of these adsorbates were further determined by Rietveld refinements of synchrotron powder X-ray diffraction patterns of MIL-47 crystal samples saturated with individual C8 aromatics at room temperature,[244,246] and by GCMC molecular simulations at high temperature (343K)[400]. The refined structures show that all three xylene isomers form pairs within a pore segment at a loading of one pair per segment with a repeating distance of 6.8 Å along the *a*-axis, commensurate with the symmetry of crystal lattice. This accounts for 4 xylene molecules/UC. The results are in good agreement with the experimental sorption data of *p*- and *o*-xylene and are confirmed by the simulated adsorption isotherms performed at 343K. The orientations and relative arrangement of the xylene isomers, however, are different and such differences are attributed to the molecular geometry and pore structure. The *p*-xylene pair align their benzene rings nearly parallel to each other and to the bdc of the pore wall, with their methyl groups being staggered to each other. This packing is most effective for a strong π-π interaction. The relative alignment of the *o*-xylene pair is similar to *p*-xylene and their CH_3 groups are also in a staggered configuration, but with a small angle between the two benzene rings the packing is less efficient. For *m*-xylene, the steric constraints between the aromatic ring of one molecule and a methyl group from a neighboring molecule force the pair to deviate from the arrangement most favorable for π-π interaction.

Different from the three xylene isomers, adsorption of C8 ethylbenzene causes significant changes in the lattice parameters of MIL-47. The relatively bulky ethyl group precludes a parallel alignment of two ethylbenzene molecules. Rather, they arrange themselves by aligning along the diagonal direction of the channel segment so that the two ethyl groups stay farthest apart from each other at the opposing corners of the rhombic-shaped pore. This arrangement favors O···H interactions between the CH_3 of the ethyl groups and the carboxylate of bdc ligands at the corners, but greatly diminishes any π-π interactions between the EB molecules and between the EB and framework. Consequently nearly equal distanced molecules stack in a zig-zag fashion within a single channel (2 EB/segment).

Separation of EB and styrene is an important part in petrochemical or petroleum refining processes[401-402]. Adsorption of styrene in MIL-47 represents another very interesting case. With a C=C double bond in place of a C-C single bond in EB, styrene is longer and more rigid than EB. Rietveld PXRD refinement reveals that while the molecules pair up as in the case of xylenes, the steric constraints make the commensurate stacking impossible to the unit cell dimensions.[240] As a result, tripling of the original length of *a*-axis is required to fit in two pairs of molecules within a single channel (four pairs per triple unit cell).

n-Octane, a C8 aliphatic molecule, is found to have higher adsorption enthalpy than the xylenes. This higher energy is a result of multiple O···H interactions between *n*-octane and the 1D chain of corner-sharing VO_6 of the MIL-47 framework. The parallel arrangement of *n*-octane molecules with respect to the VO_6 chain maximizes such interactions and results

in 1 molecule per channel segment, as shown in Fig. 55c. The simulated results are consistent with the experimental observations, which gives 23 wt% uptake at 70 °C (corresponding to 1.9 molecules/UC)[244].

CBMC simulations on lighter C1-C4 alkanes at 303K show that these molecules do not exhibit commensurate adsorption in MIL-47.[33] The alkane molecules are randomly distributed within the pore space. The adsorption capacity increases as alkane length decreases. The simulated isotherms agree well with rescaled experimental data reported earlier.

3.3.3.8. [M^{III}(OH)(bdc)] (M = Al, Cr, Fe and Ga) (MIL-53)

MIL-53 or [M^{III}(OH)(bdc)], where M denotes Al[281], Cr[389-390], Fe[403], or Ga[404], adopts the same structural topology as MIL-47as. In a MIL-53 crystal lattice, corner-sharing $MO_4(OH)_2$ (M = Al^{3+}, Cr^{3+}, Fe^{3+} or Ga^{3+}) octahedra bridged by bdc ligands yield a 3D extended network containing 1D straight channels that feature diamond shaped cross section, as in the case of MIL-47. There are three structure forms, MIL-53as (as-synthesized form), MIL-53ht (guest-free high temperature form, Fig. 45h) and MIL-53lt (hydrated low temperature form). Unlike MIL-47as, for which metal (V) undergoes an oxidation (V^{3+} to V^{4+}) upon guest removal at elevated temperatures, the metal ion (M) in the guest-free form of MIL-53as, namely MIL-53ht, retains its oxidation sate (III). This is also the case for MIL-53-lt, the hydrated structure formed spontaneously by adsorbing water in air upon cooling of the high temperature phase MIL-53ht. The three structures share the same type of 1D chains built on corner-sharing $MO_4(OH)_2$ octahedra, although their space groups and pore dimensions are all different. The cross-sections of the cages

are 7.5×9.2 Å, 8.6×8.6 Å and 3.1×14.9 Å, for the Cr-based MIL-53as, MIL-53ht and MIL-53lt phases, respectively[389-390] and 7.3×7.7 Å, 8.5×8.5 Å and 2.6×13.6 Å for the Al-based MIL-53as, MIL-53ht and MIL-53lt phases, respectively.[245,281] In addition, helium simulation was carried out to evaluate the window size of MIL-53ht(Al), which gives an estimated value of 7.2×5.3 Å (measured between the centers of the outmost He atoms), significantly smaller than the dimensions of the cages (11.2×6.9 Å), thus, dividing the straight channels into segments (6.6 Å in length). Intensive and comprehensive investigations of the structure flexibility and adsorption properties of these compounds with different M^{3+} metal centers have been reported.[23,36,85,240,245-246,250,270,281,389,405-408]

The single-component liquid-phase adsorption isotherms of C8 alkylaromatics in hexane were measured on MIL-53(Al) at room temperature (25 °C).[245] Both *o*- and *p*-xylene reached a plateau uptake of ~ 45-46 wt% at a bulk concentration of ~0.2 M and ~0.5 M, respectively. The adsorbed amount is fairly close to 4 molecules/UC, or 2 molecules per channel segment. The uptakes of *m*-xylene and ethylbenzene were significantly lower at the maximum concentration of the experiment and far from reaching saturation. Room temperature Rietveld refinements of PXRD data were carried out on C8 alkylaromatic adsorbed MIL-53ht(Al) structures at high loading. The analysis revealed significant changes in the lattice parameters upon adsorption and different adsorption behavior of the C8 isomers. The geometric arrangement of *o*-xylene allows both of its methyl groups to interact with the bdc carboxylates and thus, shows the strongest affinity to the framework. The refined structure manifests an efficient double-file packing of *o*-xylene within the channel (2 molecules/channel segment or 4

molecules/UC), commensurate with the pore structure and in excellent agreement with experimental isotherms. For *m*- and *p*-xylene, only one methyl group can be located in the close proximity of carboxylate groups and as a result, their interactions with the framework are weaker. *m*-Xylene has a higher interaction strength than *p*-xylene because its 2nd methyl group and C2 carbon of the ring can interact with aromatic rings of the framework, while such interactions are not possible for *p*-xylene. Instead, the 2nd methyl group of *p*-xylene interacts with the ring of an adjacent *p*-xylene molecule in a similar way as found in *p*-xylene loaded silicalite.[409-410] Ethylbenzene exhibits the weakest adsorbate-adsorbent binding among the four C8 isomers, because of the steric hindrance of its ethyl group that is absent in *m*- and *p*-xylene.

In addition to liquid-phase adsorption experiments, the vapor-phase adsorption isotherms of xylene isomers and ethylbenzene were measured at 110 °C by the same group.[242] The isotherms of all three xylene isomers feature a two-step profile with hysteresis, indicative of changes in the crystal structure during the adsorption process. For ethylbenzene, a kink rather than a step, was observed in its adsorption isotherm. A similar adsorption level was achieved for all four molecules at the first inception point (~0.003 bar), but at higher loadings (> 0.03 bar) the amount of ethylbenzene adsorbed is considerably less than its xylene isomers. The uptake amount of xylene molecules corresponds to ≥ 3 molecules at the maximum pressure but clearly not reaching saturation. It is reasonable to envision a maximum loading of 2 molecules per channel segment, or double-file occupancy, as verified by the Rietveld structure refinements. The refinement results on *o*-xylene adsorbed structure show that structure transformation

occurs between several phases as a function of hydrocarbon loadings, namely MIL53as(Al) (dominating at very low loadings), MIL-53iX(Al) (dominating at intermediate loadings), and MIL-53ht(Al) (dominating at high loadings). The transition from a single-file (before infection point) to double-file (after inflection point) arrangement of adsorbed molecules depends on the molecular geometry, pore symmetry and surface composition which governs the interaction strength of individual isomers with the host and their adsorption behavior.

Alkanes adsorption has also been reported on several MIL-53(M) compounds (M = Al[251], Cr[33,88,248,251], Fe[270]). For MIL-53(Al) and MIL-53(Cr), generally the adsorption capacity increases as the size of alkane decreases. Most of the reported isotherms are classical Type-I, with a few exceptions for longer alkanes that show small kinks in their isotherms. In contrast, the gas adsorption behavior of MIL-53(Fe) is very different from its Al- or Cr-analogues. Apparent gate opening effect was observed for small alkane molecules. This could be attributed to higher flexibility of the MIL-53(Fe) structure, where very narrow pores prevent most gases from entering, and "gate" opens only in the cases of certain small adsorbates when their pressure reaches a threshold.[403,411-413]

3.4. Commensurate adsorption in other porous structures

All porous structures discussed in the preceding section have a common feature in that they are three-dimensional (3D) frameworks. However, commensurate adsorption is not limited to 3D structures. The phenomenon has also been observed in other types of porous networks, such as two-dimensional (2D) interdigitated layer structures. Here we briefly discuss two interesting examples.

3.4.1. $[Cu(dhbc)_2(4,4'\text{-bpy})]\cdot H_2O$

The structure of $[Cu(dhbc)_2(4,4'\text{-bpy})]\cdot H_2O$ (H_2dhbc = 2,5-dihydroxybenzoic acid) embraces 1D open channels parallel to the *a*-axis, formed by interdigitation of the adjacent 2D layers (Fig. 16a).[198] Within the layer, the Cu(II) atoms form 1D linear chains through the linkage of 4,4'-bpy which are further connected via dhbc to give rise to a 2D network. The channel segment has an irregular shape, and is composed of two parts (*a* and *b*, as indicated in Fig. 56b). The dimensions of Part *a* and Part *b* are 2.9 × 4.8 Å and 4.7 × 2.5 Å, respectively, estimated by He simulation (see Fig. 56b). There is no clear boundary between the two parts, but the sum of the two gives the overall length of the segment (8.2 Å). Each unit cell contains 2 segments. Experimental adsorption isotherms were measured for selected paraffins and aromatic hydrocarbons including benzene, toluene, *p*-xylene, propane, *n*-butane, *n*-pentane, and *n*-hexane at 30, 40, and 50 °C. Benzene shows an adsorption level of more than 2 molecules/UC. Toluene serves a good case of commensurate adsorption. Its experimental uptake was 1.8 molecules/UC, very close to the simulated data of two molecules/UC or one molecule per segment. The fact that the adsorption amount remains the same at different temperatures (30 and 40 °C, Fig. 57c) further verifies the adsorption is commensurate to the pore segment. Being longer and more rigid, *p*-xylene has the lowest uptake among the three aromatic adsorbates. The adsorbed amount was 1 molecule per two segments, and thus, a case of incommensurate adsorption. The same trend was found for the selected paraffins. Higher uptake was achieved for smaller members of the series. The uptakes are in the descending order of propane, *n*-butane, *n*-pentane and *n*-hexane, corresponding to 0.99,

0.82, 0.76 and 0.70 molecules/UC or 0.50, 0.41, 0.38 and 0.35 molecules per segment (Fig. 57b). Therefore, none of them represent a case of commensurate adsorption.

Simulations were performed on the same hydrocarbon adsorbates to verify their adsorption behavior. Toluene molecules preferentially take the center positions at Part *b* within each segment and are oriented to face the dhbc ring to be engaged in a π-π interaction, as shown in Fig. 56c. However, the width of the toluene (5.1 Å) is a bit too large for the pore. As a result, it accommodates the shape of the segment by tilting its ring slightly. Paraffin molecules, on the other hand, prefer to stay near the center of Part *a* of the segment to have a closer contact with framework. While these results may have deviations from the real situation as the simulation experiment uses the as-made crystal structure which will most likely undergo some changes upon hydrocarbon adsorption, it is clear that experimental and simulation data agree well in the case of toluene, and it is interesting to note the incommensurate-commensurate-incommensurate (IC-C-IC) transition among benzene, toluene and *p*-xylene (Fig. 57a).

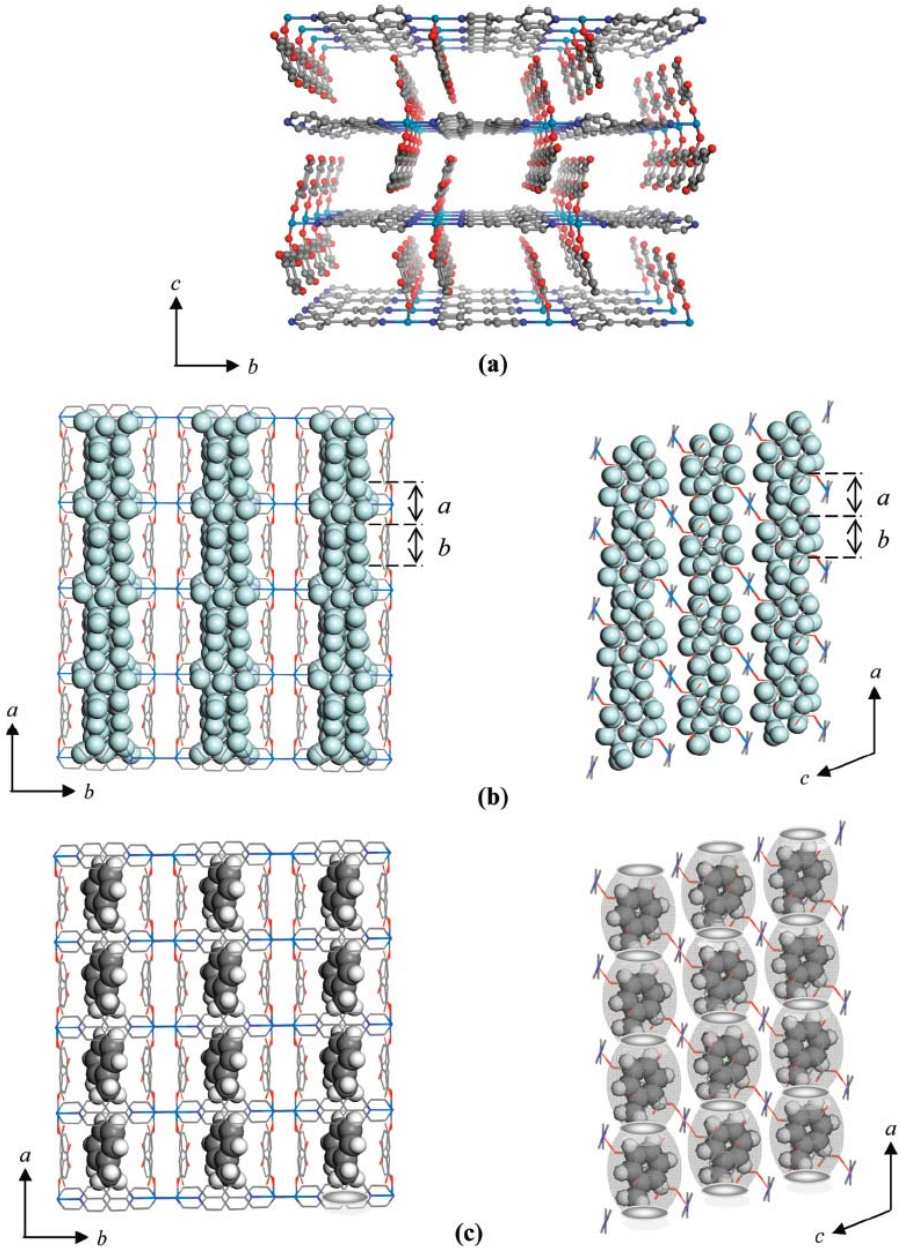

Figure 56. (a) Crystal structure of $[Cu(dhbc)_2(4,4'\text{-bpy})]\cdot H_2O$ viewed along the *a*-axis. (b) Simulated He gas adsorption (1 K and 760 torr) outlining the 1D channels, viewed along the *c*- and *b*-axes. The channel segment is composed of two parts (*a* and *b*, overall length of 8.2 Å). (c) Simulated toluene adsorption at 303 K and 17.6 torr, viewed from two directions; Color scheme: Cu (light blue), O (red), C (gray), N (dark blue), He (powder blue), H (white). Reproduced with permission from ref 67. Copyright © 2012 American Chemical Society.

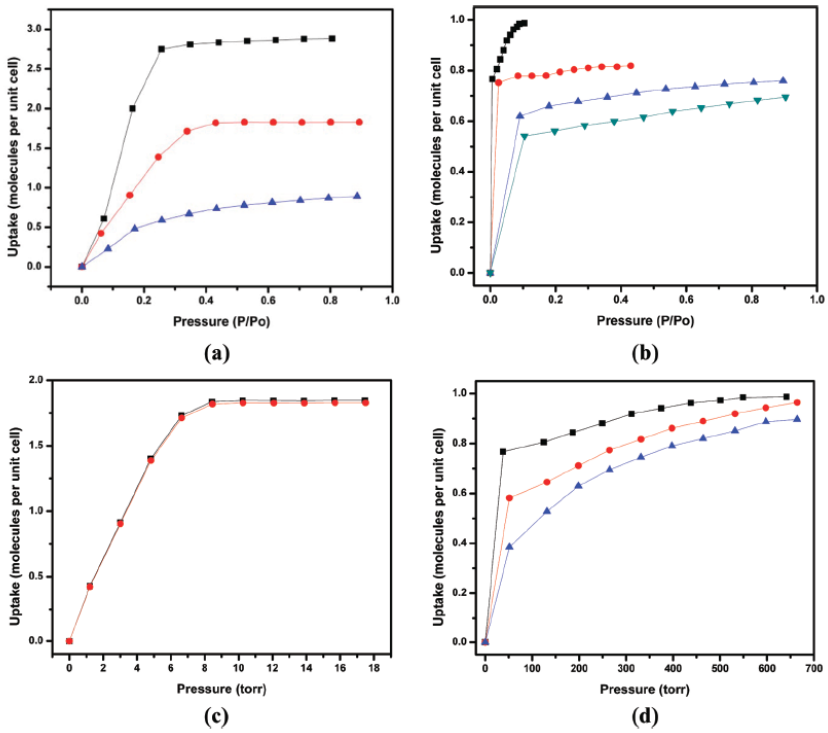

Figure 57. Selected experimental hydrocarbon adsorption isotherms in $[Cu(dhbc)_2(4,4'\text{-bpy})]\cdot H_2O$. (a) Adsorption isotherms of benzene (black), toluene (red) and *p*-xylene (blue) at 40 °C; (b) Adsorption isotherms of propane (black), *n*-butane (red), *n*-pentane (blue) and *n*-hexane (green) at 30 °C; (c) Adsorption isotherms of toluene at 30 °C (black) and 40 °C (red); (d) Adsorption isotherms of propane at 30 °C (black), 40 °C (red) and 50 °C (blue). (Po is the saturated vapor pressure at the given experimental temperature). Reproduced with permission from ref 67. Copyright © 2012 American Chemical Society.

3.4.2. $[Cd_3(btb)_2(DEF)_4]\cdot 2DEF$

$[Cd_3(btb)_2(DEF)_4]\cdot 2DEF$ (btb=1,3,5-tris(4-carboxyphenyl)benzene, DEF = N,N-diethylformamide) is another 2D structure[414] that may exhibit commensurate adsorption, as suggested from our simulation results. Two types of 1D channels (both of rhombus shaped cross section) may be generated upon stacking of the 2D bilayers. A larger one (type-A) with a cage size of 8.45×8.45 Å becomes accessible after removal of guest (non-coordinated) DEF molecules, as indicated in Fig. 18a, and a smaller one (type-B) with a cage size of 8.16×8.16 Å can be obtained if coordinated DEF molecules are removed.[414]

The structure remains intact if only the guest DEFs are taken off, while removal of both guest and coordinated DEFs will lead to a structure change. To avoid structure alternation, simulations are performed on the structure in which only type-A channels are made accessible. The neck of the channel A is estimated to be ~4.3×4.5 Å (cages dimensions: ~6.7×5.4 Å, see Fig. 58b) based on the He data using the reported crystal structure. The narrow neck cuts the 1D channel into individual segments by a repeating distance of 10.5 Å which is coincident with the length of the *a*-axis. Simulations are performed on benzene, toluene and *p*-xylene (Fig. 58c-e). For benzene, the smallest and slimmest one among the three aromatic hydrocarbons, a pair of molecules can be fit within a single segment or a single unit cell (one segment per unit cell). For larger adsorbates such as toluene and *p*-xylene only one molecule can be fit in a segment. Both are tilted so as to better accommodate the shape of the pores and to keep the methyl groups farther apart from the adjacent molecules. The simulated commensurate adsorption of these hydrocarbons certainly needs to be verified by future experimental isotherm measurements.

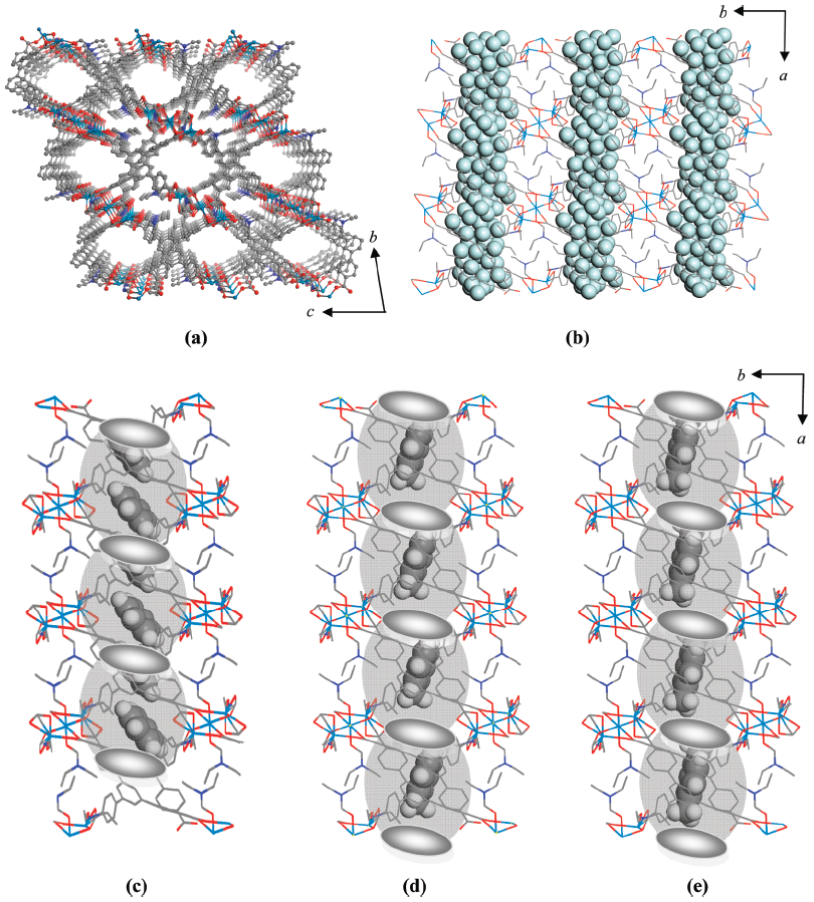

Figure 58. (a) Crystal structure of $[Cd_3(btb)_2(DEF)_4]\cdot 2DEF$. (b-e) The simulated gas adsorption in the $[Cd_3(btb)_2(DEF)_4]\cdot 2DEF$ structure. The 1D channels are parallel to the crystallographic *a*-axis: (b) He at 1 K and 760 torr; (c) benzene at 303 K and 61 torr; (d) toluene at 303 K and 17.6 torr; (e) *p*-xylene at 303 K and 5.1 torr. Color scheme: Cd (light blue), O (red), C (gray), N (dark blue), He (powder blue), H (white). Reproduced with permission from ref 67. Copyright © 2012 American Chemical Society.

3.5. Concluding remarks

As a new type of adsorbate materials with distinctly advantageous features, microporous metal organic frameworks demonstrate enormous potential for adsorption based applications, including storage, separation and purification of small gases and hydrocarbons. In this review, we introduce the concept of commensurate adsorption, a fundamentally important and interesting phenomenon that plays a key role in the adsorption processes. We illustrate that commensurate adsorption of hydrocarbons

occurs far more often in MMOFs than in zeolites and related materials, primarily as a result of vastly greater variety of framework types and richer hierarchy of complexity of the pore structures for the former. Among numerous structures in which commensurate adsorption has been observed in the vicinity of room temperature, many have 1D open channels built on pore segments of distinct shape, size and narrow pore window (aperture) that closely match with the geometries of hydrocarbon species. Clearly, the cases discussed in this review represent only a small selected group. Many existing MMOFs for which hydrocarbon adsorptions may be commensurate with their crystal symmetry and pore structures are yet to be fully recognized and investigated. It can be anticipated that further studies of this topic will reveal many more interesting features and trends, offer helpful insight and contribute to better understanding of the adsorbate-adsorbent interactions and the correlation between the crystal symmetry, pore structure and adsorption behavior of hydrocarbon adsorbates, which in turn will facilitate future design and development of new MMOF systems with enhanced functions and performance in adsorption based industrial processes.

Chaper 4: Experimental

4.1 MMOFs Synthesis

4.1.1 $Zn_2(bpdc)_2(bpee)\cdot 2DMF$ (RPM3-Zn)

Crystals of Zn2(BPDC)2(BPEE)·2DMF (**1**) were solvothermally synthesized by mixing Zn(NO3)2·6H2O (0.0892g, 0.30mmol), 4,4-biphenyldicarboxylic acid (H2BPDC, 0.0727g, 0.30mmol) and 1,2-bipyridylethene (BPEE, 0.0547g, 0.30mmol) at molar ratio of 1:1:1 in 15ml DMF solution. The reaction container was heated at 165°C for 3 days and cooled down to room temperature at the rate of 0.1°C/min. Colorless block-like crystals of 1 (0.0657g, 47% yield) were obtained by filtering, washing by DMF three times and drying in vacuum oven.

4.1.2 $Zn_2(bpdc)_2(bpe)\cdot 2DMF$ (RPM4-Zn)

A mixture of zinc (II) nitrate hexahydrate (0.2975g 1.0 mmol), 1,2-bis(4-pyridyl)-ethane-bpe (0.1842g, 1.0 mmol) and 4,4'-biphenyldicarbpxylic acid or H_2bpdc (0.2422g, 1mmol) in DMF (15 mL) and toluene (0.8 mL) was heated in a programmable oven at 170°C for 72 hours before it was cooled to room temperature at a rate of 0.1°C /min. The yellow block-shaped crystals of $Zn_2(bpdc)_2(bpe)\cdot 2DMF$ (**2**) were filtered, rinsed with DMF (10 mL) and dried under vacuum oven for 10 mins (85% yield based on zinc nitrate).

4.1.3 $Zn_2(bdc\text{-}R)_2(ted)\cdot 2DMF\cdot 0.2H_2O$ series (R=H, OH or NH_2)

4.1.3.1 $Zn_2(bdc\text{-}H)_2(ted)\cdot 2DMF\cdot 0.2H_2O$

Single crystals of $[Zn(bdc)(ted)_{0.5}]\cdot 2\ DMF\cdot 0.2H_2O$ (**3**) were grown by solvothermal reactions. A mixture of zinc(II) nitrate hexahydrate (0.156 g, 0.597 mmol), H_2bdc (0.102 g,

0.614 mmol), ted (0.036 g, 0.321 mmol), and 15 mL of DMF were transferred to a Teflon-lined autoclave and heated in an oven at 120 °C for 2 d. Single crystals of **3** (0.212 g, 83% yield) were isolated after filtering and washing the product with DMF (10 mL× 3). The polycrystalline samples were prepared by using the same molar ratio. A mixture of zinc(II) nitrate tetrahydrate (1.56 g), H_2bdc (1.02 g), ted (0.36 g), and 150 mL DMF was transferred to a 250 mL vessel. A clear solution was obtained after a sonic treatment, which dissolved all solid chemicals. The vessel was then covered and heated at 120 °C overnight. Colorless powders of **3** (1.68 g, 65.11% yield) were isolated after filtering and washing three times with 10 mL of DMF.

4.1.3.2 Zn_2(bdc-OH)$_2$(ted)·2DMF·0.2H_2O

Zn(BDC-OH)(TED)$_{0.5}$ (**4**) was prepared by a solvothermal reaction of Zn(NO_3)·6H_2O (0.089g, 0.3 mmol), BDC-OH (0.055g, 0.3 mmol) and TED (0.022g, 0.2 mmol) in 10mL of DMF. The mixture was sealed in a Parr reaction vessel and heated at 373 K for 2 days. After naturally cooling down to room temperature, the colorless rod-like single crystals of **4** (0.080g, 88% yield based on metal) were isolated by filtration and washed with DMF.

4.1.3.3 Zn_2(bdc-NH2)$_2$(ted)·2DMF·0.2H_2O

Zn(BDC-NH_2)(TED)$_{0.5}$ (**5**) was synthesized from Zn(NO_3)·6H_2O, BDC-NH_2 and TED using the same procedure described above for **4**. The reaction yielded 0.075g of **5** as grey needle crystals (82% yield based on metal).

4.1.4 $Zn_2(bdc\text{-}NH2)_2(ted)\cdot 2DMF\cdot 0.2H_2O$

0.030 g (0.049 mmol) of H_6TDPAT was dissolved in 2 mL of DMA, 2 mL of DMSO, 100 μL of H_2O, 0.164 g (0.68 mmol) of $Cu(NO_3)_2\cdot 3H_2O$. Upon adding 0.9 mL of HBF_4, the mixture was sealed in a small vial and heated at 85 ºC for 3 d. After cooling down to room temperature, blue octahedral crystals were filtered and washed with DMA. Yield 0.035 g, 83.3% (based on ligand).

4.2 Low pressure gas adsorption isotherm measurement

All low pressure gas sorption experiments were performed on a volumetric gas sorption analyzer (Autosorb-1 MP, Quantachrome Instruments). Liquid nitrogen and liquid argon were used as coolant to achieve cryogenic temperatures (77 and 87K). Ultra high purity Ar (99.995%) and H2, N2, CO, CO2, and CH4 (99.999%) were used. The Ar and N2 sorption isotherms were collected in a relative pressure range from 10-6 to 1 atmosphere at 87 and 77K, respectively. The initial outgassing process for each sample was carried out at 408K for over night (under vacuum). Outgassed samples in the amount of ~85-90mg were used for gas sorption measurements and the weight of each sample was recorded before and after outgassing to confirm the removal of guest molecules. The outgassing procedure was repeated on the same sample between experiments for 0.5~1 hour. Pore properties (e.g. pore volume, pore size, and surface area) were analyzed using Autosorb v1.50 software.

4.3 Mixed gas adsorption and desorption setup

In a gas mixture adsorption-desorption experiment a vacuum of 3kPa was applied to the activated sample and the off-gas analyzed using a Residual Gas

Analyzing Mass Spectrometer (RGA). A mixture of CO_2 in air was delivered to the sample containing test cell with the outlet valve closed but bleeding off a fraction of the gas through the small diameter tube (127μm) to the RGA (Fig. 10). In most cases the CO_2 fraction (feed concentration) was held at 20%. The gas feed flow rate was 5.7scc/m. Flow continued until the pressure in the test cell reached steady state (~80kPa). At this time the feed valve was closed (time 0:00); the gas bleed continued until the pressure reached a value of 10-13kPa. At this time the valve to the larger diameter tubing (762μm) was opened allowing the pressure to drop more rapidly.

The sorption behavior of the MMOF to the introduced air/CO_2 mixture can be illustrated by three graphs: system pressure vs. time (Fig. 11), CO_2 percentage in the exhaust vs. time and CO_2 percentage vs. system pressure (Inset of Fig. 11). Fig. 11 shows that the pressure increases rapidly as the MMOF is loaded. CO_2 breakthrough is indicated by the shoulder visible between time 55:00 and 0:00. The non-activated (as-made) MMOF (Pink) allows the gas to exit rapidly. In contrast, the activated MMOFs releases the CO_2 more slowly. The entire cycle from start to finish is typically complete in less than 30 minutes; a 12 min load and 15 min unload. The difference in adsorption performance between as made and activated is apparent as the pressure falls. The pressure drops more rapidly for the non-activated material showing practically no adsorption. It falls more slowly for the activated form indicating adsorbed gas is being released, thus extending the time at the higher pressure.

Quickly heating the sample to 50 °C promoted release of the CO_2. In Fig. 11, heating was initiated at time 0. In Fig. 11 there is a distinct increase in the length of time

that the pressure remains high for the heated MMOF, indicating rapid desorption yielding higher pressures. There is a much more rapid increase in the concentration of CO_2 at 50 than 25°C. In the inset of Fig. 11, the partial pressure (PP) of CO_2 increases to a much higher level (33 kPa) than the inlet PP (~20kPa).

4.4 High pressure adsorption measurement and data reduction

All High-pressure adsorption data in this work were collected in HPVA-100 (VTI Scientific Instruments). Ultra high purity Ar (99.995%) and H2, N2, CO, CO2, and CH4 (99.999%) were used.

High pressure adsorption data reduction is as following. The total gas uptake was calculated using the following equation:

$$Q_{tot}=Q_{exc}+100\times d_g\times V_{pore}/(1+dg\times V_{pore})$$

where Q_{tot} = total adsorption (wt %)

Q_{exc} = excess adsorption (wt %)

d_g = density of the compressed gas as a function of temperature and pressure (g/cm^3)

V_{pore} = pore volume (cm^3/g)

The density of the compressed gas, dg, was obtained from the NIST website. The pore volume was calculated from the structure.

The volumetric capacity of the sample was then calculated using:

$$C_{vol} = Q_{ads}\times d_{bulk}$$

where C_{vol} = volumetric adsorption (g/L)

Q_{ads} = quantity of H2 adsorbed (if excess adsorption is used then excess volumetric capacity is obtained. If total adsorption is used, then total volumetric capacity is obtained).

Appendix A--Virial fitting configuration for origin software

1. Obtain a copy of origin software. Install and open it.
2. File Menu > Analysis > Non-linear curve fit > Function > new (pop up small window)
3. in the small window
4. name → put the name " IsoStericHeat"
5. select "Equations" in FORM
6. Click Files and copy below info and paste into blank area. (It is important to keep the same format as shown here)

    [GENERAL INFORMATION]

    Function Name= IsoStericHeat

    Brief Description=user1

    Function Source=N/A

    Function Type=User-Defined

    Function Form=Equations

    Number Of Parameters=14

    Number Of Independent Variables=1

    Number Of Dependent Variables=1

    [FITTING PARAMETERS]

    Naming Method=User-Defined

    Names=a0,a1,a2,a3,a4,a5,a6,a7,a8,b0,b1,b2,b3,temp

Meanings=?

Initial Values=100(V),50(V),5(V),-2(V), 1(V), 0(F), 0(F), 0(F), 0(F), 10(V), 0.01(V), 0(F), 0(F)

Lower Bounds=--(X,OFF)

Upper Bounds=--(X,OFF)

Number Of Significant Digits=

[FORMULA]

y=ln(x)+((1/temp)*(a0+(a1*x)+(a2*x^2)+(a3*x^3)+(a4*x^4)+(a5*x^5)+(a6*x^6)+(a7*x^7)+(a8*x^8)))+(b0+(b1*x) +(b2*x^2)+(b3*x^3))

[CONSTRAINTS]

/*Enter general linear constraints here*/

[CONSTANTS]

[INITIALIZATIONS]

/*Scripts to be executed before fitting, a good place for complicated initialization.*/

[AFTER FITTING]

/*Scripts to be executed after fitting, a good place for generating results.*/

[INDEPENDENT VARIABLES]

x=

[DEPENDENT VARIABLES]

y=

[CONTROLS]

General Linear Constraints=Off

Initialization Scripts=On

Scripts After Fitting=Off

Number Of Duplicates=N/A

Duplicate Offset=N/A

Duplicate Unit=N/A

Generate Curves After Fitting=Yes

Curve Point Spacing=Uniform on X-Axis Scale

Generate Peaks After Fitting=Yes

Generate Peaks During Fitting=Yes

Generate Peaks with Baseline=Yes

Paste Parameters to Plot After Fitting=Yes

Paste Parameters to Notes Window After Fitting=Yes

Generate Residue After Fitting=No

Keep Parameters=No

7. Then click "Save" to have equation stored in origin.
8. Open two data sheet in Origin. Suppose we are working on 77K and 87K H2 data to estimate H2 heat of adsorption.

A. Creating correct format for adsorption data

Make two data sheet as following format. If you are working on 3 sets of room temperature (T1, T2 and T3) isotherms, make 3 data sheet for each instead.

Data1 (77K data)

1st column; P/Po (x1-axis)

2nd column; wt% (y1-axis)

3rd column; mg/g (x2-axis)

4th column; lnp(torr) (y2-axis)

Data2 (87K data)

1st column; P/Po (x1-axis)

2nd column; wt% (y1-axis)

3rd column; mg/g (x2-axis)

4th column; lnp(torr) (y2-axis)

Plot both data (using x2 and y2) in one chart

x-axis (mg/g), y-axis (lnp(torr))

B. Fitting (find coefficients of virial equation)

1. File Menu > Analysis > Non-linear curve fit > select "IsoStericHeat" in right window

2. Action > initialize

3. Action > dataset > you have three boxes now

check box "Fit multiple datasets" then click "Add data" button

4. go top box and select "y1 dep" and select column from middle box (data1_d)

Then check right number in row (1 <= row <= 31(=number of data))

Then click “Assign” button

5. go top box and select “y2 dep” and select column from middle box (data2_d)

Then check right number in row (1 <= row <= 31(=number of data))

Then click “Assign” button

9. go to third box
10. click all parameters one by one to have them “Shared” except “temp”
11. file menu; Action>fit
12. scroll all the way down in the first box
13. put 77 in temp and 87 in temp_2
14. then click “ 10 Iter” button
15. then you will see the result in the box
16. check “ Reduced Chi-sqr = 0.0035xx ”

    if “Chi-sqr” less than 0.01~0.02, fitting result is great

    if “Chi-sqr” higher than 0.03, use more variable in the first box

    (you can simply check box in “vary?” column)
17. then go to Action>result
18. click “Param.Worksheet” to generate parameter work sheet
19. then you can see “R2=0.99xx” value and several “coefficients” on the graph
20. go to “parameter worksheet” and copy “a0 to a6 and correspond error”
21. paste them in the Qst work sheet.

22. then change “C12” value from 87K data

23. then you will see Qst plot.

Biography

Haohan Wu obtained his Bachelor of Science degree in Material Science and Engineering from University of Science and Technology of China in 2007. Currently he is the Ph. D program at the department of Chemistry and Chemical Biology, Rutgers - The State University of New Jersey, under the direction of Professor Jing Li. He is a recipient of 2010 Van Dyke Award for Excellence in Research and 2012 Reid Award for Excellent in Research. His main research interests are on the adsorption-based gas storage and separation using porous materials and investigation of gas adsorption behavior and mechanism. His biggest hobby is soccer.

List of Abbreviations

1D	one dimensional
2-cim	2-chloroimidazole
22DMB	2,2-dimethylbutane
2-mim	2-methylimidazole
2D	two dimensional
3D	three dimensional
3MP	3-methylpentane
4,4’-bipy	4,4’-bipyridine
4-btapa	1,3,5-benzene tricarboxylate tris[N-(4-pyridyl)amide]
bdc	1,4-benzenedicarboxylate
bim	benzimidazole
bpdc	4,4’-biphenyldicarboxylate

bpe	1,2-bis(4-pyridyl)ethane
bpee	1,2-bis(4-pyridyl)ethene
bptc	4,4′-bipyridine-2,6,2′,6′-tetracarboxylate
btb	1,3,5-tris(4-carboxyphenyl) benzene
btc	1,3,5-benzenetricarboxylate
dabco	1,4-diazabicyclo[2.2.2]-octane
dhbc	2,5-dihydroxybenzoic acid
$C_3°$	propane
$C_3^=$	propene
CBMC	configurational-bias Monte Carlo
DEF	N,N-diethylformamide
DFT	density functional theory
DME	dimethyl-ether
DMF	N,N-dimethylformamide
dpyg	1,2-di(4-pyridyl)glycol
EB	ethyl benzene
etz	3,5-diethyl-1,2,4-triazolate
fa	formate
GC	gas chromatography
GCMC	grand canonical Monte-Carlo
gla	glutarate
H_2hfipbb	4,4′-(hexafluoroisopropylidene)bis(benzoic acid)
IF	interference

IR	infrared
LEED	low energy electron diffraction
m	meta-
*m*X	*m*-xylene
MD	molecular dynamics
Me_2trzpba	4-(3,5-dimethyl-4H-1,2,4-triazol-4-yl)benzoate
MIL	Materials of "Institut Lavoisier"
MMOFs	Microporous Metal Organic Frameworks
molec	molecule(s)
MOFs	Metal Organic Frameworks
mol	mole(s)
nHEX	*n*-hexane
NOVA	NO Void Analysis
NRS	Not reaching saturation
o	ortho-
*o*X	*o*-xylene
p	para-
P	Experimental pressure
PBU	primary building unit
Po	Saturation pressure
*p*X	*p*-xylene
PXRD	powder X-ray diffraction
pyz	pyrazine

pzdc	pyrazine-2,3-dicarboxylate
Q_{st}	isosteric heat of adsorption
R.C.	relative concentration
RPM	Rutgers Recyclable Porous Materials
SBU	secondary building unit
STP	standard temperature and pressure @ 273 K and 760 torr
tbip	5-tert butylisophthalate
tci	3,3′,3″-(2,4,6-trioxo-1,3,5-triazinane-1,3,5triyl)tripropionate
TDS	thermal desorption mass spectroscopy
TEAS	thermal energy atom scattering
UC	unit cell
VB	vinyl benzene
ZIF	zeolitic imidazolate framework

References

(1) Zhou, H.-C.; Long, J. R.; Yaghi, O. M. *Chem. Rev.* **2012**, *112*, 673.
(2) Long, J. R.; Yaghi, O. M. *Chem. Soc. Rev.* **2009**, *38*, 1213.
(3) Ferey, G. *Chemical Society Reviews* **2008**, *37*, 191.
(4) James, S. L. *Chem. Soc. Rev.* **2003**, *32*, 276.
(5) Sing, K. S. W. *Pure Appl. Chem.*, **1982**, *54*, 2201.
(6) Mueller, U.; Schubert, M.; Teich, F.; Puetter, H.; Schierle-Arndt, K.; Pastre, J. *J. Mater. Chem.* **2006**, *16*, 626.
(7) Kitagawa, S.; Kitaura, R.; Noro, S.-i. *Angew. Chem. Int. Ed.* **2004**, *43*, 2334.
(8) Rosseinsky, M. J. *Microporous Mesoporous Mater.* **2004**, *73*, 15.
(9) Rowsell, J. L. C.; Yaghi, O. M. *Microporous Mesoporous Mater.* **2004**, *73*, 3.
(10) Li, H.; Eddaoudi, M.; O'Keeffe, M.; Yaghi, O. M. *Nature* **1999**, *402*, 276.
(11) Seki, K.; Mori, W. *J. Phys. Chem. B* **2002**, *106*, 1380.
(12) Dybtsev, D. N.; Chun, H.; Kim, K. *Angew. Chem. Int. Ed.* **2004**, *43*, 5033.
(13) Pan, L.; Adams, K. M.; Hernandez, H. E.; Wang, X.; Zheng, C.; Hattori, Y.; Kaneko, K. *J. Am. Chem. Soc.* **2003**, *125*, 3062.
(14) Rosi, N. L.; Eckert, J.; Eddaoudi, M.; Vodak, D. T.; Kim, J.; O'Keeffe, M.; Yaghi, O. M. *Science* **2003**, *300*, 1127.
(15) Rowsell, J. L. C.; Millward, A. R.; Park, K. S.; Yaghi, O. M. *J. Am. Chem. Soc.* **2004**, *126*, 5666.
(16) Kesanli, B.; Cui, Y.; Smith, M. R.; Bittner, E. W.; Bockrath, B. C.; Lin, W. *Angew. Chem. Int. Ed.* **2005**, *44*, 72.
(17) Rowsell, J. L. C.; Yaghi, O. M. *Angew. Chem. Int. Ed.* **2005**, *44*, 4670.
(18) Zhao, X.; Xiao, B.; Fletcher, A. J.; Thomas, K. M.; Bradshaw, D.; Rosseinsky, M. J. *Science* **2004**, *306*, 1012.
(19) Lee, E. Y.; Jang, S. Y.; Suh, M. P. *J. Am. Chem. Soc.* **2005**, *127*, 6374.
(20) Kubota, Y.; Takata, M.; Matsuda, R.; Kitaura, R.; Kitagawa, S.; Kato, K.; Sakata, M.; Kobayashi, T. C. *Angew. Chem. Int. Ed.* **2005**, *44*, 920.
(21) Chun, H.; Dybtsev, D. N.; Kim, H.; Kim, K. *Chem.- Eur. J.* **2005**, *11*, 3521.
(22) Kaye, S. S.; Long, J. R. *J. Am. Chem. Soc.* **2005**, *127*, 6506.
(23) Ferey, G.; Latroche, M.; Serre, C.; Millange, F.; Loiseau, T.; Percheron-Guegan, A. *Chem. Commun.* **2003**, *24*, 2976.
(24) Millward, A. R.; Yaghi, O. M. *J. Am. Chem. Soc.* **2005**, *127*, 17998.
(25) O'Keeffe, M. *Chem. Soc. Rev.* **2009**, *38*, 1215.
(26) Perry Iv, J. J.; Perman, J. A.; Zaworotko, M. J. *Chem. Soc. Rev.* **2009**, *38*, 1400.
(27) Tranchemontagne, D. J.; Mendoza-Cortes, J. L.; O'Keeffe, M.; Yaghi, O. M. *Chem. Soc. Rev.* **2009**, *38*, 1257.
(28) Murray, L. J.; Dinca, M.; Long, J. R. *Chem. Soc. Rev.* **2009**, *38*, 1294.
(29) Suh, M. P.; Park, H. J.; Prasad, T. K.; Lim, D.-W. *Chem. Rev.* **2011**, *112*, 782.
(30) Getman, R. B.; Bae, Y.-S.; Wilmer, C. E.; Snurr, R. Q. *Chem. Rev.* **2011**, *112*, 703.
(31) Wu, H.; Reali, R. S.; Smith, D. A.; Trachtenberg, M. C.; Li, J. *Chem.- Eur. J.* **2010**, *16*, 13951.

(32) Zhang, J. M.; Wu, H. H.; Emge, T. J.; Li, J. *Chem. Commun.* **2010**, *46*, 9152.
(33) Rosenbach Jr, N.; Ghoufi, A.; Deroche, I.; Llewellyn, P. L.; Devic, T.; Bourrelly, S.; Serre, C.; Ferey, G.; Maurin, G. *Phys. Chem. Chem. Phys.* **2010**, *12*, 6428.
(34) Kishan, M. R.; Tian, J.; Thallapally, P. K.; Fernandez, C. A.; Dalgarno, S. J.; Warren, J. E.; McGrail, B. P.; Atwood, J. L. *Chem. Commun.* **2010**, *46*, 538.
(35) Devic, T.; Horcajada, P.; Serre, C.; Salles, F.; Maurin, G.; Moulin, B.; Heurtaux, D.; Clet, G.; Vimont, A.; Greneche, J. M.; Le Ouay, B.; Moreau, F.; Magnier, E.; Filinchuk, Y.; Marrot, J.; Lavalley, J. C.; Daturi, M.; Ferey, G. *J. Am. Chem. Soc.* **2010**, *132*, 1127.
(36) Boutin, A.; Coudert, F. o.-X.; Springuel-Huet, M.-A.; Neimark, A. V.; Férey, G. r.; Fuchs, A. H. *J. Phys. Chem. C* **2010**, *114*, 22237.
(37) Czaja, A. U.; Trukhan, N.; Muller, U. *Chemical Society Reviews* **2009**, *38*, 1284.
(38) Pan, L.; Parker, B.; Huang, X.; Olson, D. H.; Lee; Li, J. *J. Am. Chem. Soc.* **2006**, *128*, 4180.
(39) Pan, L.; Olson, D. H.; Ciemnolonski, L. R.; Heddy, R.; Li, J. *Angew. Chem. Int. Ed.* **2006**, *45*, 616.
(40) Li, J. R.; Kuppler, R. J.; Zhou, H. C. *Chemical Society Reviews* **2009**, *38*, 1477.
(41) Sircar, S.; Wu, H.; Li, J.; Lueking, A. D. *Langmuir* **2011**, *27*, 14169.
(42) Lee, C. Y.; Bae, Y.-S.; Jeong, N. C.; Farha, O. K.; Sarjeant, A. A.; Stern, C. L.; Nickias, P.; Snurr, R. Q.; Hupp, J. T.; Nguyen, S. T. *J. Am. Chem. Soc.* **2011**, *133*, 5228.
(43) Saha, D.; Bao, Z. B.; Jia, F.; Deng, S. G. *Environ. Sci. Technol.* **2010**, *44*, 1820.
(44) Zacher, D.; Shekhah, O.; Woll, C.; Fischer, R. A. *Chem. Soc. Rev.* **2009**, *38*, 1418.
(45) Li, K.; Olson, D. H.; Seidel, J.; Emge, T. J.; Gong, H.; Zeng, H.; Li, J. *J. Am. Chem. Soc.* **2009**, *131*, 10368.
(46) Yoon, M.; Srirambalaji, R.; Kim, K. *Chem. Rev.* **2011**, *112*, 1196.
(47) Ma, L. Q.; Abney, C.; Lin, W. B. *Chem. Soc. Rev.* **2009**, *38*, 1248.
(48) Lee, J.; Farha, O. K.; Roberts, J.; Scheidt, K. A.; Nguyen, S. T.; Hupp, J. T. *Chem. Soc. Rev.* **2009**, *38*, 1450.
(49) Farrusseng, D.; Aguado, S.; Pinel, C. *Angew. Chem. Int. Edit.* **2009**, *48*, 7502.
(50) Wang, C.; Zhang, T.; Lin, W. *Chem. Rev.* **2011**, *112*, 1084.
(51) Demessence, A.; Horcajada, P.; Serre, C.; Boissiere, C.; Grosso, D.; Sanchez, C.; Ferey, G. *Chem. Commun.* **2009**, 7149.
(52) Guo, Z.; Cao, R.; Wang, X.; Li, H.; Yuan, W.; Wang, G.; Wu, H.; Li, J. *Journal of the American Chemical Society* **2009**, *131*, 6894.
(53) McKinlay, A. C.; Morris, R. E.; Horcajada, P.; Ferey, G.; Gref, R.; Couvreur, P.; Serre, C. *Angew. Chem. Int. Ed.* **2010**, *49*, 6260.
(54) Sun, C.-Y.; Qin, C.; Wang, C.-G.; Su, Z.-M.; Wang, S.; Wang, X.-L.; Yang, G.-S.; Shao, K.-Z.; Lan, Y.-Q.; Wang, E.-B. *Adv. Mater.* **2011**, *23*, 5629.
(55) Horcajada, P.; Gref, R.; Baati, T.; Allan, P. K.; Maurin, G.; Couvreur, P.; Ferey, G.; Morris, R. E.; Serre, C. *Chemical Review* **2012**, *112*, 1232.
(56) Nijem, N.; Kong, L.; Zhao, Y.; Wu, H.; Li, J.; Langreth, D. C.; Chabal, Y. J. *Journal of the American Chemical Society* **2011**, *133*, 4782.

(57) Lan, A.; Padmanabhan, M.; Li, K.; Wu, H.; Emge, T. J.; Hong, M.; Li, J. *Inorganica Chimica Acta* **2011**, *366*, 68.
(58) Banerjee, D.; Kim, S. J.; Wu, H.; Xu, W.; Borkowski, L. A.; Li, J.; Parise, J. B. *Inorganic Chemistry* **2011**, *50*, 208.
(59) Nijem, N.; Veyan, J.-F.; Kong, L.; Wu, H.; Zhao, Y.; Li, J.; Langreth, D. C.; Chabal, Y. J. *Journal of the American Chemical Society* **2010**, *132*, 14834.
(60) Banerjee, D.; Kim, S. J.; Li, W.; Wu, H.; Li, J.; Borkowski, L. A.; Philips, B. L.; Parise, J. B. *Crystal Growth & Design* **2010**, *10*, 2801.
(61) Doukelis, A.; Vorrias, I.; Grammelis, P.; Kakaras, E.; Whitehouse, M.; Riley, G. *Fuel* **2009**, *88*, 2428.
(62) Lan, A.; Li, K.; Wu, H.; Olson, D. H.; Emge, T. J.; Ki, W.; Hong, M.; Li, J. *Angewandte Chemie-International Edition* **2009**, *48*, 2334.
(63) Huang, G.; Yang, C.; Xu, Z.; Wu, H.; Li, J.; Zeller, M.; Hunter, A. D.; Chui, S. S.-Y.; Che, C.-M. *Chemistry of Materials* **2009**, *21*, 541.
(64) Xie, Y.; Yan, Y.; Wu, H.-H.; Yong, G.-P.; Cui, Y.; Wang, Z.-Y.; Pan, L.; Li, J.; Fan, R.; Li, R.-P.; Tian, Y.-C.; Pan, G.-Q.; Sheng, L.-S.; Li, X. *Inorganica Chimica Acta* **2007**, *360*, 1669.
(65) Xie, Y.; Wu, H.-H.; Yong, G.-P.; Wang, Z.-Y.; Fan, R.; Li, R.-P.; Pan, G.-Q.; Tian, Y.-C.; Sheng, L.-S.; Pan, L.; Li, J. *Journal of Molecular Structure* **2007**, *833*, 88.
(66) Wu, H.; Yao, K.; Zhu, Y.; Li, B.; Shi, Z.; Krishna, R.; Li, J. *Journal of Physical Chemistry C* **2012**, *116*, 16609.
(67) Wu, H.; Gong, Q.; Olson, D. H.; Li, J. *Chemical Reviews* **2012**, *112*, 836.
(68) Nijem, N.; Wu, H.; Canepa, P.; Marti, A.; Balkus, K. J., Jr.; Thonhauser, T.; Li, J.; Chabal, Y. J. *Journal of the American Chemical Society* **2012**, *134*, 15201.
(69) Li, B.; Zhang, Z.; Li, Y.; Yao, K.; Zhu, Y.; Deng, Z.; Yang, F.; Zhou, X.; Li, G.; Wu, H.; Nijem, N.; Chabal, Y. J.; Lai, Z.; Han, Y.; Shi, Z.; Feng, S.; Li, J. *Angewandte Chemie-International Edition* **2012**, *51*, 1412.
(70) Lee, J. Y.; Wu, H.; Li, J. *International Journal of Hydrogen Energy* **2012**, *37*, 10473.
(71) Zhao, Y.; Wu, H.; Emge, T. J.; Gong, Q.; Nijem, N.; Chabal, Y. J.; Kong, L.; Langreth, D. C.; Liu, H.; Zeng, H.; Li, J. *Chemistry-a European Journal* **2011**, *17*, 5101.
(72) Wu, H.; Zhang, Z.; Zhao, Y.; Zhang, J.; Li, J. *Abstracts of Papers of the American Chemical Society* **2011**, *242*.
(73) Sircar, S.; Wu, H.; Li, J.; Lueking, A. D. *Langmuir* **2011**, *27*, 14169.
(74) Nijem, N.; Thissen, P.; Yao, Y.; Longo, R. C.; Roodenko, K.; Wu, H.; Zhao, Y.; Cho, K.; Li, J.; Langreth, D. C.; Chabal, Y. J. *Journal of the American Chemical Society* **2011**, *133*, 12849.
(75) Zhang, J.; Wu, H.; Emge, T. J.; Li, J. *Chemical Communications* **2010**, *46*, 9152.
(76) Wu, H.; Reali, R. S.; Smith, D. A.; Trachtenberg, M. C.; Li, J. *Chemistry-a European Journal* **2010**, *16*, 13951.
(77) Lan, A.; Li, K.; Wu, H.; Kong, L.; Nijem, N.; Olson, D. H.; Emge, T. J.; Chabal, Y. J.; Langreth, D. C.; Hong, M.; Li, J. *Inorganic Chemistry* **2009**, *48*, 7165.

(78) Heinberg, R. *The Party's Over: Oil, War, and the Fate of Industrial Societies*; New Society Publishers: Gabriola Island, Canada, 2005.
(79) Sumida, K.; Rogow, D. L.; Mason, J. A.; McDonald, T. M.; Bloch, E. D.; Herm, Z. R.; Bae, T.-H.; Long, J. R. *Chem. Rev.* **2011**, *112*, 724.
(80) Lan, A. J.; Li, K. H.; Wu, H. H.; Kong, L. Z.; Nijem, N.; Olson, D. H.; Emge, T. J.; Chabal, Y. J.; Langreth, D. C.; Hong, M. C.; Li, J. *Inorg. Chem.* **2009**, *48*, 7165.
(81) Ferey, G.; Serre, C. *Chemical Society Reviews* **2009**, *38*, 1380.
(82) Walton, K. S.; Millward, A. R.; Dubbeldam, D.; Frost, H.; Low, J. J.; Yaghi, O. M.; Snurr, R. Q. *J. Am. Chem. Soc.* **2008**, *130*, 406.
(83) Choi, H. S.; Suh, M. P. *Angew. Chem. Int. Edit.* **2009**, *48*, 6865.
(84) Caskey, S. R.; Wong-Foy, A. G.; Matzger, A. J. *J. Am. Chem. Soc.* **2008**, *130*, 10870.
(85) Bourrelly, S.; Llewellyn, P. L.; Serre, C.; Millange, F.; Loiseau, T.; Férey, G. *J. Am. Chem. Soc.* **2005**, *127*, 13519.
(86) Bao, L.; Trachtenberg, M. C. *Chem. Eng. Sci.* **2005**, *60*, 6868.
(87) Choi, H. J.; Dincai, M.; Long, J. R. *J. Am. Chem. Soc.* **2008**, *130*, 7848.
(88) Llewellyn, P. L.; Maurin, G.; Devic, T.; Loera-Serna, S.; Rosenbach, N.; Serre, C.; Bourrelly, S.; Horcajada, P.; Filinchuk, Y.; Férey, G. r. *J. Am. Chem. Soc.* **2008**, *130*, 12808.
(89) Llewellyn, P. L.; Bourrelly, S.; Serre, C.; Filinchuk, Y.; Férey, G. *Angew. Chem. Int. Ed.* **2006**, *45*, 7751.
(90) Lee, J. Y.; Olson, D. H.; Pan, L.; Emge, T. J.; Li, J. *Adv. Funct. Mater.* **2007**, *17*, 1255.
(91) Zhao, Y.; Wu, H.; Emge, T. J.; Gong, Q.; Nijem, N.; Chabal, Y. J.; Kong, L.; Langreth, D. C.; Liu, H.; Zeng, H.; Li, J. *Chemistry- A European Journal* **2011**, *17*, 5101.
(92) Li, K.; Lee, J.; Olson, D. H.; Emge, T. J.; Bi, W.; Eibling, M. J.; Li, J. *Chem. Commun.* **2008**, 6123.
(93) Bae, Y. S.; Lee, C. H. *Carbon* **2005**, *43*, 95.
(94) Liu, B.; Yang, Q.; Xue, C.; Zhong, C.; Chen, B.; Smit, B. *Journal of Physical Chemistry C* **2008**, *112*, 9854.
(95) Cavenati, S.; Grande, C. A.; Rodrigues, A. E. *J. Chem. Eng. Data* **2004**, *49*, 1095.
(96) Yazaydin, A. O.; Benin, A. I.; Faheem, S. A.; Jakubczak, P.; Low, J. J.; Willis, R. R.; Snurr, R. Q. *Chem. Mater.* **2009**, *21*, 1425.
(97) Siriwardane, R. V.; Shen, M. S.; Fisher, E. P.; Poston, J. A. *Energy & Fuels* **2001**, *15*, 279.
(98) Li, B.; Zhang, Z.; Li, Y.; Yao, K.; Zhu, Y.; Deng, Z.; Yang, F.; Zhou, X.; Li, G.; Wu, H.; Nijem, N.; Chabal, Y. J.; Lai, Z.; Han, Y.; Shi, Z.; Feng, S.; Li, J. *Angew. Chem. Int. Ed.* **2012**, *51*, 1412.
(99) Banerjee, R.; Furukawa, H.; Britt, D.; Knobler, C.; O'Keeffe, M.; Yaghi, O. M. *J. Am. Chem. Soc.* **2009**, *131*, 3875.
(100) Franchi, R. S.; Harlick, P. J. E.; Sayari, A. *Ind. Eng. Chem. Res.* **2005**, *44*, 8007.
(101) Bae, Y. S.; Farha, O. K.; Spokoyny, A. M.; Mirkin, C. A.; Hupp, J. T.; Snurr, R. Q. *Chem. Commun.* **2008**, *35*, 4135.
(102) Keskin, S.; Liu, J.; Johnson, J. K.; Sholl, D. S. *Langmuir* **2008**, *24*, 8254.

(103) Britt, D.; Furukawa, H.; Wang, B.; Glover, T. G.; Yaghi, O. M. *PNAS* **2009**, *106*, 20637.
(104) Schlapbach, L.; Zuttel, A. *Nature* **2001**, *414*, 353.
(105) Suh, M. P.; Park, H. J.; Prasad, T. K.; Lim, D.-W. *Chemical Review* **2012**, *112*, 782.
(106) Hu, Y. H.; Zhang, L. *Adv. Mater.* **2010**, *22*, E117.
(107) Mouawad, J. *New York Times* **2009**.
(108) http://www.naturalgas.org/overview/background.asp.
(109) Ma, S. Q.; Zhou, H. C. *Chem. Commun.* **2010**, *46*, 44.
(110) Furukawa, H.; Yaghi, O. M. *J. Am. Chem. Soc.* **2009**, *131*, 8875.
(111) Morris, R. E.; Wheatley, P. S. *Angew. Chem. Int. Edit.* **2008**, *47*, 4966.
(112) Ma, S. Q.; Sun, D. F.; Simmons, J. M.; Collier, C. D.; Yuan, D. Q.; Zhou, H. C. *J. Am. Chem. Soc.* **2008**, *130*, 1012.
(113) Liu, D.; Wu, H.; Wang, S.; Xie, Z.; Li, J.; Lin, W. *Chemical Science* **2012**, *3*, 3032.
(114) Mendoza-Cortés, J. L.; Han, S. S.; Furukawa, H.; Yaghi, O. M.; Goddard, W. A. *J. Phys. Chem. A* **2010**, *114*, 10824.
(115) Beaume, R.; Suzanne, J.; Coulomb, J. P.; Glachant, A.; Bomchil, G. *Surf. Sci.* **1984**, *137*, L117.
(116) Phillips, J. M. *Phys. Rev. B* **1984**, *29*, 4821.
(117) Koch, S. W.; Rudge, W. E.; Abraham, F. F. *Surf. Sci.* **1984**, *145*, 329.
(118) Stephens, P. W.; Heiney, P. A.; Birgeneau, R. J.; Horn, P. M.; Moncton, D. E.; Brown, G. S. *Phys. Rev. B* **1984**, *29*, 3512.
(119) Zhang, Q. M.; Kim, H. K.; Chan, M. H. W. *Phys. Rev. B* **1985**, *32*, 1820.
(120) Gameson, I.; Rayment, T. *Chem. Phys. Lett.* **1986**, *123*, 150.
(121) Hong, H.; Peters, C. J.; Mak, A.; Birgeneau, R. J.; Horn, P. M.; Suematsu, H. *Phys. Rev. B* **1987**, *36*, 7311.
(122) Jiang, S. Y.; Gubbins, K. E.; Zollweg, J. A. *Mol. Phys.* **1993**, *80*, 103.
(123) Shrimpton, N. D.; Steele, W. A. *Phys. Rev. B* **1991**, *44*, 3297.
(124) Bruch, L. W.; Novaco, A. D. *Phys. Rev. B* **2008**, *77*, 125435.
(125) Freimuth, H.; Wiechert, H.; Lauter, H. J. *Surf. Sci.* **1987**, *189*, 548.
(126) Lauter, H. J.; Frank, V. L. P.; Leiderer, P.; Wiechert, H. *Physica B* **1989**, *156*, 280.
(127) Novaco, A. D. *Phys. Rev. B* **1992**, *46*, 8178.
(128) Frank, V. L. P.; Lauter, H. J.; Leiderer, P. *Phys. Rev. Lett.* **1988**, *61*, 436.
(129) Weimer, W.; Knorr, K.; Wiechert, H. *Phys. Rev. Lett.* **1988**, *61*, 1623.
(130) Rabedeau, T. A. *Phys. Rev. B* **1989**, *39*, 9643.
(131) Greywall, D. S. *Phys. Rev. B* **1993**, *47*, 309.
(132) Feng, Y. P.; Chan, M. H. W. *Phys. Rev. Lett.* **1990**, *64*, 2148.
(133) Kortmann, K. D.; Leinbock, B.; Wiechert, H.; Fain, S. C.; Stusser, N. *Physica B* **1997**, *234*, 167.
(134) Hansen, F. Y.; Bruch, L. W. *Phys. Rev. B* **1995**, *51*, 2515.
(135) Hansen, F. Y.; Bruch, L. W.; Taub, H. *Phys. Rev. B* **1996**, *54*, 14077.
(136) Poelsema, B.; Verheij, L. K.; Comsa, G. *Surf. Sci.* **1985**, *152*, 851.
(137) Kern, K.; David, R.; Palmer, R. L.; Comsa, G. *Phys. Rev. Lett.* **1986**, *56*, 620.
(138) Black, J. E.; Janzen, A. *Phys. Rev. B* **1989**, *39*, 6238.

(139) Kern, K.; Zeppenfeld, P.; David, R.; Comsa, G. *Phys. Rev. Lett.* **1987**, *59*, 79.
(140) Ramseyer, C.; Hoang, P. N. M.; Girardet, C. *Phys. Rev. B* **1994**, *49*, 2861.
(141) Ramseyer, C.; Pouthier, V.; Girardet, C.; Zeppenfeld, P.; Buchel, M.; Diercks, V.; Comsa, G. *Phys. Rev. B* **1997**, *55*, 13203.
(142) Berndt, W. *Surf. Sci.* **1989**, *219*, 161.
(143) Schmiedl, R.; Nichtlpecher, W.; Heinz, K.; Muller, K.; Christmann, K. *Surf. Sci.* **1990**, *235*, 186.
(144) Nichtlpecher, W.; Stammler, W.; Heinz, K.; Muller, K. *Phys. Rev. B* **1991**, *43*, 6946.
(145) Yang, S. H.; Phillips, J. M. *Phys. Rev. B* **2007**, *75*, 235408.
(146) Schuster, R.; Robinson, I. K.; Kuhnke, K.; Ferrer, S.; Alvarez, J.; Kern, K. *Phys. Rev. B* **1996**, *54*, 17097.
(147) Marinelli, F.; Grillet, Y.; Pellenq, R. J. M. *Mol. Phys.* **1999**, *97*, 1207.
(148) Olson, D. H.; Kokotailo, G. T.; Lawton, S. L.; Meier, W. M. *J. Phys. Chem.* **1981**, *85*, 2238.
(149) Reischman, P. T.; Schmitt, K. D.; Olson, D. H. *J. Phys. Chem.* **1988**, *92*, 5165.
(150) Olson, D. H.; Reischman, P. T. *Zeolites* **1996**, *17*, 434.
(151) Makowski, W.; Majda, D. *Appl. Surf. Sci.* **2005**, *252*, 707.
(152) Richards, R. E.; Rees, L. V. C. *Langmuir* **1987**, *3*, 335.
(153) Sun, X. Y.; Li, J. W.; Li, Y. X.; Yan, S. C.; Chen, B. H. *Chem. Res. Chin. Univ.* **2009**, *25*, 377.
(154) Barrett, P. A.; Boix, T.; Puche, M.; Olson, D. H.; Jordan, E.; Koller, H.; Camblor, M. A. *Chem. Commun.* **2003**, 2114.
(155) Olson, D. H.; Yang, X.; Camblor, M. A. *J. Phys. Chem. B* **2004**, *108*, 11044.
(156) Floquet, N.; Coulomb, J. P.; Bellat, J. P.; Simon, J. M.; Weber, G.; Andre, G. *J. Phys. Chem. C* **2007**, *111*, 18182.
(157) Floquet, N.; Simon, J. M.; Coulomb, J. P.; Bellat, J. P.; Weber, G.; Andre, G. *Microporous Mesoporous Mater.* **2009**, *122*, 61.
(158) Morell, H.; Angermund, K.; Lewis, A. R.; Brouwer, D. H.; Fyfe, C. A.; Gies, H. *Chem. Mater.* **2002**, *14*, 2192.
(159) Gutiérrez-Sevillano, J. J.; Dubbeldam, D.; Rey, F.; Valencia, S.; Palomino, M.; Martín-Calvo, A.; Calero, S. a. *J. Phys. Chem. C* **2010**, *114*, 14907.
(160) Zhu, W.; Kapteijn, F.; Moulijn, J. A. *Phys. Chem. Chem. Phys.* **2000**, *2*, 1989.
(161) Smit, B.; Maesen, T. L. M. *Nature* **1995**, *374*, 42.
(162) Manos, G.; Dunne, L. J.; Chaplin, M. F.; Du, Z. M. *Chem. Phys. Lett.* **2001**, *335*, 77.
(163) van Well, W. J. M.; Wolthuizen, J. P.; Smit, B.; van Hooff, J. H. C.; van Santen, R. A. *Angew. Chem. Int. Ed.* **1995**, *34*, 2543.
(164) Vlugt, T. J. H.; Krishna, R.; Smit, B. *J. Phys. Chem. B* **1999**, *103*, 1102.
(165) Calero, S.; Smit, B.; Krishna, R. *J. Catal.* **2001**, *202*, 395.
(166) Krishna, R.; Calero, S.; Smit, B. *Chem. Eng. J.* **2002**, *88*, 81.
(167) Song, L.; Sun, Z.-L.; Ban, H.-Y.; Dai, M.; Rees, L. *Adsorption* **2005**, *11*, 325.
(168) Mentzen, B. F. *Mater. Res. Bull.* **1987**, *22*, 337.
(169) Mentzen, B. F. *Mater. Res. Bull.* **1987**, *22*, 489.
(170) Mentzen, B. F. *Mater. Res. Bull.* **1992**, *27*, 953.

(171) Mohanty, S.; Davis, H. T.; McCormick, A. V. *Chem. Eng. Sci.* **2000**, *55*, 2779.
(172) Mohanty, S.; Davis, H. T.; McCormick, A. V. *AlChE J.* **2000**, *46*, 1662.
(173) Dubbeldam, D.; Smit, B. *J. Phys. Chem. B* **2003**, *107*, 12138.
(174) Dubbeldam, D.; Calero, S.; Maesen, T. L. M.; Smit, B. *Angew. Chem. Int. Ed.* **2003**, *42*, 3624.
(175) Dubbeldam, D.; Calero, S.; Maesen, T. L. M.; Smit, B. *Phys. Rev. Lett.* **2003**, *90*, 245901.
(176) Krishna, R. *J. Phys. Chem. C* **2009**, *113*, 19756.
(177) Krishna, R.; van Baten, J. M. *Separation and Purification Technology* **2008**, *60*, 315.
(178) Denayer, J. F. M.; Devriese, L. I.; Couck, S.; Martens, J.; Singh, R.; Webley, P. A.; Baron, G. V. *J. Phys. Chem. C* **2008**, *112*, 16593.
(179) Santilli, D. S. *J. Catal.* **1986**, *99*, 335.
(180) Daems, I.; Singh, R.; Baron, G.; Denayer, J. *Chem. Commun.* **2007**, *13*, 1316.
(181) Connolly, M. L. *J. Appl. Crystallogr.* **1983**, *16*, 548.
(182) Shah, D. B.; Guo, C.-J.; Hayhurst, D. T. *J. Chem. Soc., Faraday Trans.* **1995**, *91*, 1143.
(183) Hayhurst, D. T.; Lee, J. C. *New Developments in Zeolites Science and Technology*; Kodansha Ltd, Japan, 1986.
(184) Lee, J.; Li, J.; Jagiello, J. *J. Solid State Chem.* **2005**, *178*, 2527.
(185) Lee, J. Y.; Pan, L.; Kelly, S. P.; Jagiello, J.; Emge, T. J.; Li, J. *Adv. Mater.* **2005**, *17*, 2703.
(186) Wang, Q. M.; Shen, D.; Bülow, M.; Ling Lau, M.; Deng, S.; Fitch, F. R.; Lemcoff, N. O.; Semanscin, J. *Microporous Mesoporous Mater.* **2002**, *55*, 217.
(187) Duren, T.; Bae, Y. S.; Snurr, R. Q. *Chem. Soc. Rev.* **2009**, *38*, 1237.
(188) Fletcher, A. J.; Cussen, E. J.; Bradshaw, D.; Rosseinsky, M. J.; Thomas, K. M. *J. Am. Chem. Soc.* **2004**, *126*, 9750.
(189) Eddaoudi, M.; Kim, J.; Rosi, N.; Vodak, D.; Wachter, J.; O'Keeffe, M.; Yaghi, O. M. *Science* **2002**, *295*, 469.
(190) Düren, T.; Sarkisov, L.; Yaghi, O. M.; Snurr, R. Q. *Langmuir* **2004**, *20*, 2683.
(191) Matsuda, R.; Kitaura, R.; Kitagawa, S.; Kubota, Y.; Belosludov, R. V.; Kobayashi, T. C.; Sakamoto, H.; Chiba, T.; Takata, M.; Kawazoe, Y.; Mita, Y. *Nature* **2005**, *436*, 238.
(192) Han, S. S.; Mendoza-Cortes, J. L.; Goddard, W. A. *Chem. Soc. Rev.* **2009**, *38*, 1460.
(193) Farha, O. K.; Bae, Y. S.; Hauser, B. G.; Spokoyny, A. M.; Snurr, R. Q.; Mirkin, C. A.; Hupp, J. T. *Chem. Commun.* **2010**, *46*, 1056.
(194) Llewellyn, P. L.; Bourrelly, S.; Serre, C.; Vimont, A.; Daturi, M.; Hamon, L.; De Weireld, G.; Chang, J. S.; Hong, D. Y.; Hwang, Y. K.; Jhung, S. H.; Ferey, G. *Langmuir* **2008**, *24*, 7245.
(195) Sarkisov, L.; Düren, T.; Snurr, R. Q. *Mol. Phys.* **2004**, *102*, 211
(196) Demessence, A.; D'Alessandro, D. M.; Foo, M. L.; Long, J. R. *J. Am. Chem. Soc.* **2009**, *131*, 8784.
(197) Park, H. J.; Suh, M. P. *Chem.- Eur. J.* **2008**, *14*, 8812.
(198) Kitaura, R.; Seki, K.; Akiyama, G.; Kitagawa, S. *Angew. Chem. Int. Ed.* **2003**, *42*, 428.

(199) Xu, Q.; Liu, D. H.; Yang, Q. Y.; Zhong, C. L.; Mi, J. G. *J. Mater. Chem.* **2010**, *20*, 706.
(200) Li, K.; Olson, D. H.; Lee, J. Y.; Bi, W.; Wu, K.; Yuen, T.; Xu, Q.; Li, J. *Adv. Funct. Mater.* **2008**, *18*, 2205.
(201) Llewellyn, P. L.; Bourrelly, S.; Serre, C.; Filinchuk, Y.; Ferey, G. *Angew. Chem.-Int. Edit.* **2006**, *45*, 7751.
(202) Dybtsev, D. N.; Chun, H.; Yoon, S. H.; Kim, D.; Kim, K. *Journal of the American Chemical Society* **2003**, *126*, 32.
(203) Dincă, M.; Long, J. R. *J. Am. Chem. Soc.* **2005**, *127*, 9376.
(204) Surblé, S.; Millange, F.; Serre, C.; Düren, T.; Latroche, M.; Bourrelly, S.; Llewellyn, P. L.; Férey, G. *J. Am. Chem. Soc.* **2006**, *128*, 14889.
(205) Loiseau, T.; Lecroq, L.; Volkringer, C.; Marrot, J.; Férey, G.; Haouas, M.; Taulelle, F.; Bourrelly, S.; Llewellyn, P. L.; Latroche, M. *J. Am. Chem. Soc.* **2006**, *128*, 10223.
(206) Navarro, J. A. R.; Barea, E.; Rodríguez-Diéguez, A.; Salas, J. M.; Ania, C. O.; Parra, J. B.; Masciocchi, N.; Galli, S.; Sironi, A. *J. Am. Chem. Soc.* **2008**, *130*, 3978.
(207) Banerjee, R.; Phan, A.; Wang, B.; Knobler, C.; Furukawa, H.; O'Keeffe, M.; Yaghi, O. M. *Science* **2008**, *319*, 939.
(208) Wang, B.; Cote, A. P.; Furukawa, H.; O/'Keeffe, M.; Yaghi, O. M. *Nature* **2008**, *453*, 207.
(209) Chen, B.; Ji, Y.; Xue, M.; Fronczek, F. R.; Hurtado, E. J.; Mondal, J. U.; Liang, C.; Dai, S. *Inorg. Chem.* **2008**, *47*, 5543.
(210) Xue, M.; Ma, S.; Jin, Z.; Schaffino, R. M.; Zhu, G.-S.; Lobkovsky, E. B.; Qiu, S.-L.; Chen, B. *Inorg. Chem.* **2008**, *47*, 6825.
(211) Moon, H. R.; Kobayashi, N.; Suh, M. P. *Inorg. Chem.* **2006**, *45*, 8672.
(212) Hamon, L.; Leclerc, H.; Ghoufi, A.; Oliviero, L.; Travert, A.; Lavalley, J.-C.; Devic, T.; Serre, C.; Férey, G. r.; De Weireld, G.; Vimont, A.; Maurin, G. *J. Phys. Chem. C* **2011**, *115*, 2047.
(213) Grant Glover, T.; Peterson, G. W.; Schindler, B. J.; Britt, D.; Yaghi, O. *Chem. Eng. Sci.* **2011**, *66*, 163.
(214) Ma, S.; Wang, X.-S.; Yuan, D.; Zhou, H.-C. *Angew. Chem. Int. Ed.* **2008**, *47*, 4130.
(215) Bae, Y.-S.; Farha, O. K.; Spokoyny, A. M.; Mirkin, C. A.; Hupp, J. T.; Snurr, R. Q. *Chemical Communications* **2008**, 4135.
(216) Dincă, M.; Yu, A. F.; Long, J. R. *J. Am. Chem. Soc.* **2006**, *128*, 8904.
(217) Ma, S.; Wang, X.-S.; Collier, C. D.; Manis, E. S.; Zhou, H.-C. *Inorg. Chem.* **2007**, *46*, 8499.
(218) Zou, Y.; Hong, S.; Park, M.; Chun, H.; Lah, M. S. *Chem. Commun.* **2007**, *48*, 5182.
(219) Li, C.-J.; Lin, Z.-j.; Peng, M.-X.; Leng, J.-D.; Yang, M.-M.; Tong, M.-L. *Chem. Commun.* **2008**, 6348.
(220) Li, Y.; Yang, R. T. *Langmuir* **2007**, *23*, 12937.
(221) Humphrey, S. M.; Chang, J.-S.; Jhung, S. H.; Yoon, J. W.; Wood, P. T. *Angew. Chem. Int. Ed.* **2007**, *46*, 272.
(222) Yoon, J. W.; Jhung, S. H.; Hwang, Y. K.; Humphrey, S. M.; Wood, P. T.; Chang, J. S. *Adv. Mater.* **2007**, *19*, 1830.

(223) Li, J.-R.; Tao, Y.; Yu, Q.; Bu, X.-H.; Sakamoto, H.; Kitagawa, S. *Chem.- Eur. J.* **2008**, *14*, 2771.
(224) Cheon, Y. E.; Suh, M. P. *Chem.- Eur. J.* **2008**, *14*, 3961.
(225) Thallapally, P. K.; Tian, J.; Radha Kishan, M.; Fernandez, C. A.; Dalgarno, S. J.; McGrail, P. B.; Warren, J. E.; Atwood, J. L. *Journal of the American Chemical Society* **2008**, *130*, 16842.
(226) Bae, Y.-S.; Mulfort, K. L.; Frost, H.; Ryan, P.; Punnathanam, S.; Broadbelt, L. J.; Hupp, J. T.; Snurr, R. Q. *Langmuir* **2008**, *24*, 8592.
(227) Seki, K. *Phys. Chem. Chem. Phys.* **2002**, *4*, 1968.
(228) Maji, T. K.; Mostafa, G.; Matsuda, R.; Kitagawa, S. *J. Am. Chem. Soc.* **2005**, *127*, 17152.
(229) Chen, B.; Ma, S.; Hurtado, E. J.; Lobkovsky, E. B.; Zhou, H.-C. *Inorg. Chem.* **2007**, *46*, 8490.
(230) Ma, S.; Wang, X.-S.; Manis, E. S.; Collier, C. D.; Zhou, H.-C. *Inorg. Chem.* **2007**, *46*, 3432.
(231) Hayashi, H.; Cote, A. P.; Furukawa, H.; O/'Keeffe, M.; Yaghi, O. M. *Nat. Mater.* **2007**, *6*, 501.
(232) Maji, T. K.; Matsuda, R.; Kitagawa, S. *Nat. Mater.* **2007**, *6*, 142.
(233) Chen, B.; Ma, S.; Hurtado, E. J.; Lobkovsky, E. B.; Liang, C.; Zhu, H.; Dai, S. *Inorg. Chem.* **2007**, *46*, 8705.
(234) Chen, B.; Ma, S.; Zapata, F.; Fronczek, F. R.; Lobkovsky, E. B.; Zhou, H.-C. *Inorg. Chem.* **2007**, *46*, 1233.
(235) Tanaka, D.; Nakagawa, K.; Higuchi, M.; Horike, S.; Kubota, Y.; Kobayashi, T. C.; Takata, M.; Kitagawa, S. *Angew. Chem. Int. Ed.* **2008**, *47*, 3914.
(236) Xiao, B.; Wheatley, P. S.; Zhao, X. B.; Fletcher, A. J.; Fox, S.; Rossi, A. G.; Megson, I. L.; Bordiga, S.; Regli, L.; Thomas, K. M.; Morris, R. E. *J. Am. Chem. Soc.* **2007**, *129*, 1203.
(237) Ingleson, M. J.; Heck, R.; Gould, J. A.; Rosseinsky, M. J. *Inorg. Chem.* **2009**, *48*, 9986.
(238) McKinlay, A. C.; Xiao, B.; Wragg, D. S.; Wheatley, P. S.; Megson, I. L.; Morris, R. E. *J. Am. Chem. Soc.* **2008**, *130*, 10440.
(239) Bárcia, P. S.; Zapata, F.; Silva, J. A. C.; Rodrigues, A. E.; Chen, B. *J. Phys. Chem. B* **2007**, *111*, 6101.
(240) Maes, M.; Vermoortele, F.; Alaerts, L.; Couck, S.; Kirschhock, C. E. A.; Denayer, J. F. M.; De Vos, D. E. *J. Am. Chem. Soc.* **2010**, *132*, 15277.
(241) Maes, M.; Alaerts, L.; Vermoortele, F.; Ameloot, R.; Couck, S.; Finsy, V.; Denayer, J. F. M.; De Vos, D. E. *J. Am. Chem. Soc.* **2010**, *132*, 2284.
(242) Finsy, V.; Kirschhock, C. E. A.; Vedts, G.; Maes, M.; Alaerts, L.; De Vos, D. E.; Baron, G. V.; Denayer, J. F. M. *Chem.- Eur. J.* **2009**, *15*, 7724.
(243) Alaerts, L.; Maes, M.; van der Veen, M. A.; Jacobs, P. A.; De Vos, D. E. *Phys. Chem. Chem. Phys.* **2009**, *11*, 2903.
(244) Finsy, V.; Verelst, H.; Alaerts, L.; De Vos, D.; Jacobs, P. A.; Baron, G. V.; Denayer, J. F. M. *J. Am. Chem. Soc.* **2008**, *130*, 7110.

(245) Alaerts, L.; Maes, M.; Giebeler, L.; Jacobs, P. A.; Martens, J. A.; Denayer, J. F. M.; Kirschhock, C. E. A.; De Vos, D. E. *J. Am. Chem. Soc.* **2008**, *130*, 14170.
(246) Alaerts, L.; Kirschhock, C. E. A.; Maes, M.; van der Veen, M. A.; Finsy, V.; Depla, A.; Martens, J. A.; Baron, G. V.; Jacobs, P. A.; Denayer, J. F. M.; De Vos, D. E. *Angew. Chem. Int. Ed.* **2007**, *46*, 4293.
(247) Ma, S.; Sun, D.; Wang, X.-S.; Zhou, H.-C. *Angew. Chem. Int. Ed.* **2007**, *46*, 2458.
(248) Trung, T. K.; Déroche, I.; Rivera, A.; Yang, Q.; Yot, P.; Ramsahye, N.; Vinot, S. D.; Devic, T.; Horcajada, P.; Serre, C.; Maurin, G.; Trens, P. *Microporous Mesoporous Mater.* **2011**, *140*, 114.
(249) Olson, D.; Lan, A.; Seidel, J.; Li, K.; Li, J. *Adsorption* **2010**, *16*, 559.
(250) Coudert, F. o.-X.; Mellot-Draznieks, C.; Fuchs, A. H.; Boutin, A. *J. Am. Chem. Soc.* **2009**, *131*, 3442.
(251) Trung, T. K.; Trens, P.; Tanchoux, N.; Bourrelly, S.; Llewellyn, P. L.; Loera-Serna, S.; Serre, C.; Loiseau, T.; Fajula, F. o.; Férey, G. r. *J. Am. Chem. Soc.* **2008**, *130*, 16926.
(252) Lee, J. Y.; Olson, D. H.; Pan, L.; Emge, T. J.; Li, J. *Advanced Functional Materials* **2007**, *17*, 1255.
(253) Uchida, S.; Kawamoto, R.; Tagami, H.; Nakagawa, Y.; Mizuno, N. *J. Am. Chem. Soc.* **2008**, *130*, 12370.
(254) Ghosh, S. K.; Bureekaew, S.; Kitagawa, S. *Angew. Chem. Int. Ed.* **2008**, *47*, 3403.
(255) Zhang, J.-P.; Chen, X.-M. *J. Am. Chem. Soc.* **2008**, *130*, 6010.
(256) Maji, T. K.; Uemura, K.; Chang, H.-C.; Matsuda, R.; Kitagawa, S. *Angew. Chem. Int. Ed.* **2004**, *43*, 3269.
(257) Lin, X.; Blake, A. J.; Wilson, C.; Sun, X. Z.; Champness, N. R.; George, M. W.; Hubberstey, P.; Mokaya, R.; Schröder, M. *J. Am. Chem. Soc.* **2006**, *128*, 10745.
(258) Sun, X. Q.; Wick, C. D.; Thallapally, P. K.; McGrail, B. P.; Dang, L. X. *J. Phys. Chem. B* **2011**, *115*, 2842.
(259) Lincke, J.; Lassig, D.; Moellmer, J.; Reichenbach, C.; Puls, A.; Moeller, A.; Glaser, R.; Kalies, G.; Staudt, R.; Krautscheid, H. *Microporous Mesoporous Mater.* **2011**, *142*, 62.
(260) Xu, G. H.; Zhang, X. G.; Guo, P.; Pan, C. L.; Zhang, H. J.; Wang, C. *J. Am. Chem. Soc.* **2010**, *132*, 3656.
(261) Liu, Q. K.; Ma, J. P.; Dong, Y. B. *J. Am. Chem. Soc.* **2010**, *132*, 7005.
(262) Meyers, R. A. *Handbook of Petroleum Refining processes, Mcgraw-Hill, INC.* **1986**.
(263) Yang, R. T. *Adsorbents: Fundamentals and Applications, John Wiley & Sons, Hoboken,* **2003**.
(264) Yang, R. T. *Gas Separation by Adsorption Progress, Butterworth, Boston,* **1987.**
(265) Rouquerol, F.; Rouquerol, I.; Sing, K. *Adsorption by Powders and Porous Solids-Principles Methodology and Applications, Academic Press, London,* **1999.**
(266) Auerbach, S. M.; Carrado, K. A.; Dutta, P. K. *Handbook of Zeolite Science and Technology*; Marcel Dekker, Inc., New York, 2003.
(267) Keller, J. U.; Staudt, R. *Gas Adsorption Equilibria, Experimental Methods and Adsorptive Isotherms, Springer Science+Business Media, Inc., Boston,* **2005**.

(268) Lan, A. J.; Li, K. H.; Wu, H. H.; Olson, D. H.; Emge, T. J.; Ki, W.; Hong, M. C.; Li, J. *Angew. Chem. Int. Edit.* **2009**, *48*, 2334.
(269) Uemura, K.; Yamasaki, Y.; Komagawa, Y.; Tanaka, K.; Kita, H. *Angew. Chem.* **2007**, *119*, 6782.
(270) Llewellyn, P. L.; Horcajada, P.; Maurin, G.; Devic, T.; Rosenbach, N.; Bourrelly, S.; Serre, C.; Vincent, D.; Loera-Serna, S.; Filinchuk, Y.; Férey, G. *J. Am. Chem. Soc.* **2009**, *131*, 13002.
(271) Kitaura, R.; Fujimoto, K.; Noro, S.-i.; Kondo, M.; Kitagawa, S. *Angew. Chem. Int. Ed.* **2002**, *41*, 133.
(272) Hasegawa, S.; Horike, S.; Matsuda, R.; Furukawa, S.; Mochizuki, K.; Kinoshita, Y.; Kitagawa, S. *J. Am. Chem. Soc.* **2007**, *129*, 2607.
(273) Zhang, J.; Wu, H.; Emge, T. J.; Li, J. *Chem. Commun.* **2010**, *46*, 9152.
(274) Samsonenko , D. G.; Kim, H.; Sun, Y.; Kim, G.-H.; Lee, H.-S.; Kim, K. *Chem.- Asian J.* **2007**, *2*, 484.
(275) Gucuyener, C.; van den Bergh, J.; Gascon, J.; Kapteijn, F. *J. Am. Chem. Soc.* **2010**, *132*, 17704.
(276) Wang, Z.; Zhang, B.; Kurmoo, M.; Green, M. A.; Fujiwara, H.; Otsuka, T.; Kobayashi, H. *Inorg. Chem.* **2005**, *44*, 1230.
(277) Dybtsev, D. N.; Chun, H.; Yoon, S. H.; Kim, D.; Kim, K. *J. Am. Chem. Soc.* **2004**, *126*, 32.
(278) Krishna, R.; van Baten, J. M. *Mol. Simul.* **2009**, *35*, 1098.
(279) Lamia, N.; Jorge, M.; Granato, M. A.; Almeida Paz, F. A.; Chevreau, H.; Rodrigues, A. E. *Chem. Eng. Sci.* **2009**, *64*, 3246.
(280) Hartmann, M.; Kunz, S.; Himsl, D.; Tangermann, O.; Ernst, S.; Wagener, A. *Langmuir* **2008**, *24*, 8634.
(281) Loiseau, T.; Serre, C.; Huguenard, C.; Fink, G.; Taulelle, F.; Henry, M.; Bataille, T.; Férey, G. *Chem.- Eur. J.* **2004**, *10*, 1373.
(282) Barthelet, K.; Marrot, J.; Riou, D.; Férey, G. *Angew. Chem. Int. Ed.* **2002**, *41*, 281.
(283) Eldridge, R. B. *Ind. Eng. Chem. Res.* **1993**, *32*, 2208.
(284) Moulijn, J. A.; Makkee, M.; van Diepen, A. *Process Technology*; Wiley: Chichester, England, 2001.
(285) Park, K. S.; Ni, Z.; Côté, A. P.; Choi, J. Y.; Huang, R.; Uribe-Romo, F. J.; Chae, H. K.; O'Keeffe, M.; Yaghi, O. M. *PNAS* **2006**, *103*, 10186.
(286) Huang, X.-C.; Lin, Y.-Y.; Zhang, J.-P.; Chen, X.-M. *Angew. Chem. Int. Ed.* **2006**, *45*, 1557.
(287) Krishna, R.; van Baten, J. M. *Microporous Mesoporous Mater.* **2011**, *137*, 83.
(288) Zhu, W.; Kapteijn, F.; A. Moulijn, J. *Chem. Commun.* **1999**, *24*, 2453.
(289) Hedin, N.; DeMartin, G. J.; Roth, W. J.; Strohmaier, K. G.; Reyes, S. C. *Microporous Mesoporous Mater.* **2008**, *109*, 327.
(290) Ruthven, D. M.; Reyes, S. C. *Microporous Mesoporous Mater.* **2007**, *104*, 59.
(291) Gascon, J.; Blom, W.; van Miltenburg, A.; Ferreira, A.; Berger, R.; Kapteijn, F. *Microporous Mesoporous Mater.* **2008**, *115*, 585.

(292) ter Horst, J. H.; Bromley, S. T.; van Rosmalen, G. M.; Jansen, J. C. *Microporous Mesoporous Mater.* **2002**, *53*, 45.
(293) Olson, D. H.; Camblor, M. A.; Villaescusa, L. A.; Kuehl, G. H. *Microporous Mesoporous Mater.* **2004**, *67*, 27.
(294) Krishna, R.; van Baten, J. M. *J. Phys. Chem. C* **2010**, *114*, 18017.
(295) Krishna, R.; van Baten, J. M. *Phys. Chem. Chem. Phys.* **2011**, *13*, 10593.
(296) Pramanik, S.; Zheng, C.; Zhang, X.; Emge, T. J.; Li, J. *J. Am. Chem. Soc.* **2011**, *133*, 4153.
(297) Yoon, J. W.; Seo, Y.-K.; Hwang, Y. K.; Chang, J.-S.; Leclerc, H.; Wuttke, S.; Bazin, P.; Vimont, A.; Daturi, M.; Bloch, E.; Llewellyn, P. L.; Serre, C.; Horcajada, P.; Grenèche, J.-M.; Rodrigues, A. E.; Férey, G. *Angew. Chem. Int. Ed.* **2010**, *49*, 5949.
(298) Bux, H.; Chmelik, C.; Krishna, R.; Caro, J. *J. Membr. Sci.* **2011**, *369*, 284.
(299) Dubbeldam, D.; Galvin, C. J.; Walton, K. S.; Ellis, D. E.; Snurr, R. Q. *J. Am. Chem. Soc.* **2008**, *130*, 10884.
(300) Lowell, S. S., J.; Thomas, M.A.; Thommes, M. *Characterization of Porous Solids and Powders: Surface Area, Porosity and Density*; ; Springer, 2006.
(301) Keller, J. U.; Robens, E.; Hohenesche, C. d. F. v. *Stud. Surf. Sci. Catal.* **2002**, *144*, 387.
(302) Mikhail, R. S.; Robens, E. *Microstructure and Thermal Analysis of Solid Surfaces, Wiley, Chichester.* **1983**.
(303) Kaneko, K.; Ohba, T.; Hattori, Y.; Sunaga, M.; Tanaka, H.; Kanoh, H. *Stud. Surf. Sci. Catal.* **2002**, *144*, 11.
(304) Sing, K. S. W.; Everett, D. H.; Haul, R. A. W.; Moscou, L.; Pierotti, R. A.; Rouquerol, J.; Siemieniewska, T. *Pure Appl. Chem.* **1985**, *57*, 603.
(305) Pan, L.; Liu, H. M.; Lei, X. G.; Huang, X. Y.; Olson, D. H.; Turro, N. J.; Li, J. *Angew. Chem. Int. Edit.* **2003**, *42*, 542.
(306) Ruthven, D. M. *Principles of Adsorption and adsorption processes*; John Wiley & Sons, Inc.: New York, 1984.
(307) Ocakoglu, R. A.; Denayer, J. F. M.; Marin, G. B.; Martens, J. A.; Baron, G. V. *J. Phys. Chem. B* **2002**, *107*, 398.
(308) Llewellyn, P. L.; Maurin, G. *Comptes Rendus Chimie* **2005**, *8*, 283.
(309) Salles, F.; Maurin, G.; Serre, C.; Llewellyn, P. L.; Knöfel, C.; Choi, H. J.; Filinchuk, Y.; Oliviero, L.; Vimont, A.; Long, J. R.; Férey, G. r. *J. Am. Chem. Soc.* **2010**, *132*, 13782.
(310) Salles, F.; Kolokolov, D. I.; Jobic, H.; Maurin, G.; Llewellyn, P. L.; Devic, T.; Serre, C.; Ferey, G. r. *J. Phys. Chem. C* **2009**, *113*, 7802.
(311) Chmelik, C.; Karger, J. *Chem. Soc. Rev.* **2010**, *39*, 4864.
(312) Heinke, L.; Tzoulaki, D.; Chmelik, C.; Hibbe, F.; van Baten, J. M.; Lim, H.; Li, J.; Krishna, R.; Karger, J. *Phys. Rev. Lett.* **2009**, *102*, 065901.
(313) Tzoulaki, D.; Heinke, L.; Lim, H.; Li, J.; Olson, D.; Caro, J.; Krishna, R.; Chmelik, C.; Kärger, J. *Angew. Chem. Int. Ed.* **2009**, *48*, 3525.
(314) Chmelik, C.; Heinke, L.; Kortunov, P.; Li, J.; Olson, D.; Tzoulaki, D.; Weitkamp, J.; Kärger, J. *ChemPhysChem* **2009**, *10*, 2623.

(315) Chmelik, C.; Hibbe, F.; Tzoulaki, D.; Heinke, L.; Caro, J.; Li, J.; Kärger, J. *Microporous Mesoporous Mater.* **2010**, *129*, 340.
(316) Hibbe, F.; Chmelik, C.; Heinke, L.; Pramanik, S.; Li, J.; Ruthven, D. M.; Tzoulaki, D.; Kärger, J. r. *J. Am. Chem. Soc.* **2011**, *133*, 2804.
(317) Leach, A. R. *Molecular Modelling Principles and Applications*; 2nd ed.; Prentice Hall: London, 2001.
(318) Smit, B.; Maesen, T. L. M. *Chem. Rev.* **2008**, *108*, 4125.
(319) June, R. L.; Bell, A. T.; Theodorou, D. N. *J. Phys. Chem.* **1992**, *96*, 1051.
(320) Runnebaum, R. C.; Maginn, E. J. *J. Phys. Chem. B* **1997**, *101*, 6394.
(321) Schuring, D.; Jansen, A. P. J.; van Santen, R. A. *J. Phys. Chem. B* **2000**, *104*, 941.
(322) Smit, B.; Daniel J. C. Loyens, L.; L. M. M. Verbist, G. *Faraday Discuss.* **1997**, *106*, 93.
(323) Webb, E. B.; Grest, G. S.; Mondello, M. *J. Phys. Chem. B* **1999**, *103*, 4949.
(324) Frenkel, D.; Smit, B. *Understanding Molecular Simulations: from Algorithms to Applications*; 2nd ed.; Academic Press: San Diego, 2002.
(325) Harris, J.; Rice, S. A. *J. Chem. Phys.* **1988**, *89*, 5898.
(326) Siepmann, J. I.; Frenkel, D. *Mol. Phys.* **1992**, *75*, 59
(327) Frenkel, D.; et al. *J. Phys.: Condens. Matter* **1992**, *4*, 3053.
(328) Chmelik, C.; Heinke, L.; Karger, J.; Schmidt, W.; Shah, D. B.; van Baten, J. M.; Krishna, R. *Chem. Phys. Lett.* **2008**, *459*, 141.
(329) Granato, M. A.; Vlugt, T. J. H.; Rodrigues, A. E. *Ind. Eng. Chem. Res.* **2007**, *46*, 321.
(330) Daems, I.; Baron, G. V.; Punnathanam, S.; Snurr, R. Q.; Denayer, J. F. M. *J. Phys. Chem. C* **2007**, *111*, 2191.
(331) Krishna, R.; van Baten, J. M. *Chem. Phys. Lett.* **2006**, *420*, 545.
(332) Jobic, H.; Laloue, N.; Laroche, C.; van Baten, J. M.; Krishna, R. *J. Phys. Chem. B* **2006**, *110*, 2195.
(333) Garcia-Perez, E.; Dubbeldam, D.; Maesen, T. L. M.; Calero, S. *J. Phys. Chem. B* **2006**, *110*, 23968.
(334) van Baten, J. M.; Krishna, R. *Microporous Mesoporous Mater.* **2005**, *84*, 179.
(335) Lu, L. H.; Wang, Q.; Liu, Y. C. *J. Phys. Chem. B* **2005**, *109*, 8845.
(336) Krishna, R.; van Baten, J. M. *J. Phys. Chem. B* **2005**, *109*, 6386.
(337) Lu, L. H.; Wang, Q.; Liu, Y. C. *Langmuir* **2003**, *19*, 10617.
(338) Beerdsen, E.; Dubbeldam, D.; Smit, B.; Vlugt, T. J. H.; Calero, S. *J. Phys. Chem. B* **2003**, *107*, 12088.
(339) Krishna, R.; Smit, B.; Calero, S. *Chem. Soc. Rev.* **2002**, *31*, 185.
(340) Beerdsen, E.; Smit, B.; Calero, S. *J. Phys. Chem. B* **2002**, *106*, 10659.
(341) Schenk, M.; Vidal, S. L.; Vlugt, T. J. H.; Smit, B.; Krishna, R. *Langmuir* **2001**, *17*, 1558.
(342) Krishna, R. *Chem. Eng. Res. Des.* **2001**, *79*, 182.
(343) Krishna, R.; Paschek, D. *Phys. Chem. Chem. Phys.* **2001**, *3*, 453.
(344) Vlugt, T. J. H.; Martin, M. G.; Smit, B.; Siepmann, J. I.; Krishna, R. *Mol. Phys.* **1998**, *94*, 727.

(345) van Well, W. J. M.; Cottin, X.; Smit, B.; van Hooff, J. H. C.; van Santen, R. A. *J. Phys. Chem. B* **1998**, *102*, 3952.
(346) Krishna, R.; Smit, B.; Vlugt, T. J. H. *J. Phys. Chem. A* **1998**, *102*, 7727.
(347) Du, Z. M.; Manos, G.; Vlugt, T. J. H.; Smit, B. *AlChE J.* **1998**, *44*, 1756.
(348) Bandyopadhyay, S. *Chem. Phys. Lett.* **1998**, *293*, 378.
(349) Granato, M. A.; Lamia, N.; Vlugt, T. J. H.; Rodrigues, A. E. *Ind. Eng. Chem. Res.* **2008**, *47*, 6166.
(350) Granato, M. A.; Vlugt, T. J. H.; Rodrigues, A. E. *Adsorption* **2008**, *14*, 763.
(351) Dijkstra, M. *J. Chem. Phys.* **1997**, *107*, 3277.
(352) Martin, M. G.; Siepmann, J. I. *J. Phys. Chem. B* **1999**, *103*, 4508.
(353) Chen, Z.; Escobedo, F. A. *J. Chem. Phys.* **2000**, *113*, 11382.
(354) Wick, C. D.; Siepmann, J. I. *Macromolecules* **2000**, *33*, 7207.
(355) Chen, B.; Siepmann, J. I. *J. Phys. Chem. B* **1999**, *103*, 5370.
(356) Maginn, E. J.; Bell, A. T.; Theodorou, D. N. *J. Phys. Chem.* **1995**, *99*, 2057.
(357) van Erp, T. S.; Dubbeldam, D.; Caremans, T. P.; Calero, S.; Martens, J. A. *J. Phys. Chem. Lett.* **2010**, *1*, 2154.
(358) Chmelik, C.; Heinke, L.; van Baten, J. M.; Krishna, R. *Microporous Mesoporous Mater.* **2009**, *125*, 11.
(359) Hansen, N.; Krishna, R.; van Baten, J. M.; Bell, A. T.; Keil, F. J. *J. Phys. Chem. C* **2009**, *113*, 235.
(360) Jiang, J.; Sandler, S. I. *Langmuir* **2006**, *22*, 5702.
(361) Zhang, L.; Wang, Q.; Wu, T.; Liu, Y.-C. *Chem.- Eur. J.* **2007**, *13*, 6387.
(362) Düren, T.; Snurr, R. Q. *J. Phys. Chem. B* **2004**, *108*, 15703.
(363) Nicholson, T. M.; Bhatia, S. K. *J. Phys. Chem. B* **2006**, *110*, 24834.
(364) Skoulidas, A. I. *J. Am. Chem. Soc.* **2004**, *126*, 1356.
(365) Babarao, R.; Jiang, J. *Langmuir* **2008**, *24*, 5474.
(366) Burchard, E. *Forcefields: studies on zeolites, molecular mechanics, framework stabilities and crystal growth*; Ph. D thesis, 1993.
(367) Spicer, L. D.; Rabinovitch, B. S. *J. Phys. Chem.* **1970**, *74*, 2445.
(368) Bowen, T. C.; Li, S.; Noble, R. D.; Falconer, J. L. *J. Membr. Sci.* **2003**, *225*, 165.
(369) Poling, B. E.; Prausnitz, J. M.; O'Connell, J. P. *The Properties of Gases and Liquids*; 5th ed.; McGraw-Hill, New York, 2001.
(370) Beck, D. W. *Zeolite Molecular Sieves*; John Wiley & Sons, New York, 1974.
(371) Ohe, S. *Computer Aided Data Book of Vapor Pressure, Data Book Publ Co, Tokyo, Japan* **1976**.
(372) Lide, D. R. *Handbook of Chemistry and Physics. CRC press. 77th edision.* **1996-1997**.
(373) *NIST chemistry webbook, NIST Standard Reference Database Number 69*.
(374) *Selected Values of properties of hydrocarbons and related compounds, American Petroluem Institute Research Project 44*; Cannegie Institute of Technology, Pittsburgh Pennsylvenia.
(375) *Seclected Values of properties of chemical compounds Manufacturing Chemists Association Research Project*; Texas A&M Univ., College Statetion, Texas.

(376) Rudek, M. M.; Katz, J. L.; Vidensky, I. V.; Zdimal, V.; Smolik, J. *J. Chem. Phys.* **1999**, *111*, 3623.
(377) Yaws, C. L. *Thermophysical Properties of Chemicals and Hydrocarbons*; William Andrew, 2008.
(378) Fitch, A. N.; Jobic, H.; Renouprez, A. *J. Phys. Chem.* **1986**, *90*, 1311.
(379) Hu, K.-N.; Hwang, L.-P. *Solid State Nucl. Magn. Reson.* **1998**, *12*, 211.
(380) Auerbach, S. M.; Bull, L. M.; Henson, N. J.; Metiu, H. I.; Cheetham, A. K. *J. Phys. Chem.* **1996**, *100*, 5923.
(381) Auerbach, S. M.; Henson, N. J.; Cheetham, A. K.; Metiu, H. I. *J. Phys. Chem.* **1995**, *99*, 10600.
(382) Datka, J. *J. Chem. Soc., Faraday Trans. 1 F* **1981**, *77*, 511.
(383) Angell, C. L.; Howell, M. V. *J. Colloid Interface Sci.* **1968**, *28*, 279.
(384) Simperler, A.; Bell, R. G.; Philippou, A.; Anderson, M. W. *J. Phys. Chem. B* **2002**, *106*, 10944.
(385) Zhu, J.; Trefiak, N.; Woo, T.; Huang, Y. *Microporous Mesoporous Mater.* **2008**, *114*, 474.
(386) Li, K.; Olson, D. H.; Li, J. *Trends in Inorg. Chem.* **2010**, *12*, 13.
(387) Li, D.; Kaneko, K. *J. Phys. Chem. B* **2000**, *104*, 8940.
(388) Kitaura, R.; Kitagawa, S.; Kubota, Y.; Kobayashi, T. C.; Kindo, K.; Mita, Y.; Matsuo, A.; Kobayashi, M.; Chang, H.-C.; Ozawa, T. C.; Suzuki, M.; Sakata, M.; Takata, M. *Science* **2002**, *298*, 2358.
(389) Serre, C.; Millange, F.; Thouvenot, C.; Noguès, M.; Marsolier, G.; Louër, D.; Férey, G. *J. Am. Chem. Soc.* **2002**, *124*, 13519.
(390) Millange, F.; Serre, C.; Ferey, G. *Chem. Commun.* **2002**, *8*, 822.
(391) Kubota, Y.; Takata, M.; Matsuda, R.; Kitaura, R.; Kitagawa, S.; Kobayashi, T. C. *Angew. Chem.* **2006**, *118*, 5054.
(392) Krishna, R.; van Baten, J. M. *Sep. Purif. Technol.* **2011**, *76*, 325.
(393) Krishna, R.; van Baten, J. M. *J. Phys. Chem. C* **2010**, *114*, 13154.
(394) Krishna, R.; van Baten, J. M. *J. Membr. Sci.* **2010**, *360*, 476.
(395) Krishna, R.; van Baten, J. M. *Langmuir* **2010**, *26*, 10854.
(396) Wang, Z.; Zhang, B.; Fujiwara, H.; Kobayashi, H.; Kurmoo, M. *Chem. Commun.* **2004**, *4*, 416.
(397) Chen, B.; Liang, C.; Yang, J.; Contreras, D. S.; Clancy, Y. L.; Lobkovsky, E. B.; Yaghi, O. M.; Dai, S. *Angew. Chem. Int. Ed.* **2006**, *45*, 1390.
(398) Kondo, M.; Okubo, T.; Asami, A.; Noro, S.-i.; Yoshitomi, T.; Kitagawa, S.; Ishii, T.; Matsuzaka, H.; Seki, K. *Angew. Chem. Int. Ed.* **1999**, *38*, 140.
(399) Jorgensen, W. L.; Severance, D. L. *J. Am. Chem. Soc.* **1990**, *112*, 4768.
(400) Castillo, J. M.; Vlugt, T. J. H.; Calero, S. *J. Phys. Chem. C* **2009**, *113*, 20869.
(401) *Kirk-Othmer Encyclopedia of Chemical Technology, John Wiley & Sons, Inc.: New York* **2008**.
(402) Greim, J.; Schwetz, K. A. *Boron Carbide, Boron Nitride, and Metal Borides*; Wiley-VCH Verlag GmbH & Co. KGaA, 2000.
(403) Whitfield, T. R.; Wang, X.; Liu, L.; Jacobson, A. J. *Solid State Sci.* **2005**, *7*, 1096.

(404) Vougo-Zanda, M.; Huang, J.; Anokhina, E.; Wang, X.; Jacobson, A. J. *Inorg. Chem.* **2008**, *47*, 11535.
(405) Wang, X.; Liu, L.; Jacobson, A. J. *Angew. Chem. Int. Ed.* **2006**, *45*, 6499.
(406) Boutin, A.; Springuel-Huet, M.-A.; Nossov, A.; Gédéon, A.; Loiseau, T.; Volkringer, C.; Férey, G.; Coudert, F.-X.; Fuchs, A. H. *Angew. Chem. Int. Ed.* **2009**, *48*, 8314.
(407) Neimark, A. V.; Coudert, F. o.-X.; Boutin, A.; Fuchs, A. H. *J. Phys. Chem. Lett.* **2009**, *1*, 445.
(408) Ghoufi, A.; Maurin, G.; Férey, G. *J. Phys. Chem. Lett.* **2010**, *1*, 2810.
(409) H. van Koningsveld, A. J. v. d. B., J. C. Jansen and R. de Goede *J. Acta Crystallogr.* **1986**, *B42*, 491.
(410) H. van Koningsveld, F. T., H. van Bekkum and J. C. Jansen *J. Acta Crystallogr.* **1989**, *B45*, 423.
(411) Millange, F.; Guillou, N.; Walton, R. I.; Greneche, J.-M.; Margiolaki, I.; Ferey, G. *Chem. Commun.* **2008**, *39*, 4732.
(412) Devautour-Vinot, S.; Maurin, G.; Henn, F.; Serre, C.; Devic, T.; Ferey, G. *Chem. Commun.* **2009**, *19*, 2733.
(413) Millange, F.; Serre, C.; Guillou, N.; Férey, G.; Walton, R. I. *Angew. Chem. Int. Ed.* **2008**, *47*, 4100.
(414) Mu, B.; Huang, Y.; Walton, K. S. *CrystEngComm* **2010**, *12*, 2347.